Alloying Effects and Temperature Dependency of Oxidation Behavior in Near-α Titanium Alloys.

楊, 陽

https://doi.org/10.15017/1866306

出版情報：九州大学, 2017, 博士（工学）, 課程博士
バージョン：
権利関係：

Alloying Effects and Temperature Dependency of Oxidation Behavior in Near-α Titanium Alloys

DISSERTATION

Presented in Partial Fulfillment of the Requirements for the Degree Doctor of Philosophy in the Graduate School of Kyushu University

By

Yang Yang

Course of Advanced Nanomaterials Science and Engineering

Graduate School of Engineering

Kyushu University

2017

ABSTRACT

Near-α Ti alloys are attractive structural materials with a high strength-to-density ratio and excellent corrosion resistance and have been applied to jet-engine components operating at high temperature. However, the interaction of Ti alloys with oxygen results in embrittlement of substrate surface of the components and causes a loss of ductile metallic material. To design high temperature resistant Ti alloy, it is important to understand mechanism and kinetics of oxidation process. In this study, the effects of elements and microstructures on oxidation behaviors of near-α Ti alloys at elevated temperatures in ambient air were investigated.

Isothermal oxidation testing of a Sn-containing and a Ga-containing near-α Ti alloys, with almost the same Al equivalent, were performed at 750 °C for up to 500 h. The replacement of Sn with Ga decreased the weight gain of the oxidation sample during oxidation, suppressed oxide growth, and improved adherence between the oxide and substrate. The lamellar structure showed a lower weight gain compared to the bimodal structure in both alloys.

Since the Ga-containing alloy showed better oxidation resistance compared to that of Sn-containing alloy, isothermal oxidation testing of the Ga-containing alloy were performed at the temperature range of 650-750 °C for up to 500 h in air. Results revealed that the alloy oxidation kinetics followed a parabolic relationship at 650 °C and a parabolic-cubic relationship at 700 and 750 °C, while

the abundance of Al_2O_3 in oxide layers increased with temperature after the dissolution of Ga_2O_3 species in the Al_2O_3 phase. The activation energy of the α-case formation was close to the magnitudes obtained for conventional titanium alloys.

Unlike conventional near-α Ti alloys, recrystallization was observed in the substrate at oxide/metal interface in the Ga-containing alloy at 700 and 750 °C but the recrystallization did not occur at 650 °C. In addition, that recrystallization was also observed in Ti-4Al, and Ti-8Al systems. It was suggested that an increase in N concentration at oxide/metal interface strongly triggered the recrystallization of grains comprising Ti_2N and Ti_3AlN from the interface. In addition, the recrystallization did not occur in Sn-containing alloy may be due to the low N concentration at oxide/metal interface. The diffusion of N may be suppressed by the formation of the Sn-rich layer at the interface.

ACKNOWLEDGEMENT

First and foremost, I would like to express my deepest and sincere gratitude to my supervisor, Prof. Tomonori Kitashima for his guidance, support and sharing his knowledge in this field. I joined the group with little background of titanium alloys. Thanks for his incredible patience and abundant discussion that allows me to survive after a long incubation time in my learning curve in this field.

I would also like to thank Dr. Toru Hara and Ms. Yuka Hara. Many fruitful discussions with them contribute a lot to the work done in this thesis. I also want to thank Mr. Koji Nakazato, Ms. Emi Utsumi and Mr. Sadao Furukawa for sharing their experience in the labs and helping me with the instruments.

I would like to greatly appreciate the constructive comments, abundant discussion and thoughtful guidance provided by Prof. Setsuo Takaki, Prof. Kazuya Kunitomo, and Prof. Toshihiro Tsuchiyama in improving my thesis. I am really grateful for their expert comments and excellent advice.

I would also like to thank Dr. Yoko Yamabe-Mitarai and all staff members of High Temperature Materials Design Group and also my friends at NIMS, for creating pleasant working environment.

Last, but not the least, I would like to express my gratitude to my parents and Dr. Yadong Yu for providing me with support, inspiration and motivation that give me strength to overcome all obstacles in my life.

VITA

December 16, 1990……...Born – Weinan, China

2007-2011……..……..Bachler Course, Energy, Power system and Automation, Department of Energy and Power Engineering, Xi'an Jiaotong University, China

2011-2014……..……..Master Course, Fluid Machinery, Department of Energy and Power Engineering, Xi'an Jiaotong University, China

2014-Present……..……..Doctor Course, Department of Physics and Chemistry, Kyushu University

PUBLICATIONS

(1) Effects of Ga, Sn addition and microstructure on oxidation behavior of near-α Ti alloy: Y.Yang, T. Kitashima, T. Hara, Y. Hara, Y. Yamabe-Mitarai, M. Hagiwara, S. Iwasaki - Oxidation of Metals, 2017. doi:10.1007/s11085-017-9741-5.

(2) Effect of temperature on oxidation behaviour of Ga-containing Near-α Ti Alloy: Y. Yang, T. Kitashima, T. Hara, Y. Hara, S. Iwasaki – Corrosion Science, under review.

(3) Effect of grain size on oxidation resistance of unalloyed titanium: Y. Yang, T. Kitashima, T. Hara, Y. Hara, Y. Yamabe-Mitarai, M. Hagiwara, L.J. Liu – Materials Science Forum, Vol. 879, 2017.

Table of Contents

LIST OF TABLES

LIST OF FIGURES

Chapter 1 Introduction

Global warming has become one of the most important environmental issues in the world and the emission of carbon dioxide (CO_2) from airplanes is one of the key sources for green gases. The reduction of aircraft weight and enhancement of gas-turbine working temperature are two important aspects of future aircraft engine development, as they could save kerosene and improve the jet-engine working efficiency, which could suppress the emission of CO_2 significantly[1, 2]. High temperature titanium alloys with high strength-to-density ratio and excellent corrosion resistance are attractive structural materials and have been applied to jet-engine components operating at high temperature.

Through years' application of titanium alloys to commercial aircrafts, the total weight of titanium alloys in Boeing 777 has reached approximately 9 % and becomes the second most abundant material applied in jet engines after Ni-based superalloys [3]. However, when exposed to gaseous environments containing oxygen, especially at elevated temperatures, the mechanical properties of titanium-alloy components degrade, limiting the high-temperature capability during service and hindering commercial application. The interaction of titanium alloys with oxygen not only results in the embrittlement of the substrate surface of components due to the high solubility of oxygen in Ti [4-7], but also causes a loss of ductile metallic material due to the formation of oxides on the surface [8, 9]. Figure 1.1 shows development of titanium alloys together with their maximum

application temperatures [2,10]. In addition, alloying elements, microstructures and also oxidizing environment strongly affect the oxidation behaviors of titanium alloys, such as the composition, porosity, thickness of oxide layer, adherence between oxide and substrate, temperature and time dependency of alpha-case thickness etc.

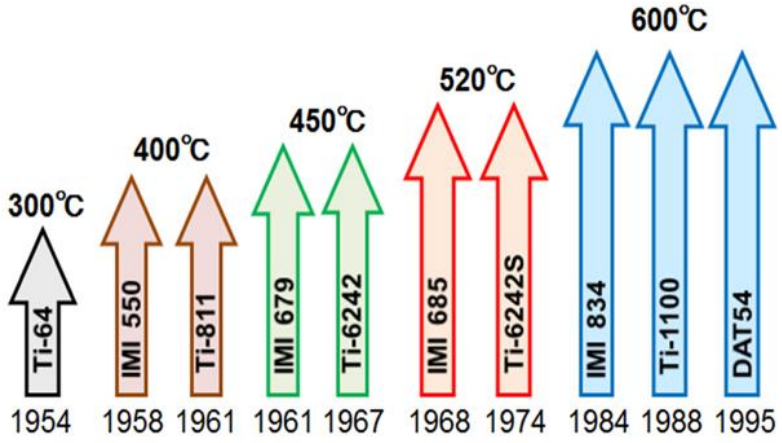

Figure 1.1 Forty years of development of titanium alloys used in jet-engines and their maximum application temperatures [2,10].

To design new titanium alloys for high temperature application in jet-engine, it is necessary to well understand the phenomena of oxidation, the mechanism and kinetics of oxidation behaviours and have better knowledge on how elements, microstructures, temperature and time affect oxide formation and oxygen penetration processes.

1.1 Aim and objective of the research

Al, Ga, and Sn, are α-stabilizing elements and they are used to promote high-temperature strength in Ti alloys by solid solution strengthening and

dispersion strengthening by the precipitation of the α_2 phase [11]. The conventional alloying element Sn accelerates oxide growth of TiO_2 and causes the spallation of oxides. In addition, Sn-added alloy showed smaller tensile strength at 650 °C at the same quantity per unit weight compared with that of Ga addition [12, 13]. However, few data and mechanism investigation of oxidation behaviour of Ga-added alloys were reported.

The present research aimed to evaluate and compare the effects of elements (Ga, Sn) and microstructures on oxidation behaviours of near-α titanium alloys at elevated temperature (650-750 °C) after long exposure time (up to 500 h) in ambient air. The objectives of the research were as follows:

(1) To investigate effects of alloying elements on the oxidation behaviours of near-α Ti alloys.

i) To characterize and compare the weight gains, oxide scales and element distributions in a Sn-containing and a Ga-containing near- α Ti alloys at 750 °C for up to 500 h.

ii) To evaluate and compare effects of two microstructures (bimodal microstructure and lamellar microstructure) on weight gains, element distributions and oxide scales in the two alloys.

iii) To investigate recrystallization phenomenon during isothermal oxidation discovered in Ga-containing alloy.

(2) To investigate the effects of temperature and time on oxidation behaviours of a Ga-containing alloy.

i) To investigate reaction rate, alpha-case formation in the Ga-containing alloy at the temperature range of 650-750 °C up to 500 h.

ii) To investigate the temperature and time dependency of recrystallization phenomenon in the Ga-containing alloy.

1.2 References

[1] J. H. Perepezko, The hotter the engine, the better, Science, 326 (2009) 1068-1069.

[2] T. Kitashima, K. S. Suresh, and Y. Yamabe-Mitarai, Present stage and future prospects of development of compressor material, Crystal Research and Technology, 50 (2015) 28-37.

[3] C. Leyens, and M. Peters: Titanium and titanium alloys, Weinheim, Wiley, 2003.

[4] R. N. Shenoy, J. Unnam, and R. K. Clark, Oxidation and embrittlement of Ti-6Al-2Sn-4Zr-2Mo alloy, Oxidation of Metals, 26 (1986) 105-124.

[5] Z. Liu, and G. Welsch, Effects of oxygen and heat treatment on the mechanical properties of alpha and beta titanium alloys, Metallurgical Transactions A, 19 (1988) 527-542.

[6] T. Kitashima, L. J. Liu, and H. Murakami, Numerical analysis of oxygen transport in alpha titanium during isothermal oxidation, Journal of The Electrochemical Society, 160 (2013) C441-C444.

[7] D. A. P. Reis, C. R. M. Silva, M. C. A. Nono, M. J. R. Barboza, F. Piorino Neto, and E. A. C. Perez, Effect of environment on the creep behavior of the Ti–6Al–4V alloy, Materials Science and Engineering: A, 399 (2005) 276-280.

[8] T. J. Johnson, M. H. Loretto, and M. W. Kearns, Oxidation of high temperature titanium alloys, in: Titanium ’92, Science and Technology, edited by F. H. Froes and I. L. Caplan, TMS, PA, 1992, pp. 2035-2042.

[9] K. S. Mcreynolds, and S. Tamirisakandala, A study on alpha-case depth in Ti-6Al-2Sn-4Zr-2Mo, Metallurgical and Materials Transactions A, 42 (2011) 1732-1736.

[10] M. Peters, J. Kumpfert, C. H. Ward, and C. Leyens, Titanium alloys for aerospace applications, Advanced Engineering Materials, 5 (2003) 419-427.

[11] C. E. Shamblen, and T. K. Redden, Creep resistance and high-temperature metallurgical stability of titanium alloys containing gallium, Metallurgical and Materials Transactions B, 3 (1972) 1299-1305.

[12] T. Kitashima, Y. Yamabe-Mitarai, S. Iwasaki, and S. Kuroda, Effects of Ga and Sn additions on the creep strength and oxidation resistance of near-α Ti alloys, Metallurgical and Material Transactions A, 47 (2016) 6394-6403.

[13] E. M. Kenina, I. I. Kornilov, and V. V. Vanilova, Effect of oxygen on the scale resistance of titanium-tin alloys, Metal Science and Heat Treatment, 14 (1972) 396-398.

Chapter 2 Background

This chapter describes the background theory to the research field and includes literature reviews for alloying elements, temperature and microstructure analysis of titanium alloys as well as diffusion induced recrystallization in binary systems.

2.1 Metallurgy of titanium alloy

Titanium, the ninth abundant element and the fourth most prevalent structural element in the Earth's crust, was discovered by William Gregor in 1791. Martin Heinrich Klaproth named the element Titanium after the Titans from the Greek mythology in 1795. In 1932, Wilhelm Justin Kroll, who first introduced a method to produce pure titanium in large scale, is recognized as the father of titanium industry.

2.1.1 Titanium crystallography

Titanium can crystallize in various crystal structures like Ca, Fe, Co, Zr, Sn, Ce and Hf. Each modification is only stable within particular temperature ranges. Pure titanium exists in two allotropic forms: a modified ideally hexagonal close packed (HCP) structure referred as α-phase at lower temperature and a body-centred cubic (BCC) structure referred as β-phase. The β-transus temperature for pure titanium is 882±2 °C [1]. The exact transformation temperature is strongly influenced by interstitial and substantial elements and

therefore depends on the purity of the metal. Fig. 2.1 schematically shows the atomic unit cells and also some crystallographic parameters of α-phase and β-phase of titanium. As shown in Fig. 2.1(a), there are three most densely packed types of lattice planes, the (0002) plane, also called basal plane, one of the three $\{10\bar{1}0\}$ planes, also called prismatic planes, and one of the six $\{10\bar{1}1\}$ planes, also called pyramidal planes for the HCP crystal structure of titanium [1]. The three axes $\overrightarrow{a_1}$, $\overrightarrow{a_2}$ and $\overrightarrow{a_3}$ are close-packed directions with indices <11$\bar{2}$0>. In Fig. 2.1(b), for BCC crystal structure of titanium, one of the six most densely packed {110} planes is illustrated.

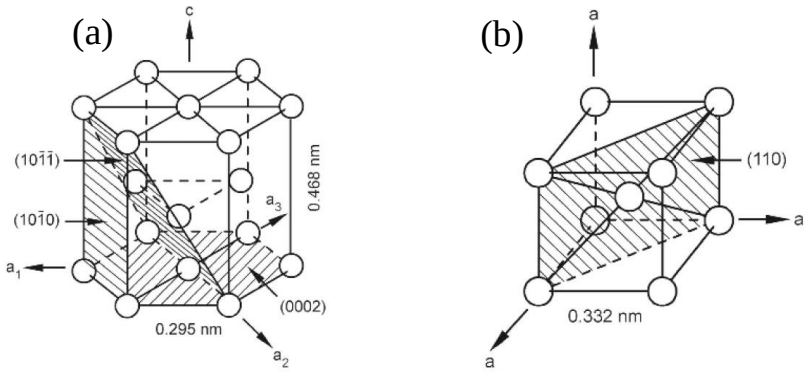

Figure 2.1 Crystal structure of HCP α-phase and BCC β-phase [1].

2.1.2 Alloy classification

As mentioned before, the transformation temperature is strongly affected by alloying elements. Elements that when dissolved in titanium increase transformation temperature through stabilizing α-phase are known as "α-stabilizers". Alloying additions that decrease the phase transformation temperature through stabilizing β-phase are referred to as "β-stabilizers". The "β-stabilizers" are divided into β-isomorphs elements, which have high solubility in

titanium, and β-eutectoid elements, which have limited solubility and tend to form intermetallic [2]. The elements that affect little the β-transus temperature are called neutral elements. Fig. 2.2 shows the effects of some alloying elements on the β transus temperature.

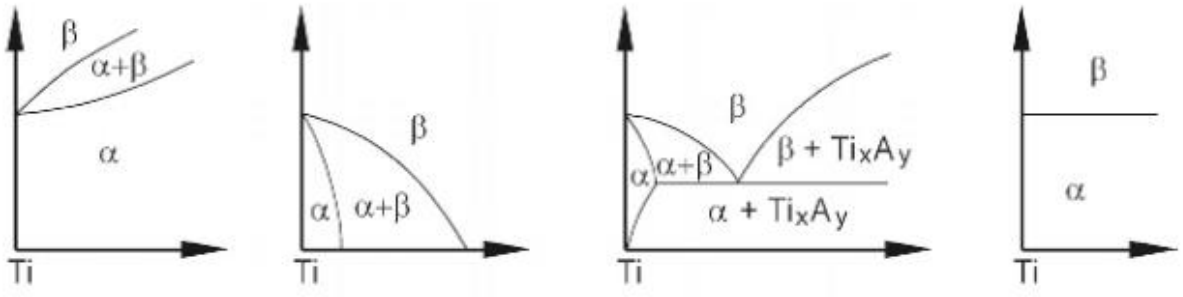

α stabilizers **β stabilizer** **neutral**

β isomorphs **β eutectoid**

(Al, O, N, C) **(V, Mo, Nb, Ta)** **(Fe, Mn, Cr, Ni, Cu, Si, H)** **(Zr)**

Figure 2.2 Effect of alloying elements on β transus temperatures [2].

As shown in Fig. 2.2, the substitutional element Al and the interstitial elements O, N, and C are all strong α stabilizers. They increase the β transus temperature with increasing solute content. Al is the most widely used alloying element in titanium alloys mainly because it raises the β transus temperature and has high solubility in both α and β phases. Fig. 2.3 is the binary Ti-Al phase diagram. As shown in Fig. 2.3, with increasing Al content, the Ti_3Al (α_2) phase will be formed. As ordered α_2 phase is brittle and its precipitation decreases ductility, the amount of Al is limited to about 6 wt. %. Moreover, the Ti-Al phase diagram is also basis for the titanium-aluminides intermetallics characterized with high strength at higher temperatures, but also with low ductility and low fracture toughness compared to conventional titanium alloys. Among the interstitial

elements, oxygen can be considered as an alloying element when oxygen content is used to obtain desired strength level, like getting different degree of CP Ti. Ga is α stabilizer element, although the solubility is lower compared to Al or O, and it can replace Al in the hexagonal ordered Ti_3Al thus increasing strength through precipitation strengthening [3]. The most frequently used β isomorphous elements are V, Mo, and Nb, which can stabilize the β phase to room temperature with sufficient concentration. For β eutectoid elements, Cr, Fe, and Si are used in many Ti alloys. Zr, Hf and Sn can lower β transus temperature only slightly and then increase it again at higher concentrations, thus considered as neutral elements. For Zr and Sn, which were applied to many commercial multicomponent alloys, are considered and counted as α stabilizers because of chemical similarity of Zr to Ti and Sn can replace Al in Ti_3Al phase [4].

Commercial titanium alloys are classified conventionally into three different categories: α, α+ β, and β alloys based on the type and the amount of alloying elements which determines the dominate phase at room temperature. Further subdivisions of Ti alloys are into two more subclasses: near-α and metastable or near-β alloys as shown schematically in Fig. 2.4.

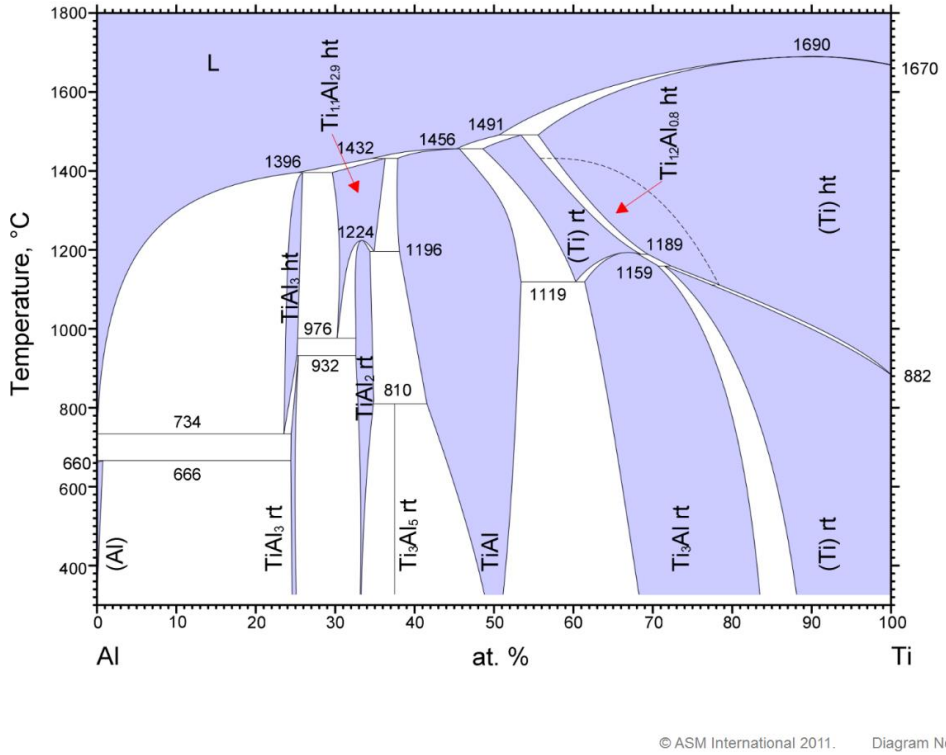

Figure 2.3 Ti-Al phase diagram [5]

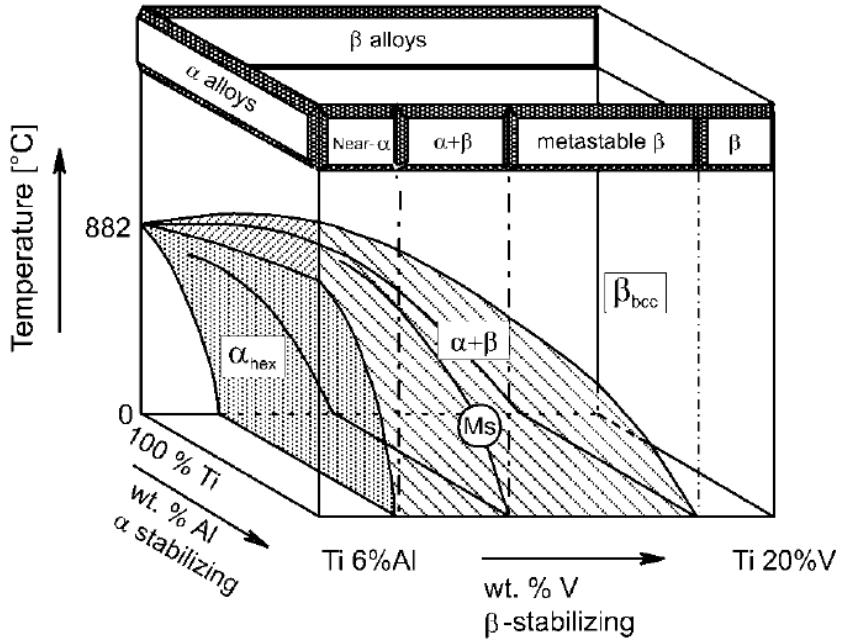

Figure 2.4 Three-dimensional phase diagram for classification of titanium alloys [6]

α alloys and near-α alloys

Unalloyed titanium and alloys of titanium with solute α stabilizers such as Al, Ga, and Sn, are HCP at ordinary temperatures. These alloys are characterized by satisfactory strength, toughness, creep resistance, and weldability. The conventional near-α alloys containing minor fractions of β stabilizers are designed for high temperature application since they have excellent creep property and high strength, which is partly due to the small addition of Si that tends to segregate on dislocations and form silicide precipitation thus preventing dislocation climb and deformation.

α + β alloys

The α + β alloys are a mixture of α and β phases and contain α (e.g. Al) and β (e.g. Mo or V) stabilizing elements in larger quantity than that in near-α alloys. One of the most popular α + β alloys is Ti-6Al-4V. Although this particular alloy is difficult to form, even in the annealed condition, α + β alloys generally exhibit good fabricability as well as high room-temperature strength and moderate elevated-temperature strength. The property of this category alloy can be controlled by heat treatment, which is used to adjust the microstructure and volume fractions of α and β phase.

β alloys and near-β alloys

This category of alloys located in α + β phase regions as shown in Fig. 2.4 and β phase do not transform to martensitic upon fast cooling quenching from β phase field. Most alloys in this class contain more than 15 wt. % β stabilizing alloying elements. They exhibit good formability, toughness and room temperature ductility. In Table 2.1, some important commercial available Ti alloys with their characteristic β transus temperature are listed.

As mentioned before, the prototypical α stabilizing and β stabilizing additions to Ti are Al and Mo, respectively. Accordingly, a classification in terms of its equivalent Al and Mo contents is very useful. According to Rosenberg [7], the equivalent Al content of an alloy contenting Al, Zr, Sn, Ga, and O is: $[Al]_{eq}$= [Al]+1/6[Zr]+1/2[Ga]+1/3[Sn]+10[O], where [x] indicates the concentration of element "x" in weight percent. The Mo equivalence can be expressed by: $[Mo]_{eq}$=[Mo]+1/5[Ta]+1/3.6[Nb]+1/2.5[W]+1/1.5[V]+1.25[Cr]+1.25[Ni]+ 1.7[Mn] +1.7[Co] +2.5[Fe]. These Al- and Mo-equivalent formats provides a rationalization for their replacement into one or another element or phase-stability classifications.

Table 2.1 Important commercial titanium alloys [1]

Commercial Name	Composition (wt.%)	T_β (°C)
α alloys		
Grade 1	CP-Ti (0.2Fe, 0.18O)	890
Grade 2	CP-Ti (0.3Fe, 0.25O)	915
Grade 3	CP-Ti (0.2Fe, 0.35O)	920
Grade 4	CP-Ti (0.5Fe, 0.40O)	950
Grade 7	Ti-0.2Pd	915
Grade 12	Ti-0.3Mo-0.8Ni	880
Ti-8-2.5	Ti-5Al-2.5Sn	1040
Ti-3-2.5	Ti-3Al-2.5V	935
α + β alloys		
Ti-811	Ti-8Al-1V-1Mo	1040
TIMET 685	Ti-6Al-5Zr-0.5Mo-0.25Si	1020
TIMET 834	Ti-5.8Al-4Sn-3.5Zr-0.5Mo-0.7Nb-0.35Si-0.06C	1045
Ti-6242	Ti-6Al-2Sn-4Zr-2Mo-0.1Si	995
Ti-64	Ti-6Al-4V (0.20O)	995
Ti-64 ELI	Ti-6Al-4V (0.13O)	975
Ti-662	Ti-6Al-4V-2Sn	945
Ti-550	Ti-4Al-2Sn-4Mo-0.5Si	975
β alloys		
Ti-6246	Ti-6Al-2Sn-4Zr-6Mo	940
Ti-17	Ti-5Al-2Sn-2Zr-4Mo-4Cr	890
SP-700	Ti-4.5Al-3V-2Mo-2Fe	900
Beta-CEZ	Ti-5Al-2Sn-2Cr-4Mo-4Zr-1Fe	890
Ti-10-2-3	Ti-10V-2Fe-3Al	800
Beta 21S	Ti-15Mo-2.7Nb-3Al-0.2Si	810
Ti-LCB	Ti-4.5Fe-6.8Mo-1.5Al	810
Ti-15-3	Ti-15V-3Cr-3Al-3Sn	760
Beta C	Ti-3Al-8V-6Cr-4Mo-4Zr	730
B120VCA	Ti-13V-11Cr-3Al	700

2.1.3 Microstructure of titanium alloys

The microstructure morphology plays important role in determining its mechanical properties. The two typical microstructures are the equiaxed microstructure, which is a result of recrystallization process, and the lamellar microstructure, which is generated by cooling from β phase field. Both types of microstructure can have a fine and a coarse microstructure based on the size of each phase. Generally, the different microstructures are generated by thermomechanical treatments. Fig. 2.5 schematically shows an outline of a complex sequence of solution heat treatment, deformation, recrystallization, aging and annealing.

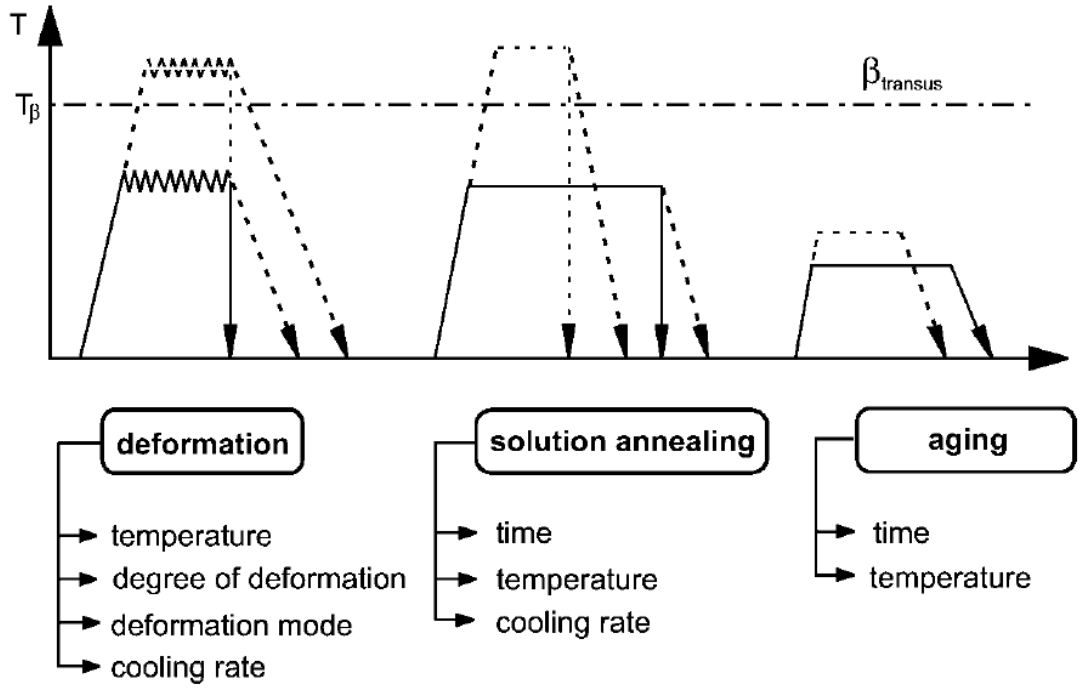

Figure 2.5 Thermomechanical treatment for titanium alloys [6].

Equiaxed Microstructure

As equiaxed microstructure is a result of recrystallization, deformation in the α + β field is necessary to introduce strain energy. After solution heat treatment at temperatures in α + β field, a recrystallized and equiaxed microstructure is developed (see Fig. 2.6). The deformation temperature and deformed percentage will affect texture strength, dislocation density etc. The solution heat treatment procedure and time affect size of equiaxed grain and annealing temperature affects the formation of Ti_3Al phase.

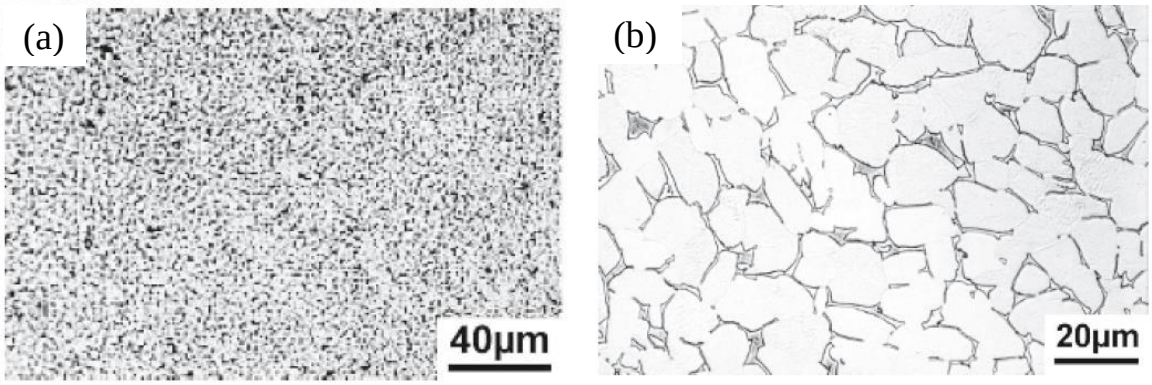

Figure 2.6 Equiaxed microstructures of (a) Ti-64 with fine equiaxed grains [1] and (b) Ti-6242 with coarse equiaxed grains [2].

Lamellar Microstructure

Lamellar microstructure can be obtained by conducting out the final procedure of annealing treatment in the β phase field as shown in Fig. 2.5. The most important parameter in the processing route is the cooling rate from β phase field in solution heat treatment procedure as shown in Fig. 2.5. It determines the characteristic features of the lamellar microstructures, such as the thickness of α lamellae (α plates), the size of α colony, and the thickness of α layers at β grain

boundaries. Fig. 2.7 shows the effect of cooling rate from the β phase field on lamellar microstructures of Ti-6242.

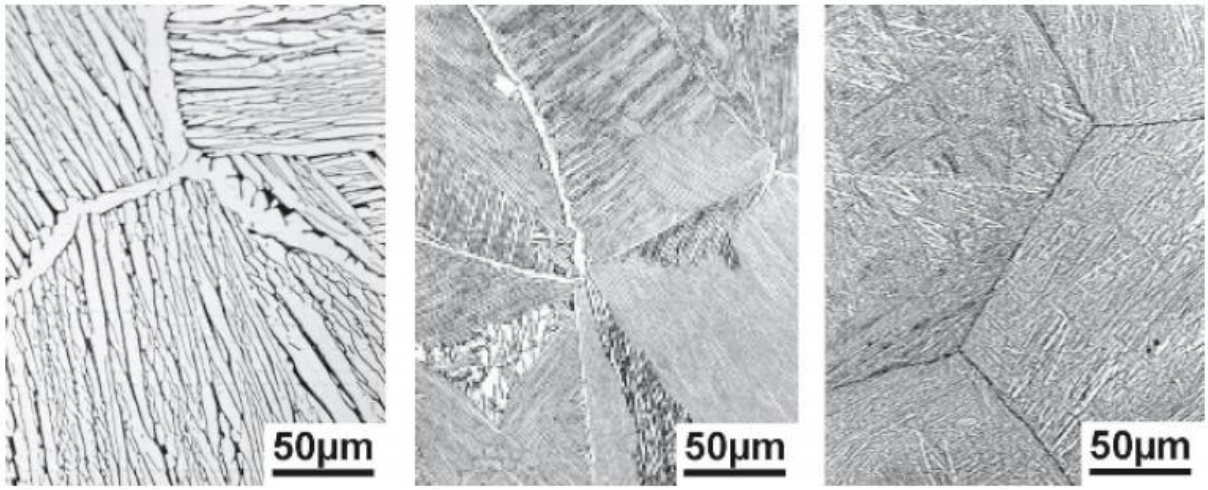

(a) 1 °C/min **(b) 100 °C/min** **(c) 8000 °C/min**

Figure 2.7 Effect of cooling rate on lamellar microstructure of Ti-6242 [1].

Bimodal Microstructure

Bimodal microstructure can be considered to be a combination of lamellar and equiaxed microstructures. It can be obtained when the solution heat treatment is performed at temperatures below β transus temperature. The solution heat treatment temperature determines the volume fraction of primary α phase and the cooling rate after solution heat treatment affect thickness of α lamellae. Fig. 2.8 shows a bimodal microstructure of Ti-64 by optical microscope and transmission electron microscope.

In the present work, Ga-containing Ti alloys have a bimodal microstructure (see Fig. 2.9 a of SEM image) and a fully lamellar microstructure (see Fig. 2.9 b of SEM image).

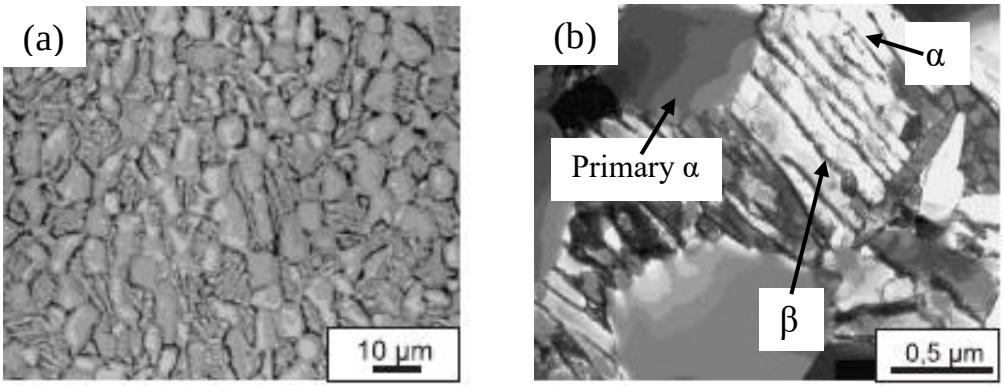

Figure 2.8 Bimodal microstructure in Ti-64 by: (a) optical microscope, and (b) transmission electron microscope [2].

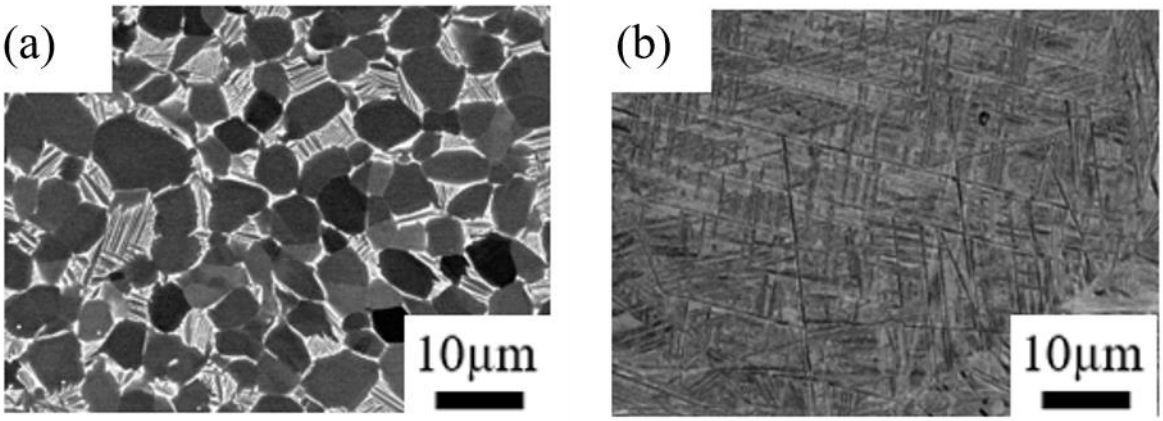

Figure 2.9 Microstructures in present study: (a) bimodal microstructure of a Ga-added titanium alloy, and (b fully lamellar microstructure of a Ga-added titanium alloy.

2.1.4 Mechanical properties of titanium alloys

The properties of Ti alloys are primarily affected by the microstructure features such as, volume fraction, and individual properties of α and β phases. In pure Ti, α phase with HCP structure is more densely packed than β phase with BCC structure and has an anisotropic crystal structure, thus exhibiting higher resistance to plastic deformation, lower ductility, lower diffusion rate, higher creep resistance and anisotropic mechanical as well as physical properties. Table

2.2 shows some physical, mechanical and technological properties of three main categories of titanium alloys.

Table 2.2 Properties of α, α + β and β titanium alloys [2].

Properties	**Class of titanium alloys**		
	α	**α + β**	**β**
Density	+	+	–
Strength	–	+	++
Ductility	–/+	+	+/–
Fracture Toughness	+	–/+	+/–
Creep Resistance	+	+/–	–
Corrosion Resistance	++	+	+/–
Oxidation Resistance	++	+/–	–
Weldability	+	+/–	–
Cold Formability	– –	–	+/–

+: beneficial; ++: significant beneficial; -: detrimental; --: significant detrimental

As shown in Table 2.2, β alloys shows higher density mainly due to alloying elements such as V and Mo, which are heavier compared to Al and O in α alloys. The class of α and near-α alloys exhibit excellent creep resistance mainly due to the limited ability of atoms to diffuse and to deform in HCP structure compared to that in BCC structure. Ti alloys exhibit poor oxidation resistance mainly due to high chemical affinity of O to Ti even at room temperature.

The improvement of mechanical properties of Ti alloys essentially lies on three ways as schematically shown in Fig. 2.10: alloying, processing and the production of composite materials.

Alloying can affect properties by adjusting chemical composition of alloy. This kind of adjustment lays the basis for strength increasing and the formation of new ordered structures. Alloying can modify the physical properties like density, elastic modulus, and also affect chemical resistances such as corrosion and oxidation.

Processing modifies and carefully balances material properties by generating proper microstructures through thermomechanical treatment. This method can optimize for strength, ductility, toughness, stress corrosion, creep resistance etc.

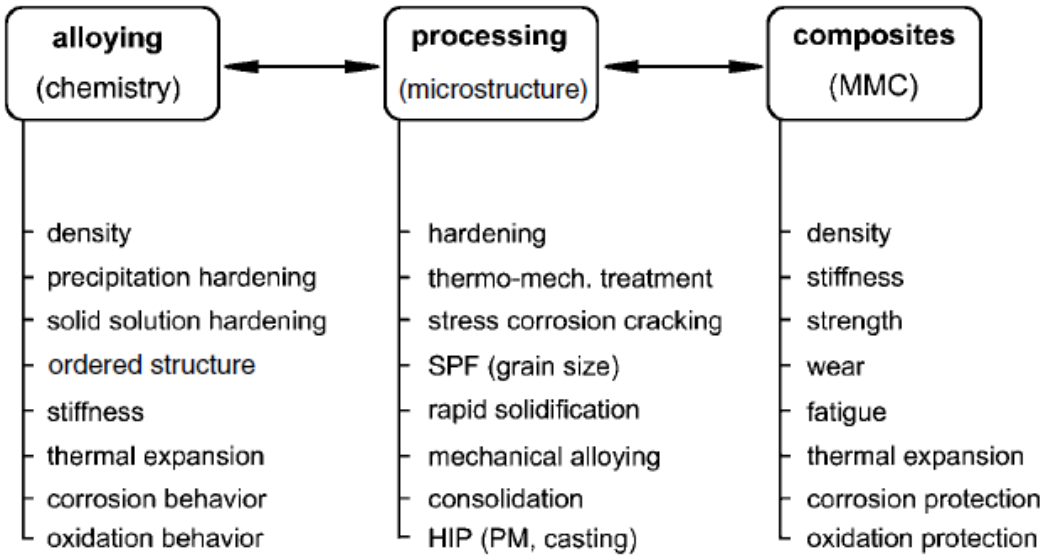

Figure 2.10 Ways for modification of properties in titanium alloys [2].

In practical application, alloying and processing are combined to obtain proper Ti alloys with specific requirement. Alloying elements composition and microstructure both determine the final mechanical properties of titanium alloys.

The quantitative influence of microstructures (fine, coarse, lamellar and equiaxed) on mechanical properties in Ti alloys are shown in Table 2.3. Fine-scale microstructure increase strength and ductility. Coarse-scale microstructure is beneficial for creep resistance and fatigue crack growth elimination. Equiaxed microstructure exhibits high fatigue strength while lamellar structure shows excellent resistance to creep and fatigue crack growth and have high fracture toughness at the same time. Bimodal microstructure shows a combination features of lamellar and equiaxed structures and have the potential of obtaining a well-balanced alloy with proper mechanical property.

Table 2.3 Microstructure effects on mechanical properties of titanium alloys [2].

Properties	**Fine**	**Coarse**	**Equiaxed**	**Lamellar**
Young's Modulus	×	×	×	+/− (texture)
Strength	+	−	+	−
Ductility	+	−	+	−
Fracture Toughness	−	+	−	+
Fracture Crack Initiation	+	−	+	−
Fracture Crack Propagation	−	+	−	+
Creep Strength	−	+	−	+
Fatigue Strength	+	−	+	−
Oxidation Rate	+	−	−	+

×: no effect; +: positive, −: negative.

Near-α Ti alloys with high-temperature strength is attractive for application [8-10] because of the ability to retain adequate low temperature toughness after long-time exposure to high atmosphere. α-stabilizers of Al, Ga, Sn are known to enhance the high-temperature strength of Ti alloys by solid solution strengthening.

In addition, the formation of α_2 phase with $D0_{19}$ structure in near-α Ti alloys increases strength by precipitation strengthening. The addition of Ga to Ti was more effective than the addition of Sn in increasing the 0.2 % proof strength and the tensile strength at room temperature and 650 °C at the same quantity per unit weight [11]. Si addition was proved to be effective in increasing high temperature tensile and creep strength in α and α+β alloys. This is partly achieved by solid solution strengthening and silicide precipitation strengthening. Si atoms interact with dislocations to increase dislocation slip energy and induce cross-slip, causing an increase in tensile strength that can be maintained to high temperature. Interstitial elements O, N, and C cause solid solution strengthening in titanium alloys, especially for O, based on the concentration of which the different grades of CP-titanium was designed [4]. O has high chemical affinity to Ti at elevated temperature and high solubility in titanium (14.3 wt %) [12]. In fact, O is often used as an alloying element to achieve desired strength levels or fatigue performance, although such strengthening usually decreases toughness [13]. Many researchers investigated the effects of oxygen on mechanical properties [14-21]. Welsch et al. [14] suggested that oxygen affected the tensile strength of Ti-6Al-4V through microstructural modifications which depend on the choice of aging parameters. Dong et al. [15] and Ebrahimi et al. [16] reported that thermal oxidation and oxygen dissolution caused a reduction of the fatigue limit of 27% in Ti-6Al-4V. Leyens et al. [17] and Ja et al. [18] showed that oxidation significantly affected tensile properties and caused a decreasing of strength and

ductility. Liu et al. [19] studied the effects of oxygen concentration and aging temperature on hardness and ductility of α and β Ti alloys. They reported that O hardened α and β alloys to the same degree with a square root dependency on concentration and it enhanced α_2 precipitation during aging.

2.2 Oxidation

In this section fundamental aspects of metal oxidation, oxidation of titanium alloys and temperature, elements, and microstructure dependency are presented.

2.2.1 Introduction

The oxidation of metals at high temperature is interdisciplinary, covering metallurgy, physic and chemistry [22]. Most metal and alloys would form corrosion products when exposed to oxidizing atmosphere between 100 and 500 °C [23]. Such corrosion products on the surface of metal and alloys play a key role in determining the properties of metal and alloys at elevated temperatures. For high temperature application, the metals or alloys are required to have high temperature oxidation resistance. To design such high temperature resistance material, the oxide growth rate should be relatively low and their mechanical properties keep stable. Temperature, alloying elements, microstructure and atmosphere all affect oxidation behaviour of metals and alloys. So, it is very important to understand the kinetics and mechanism of the oxidation process and

how alloying elements, temperature, microstructures as well as atmosphere affect such oxidation process.

2.2.2 Fundamentals of oxidation of metals

In this section, the two key aspects for the oxidation process and formation of oxides are taken out: thermodynamics of oxidation and kinetics of oxidation.

2.2.2.1 Thermodynamics of oxidation

To know high temperature corrosion reaction, it is essential to make sure whether each element can have chemical reaction with exposure atmosphere. One of the most important tool to analyse such a problem is equilibrium thermodynamics, which is helpful to find out clearly the possible chemical products with typical reaction conditions.

The reaction of a metal (M) and oxygen gas (O_2) can be simply described as the following simple chemical reaction [22]:

$$a \cdot M_{(s)} + \frac{b}{2} \cdot O_{2(g)} \leftrightarrow M_a O_{b(s)}, \tag{2.1}$$

The oxidation reaction can be thermodynamically described by the difference of Gibbs free energy ΔG between reaction product $M_a O_{b(s)}$ and reactants $M_{(s)}$ and $O_{2(g)}$. If the $\Delta G < 0$, the reaction for formation of oxide could proceed and for $\Delta G = 0$, equilibrium conditions can be established. As concentration of reactants and products affect absolute Gibbs free energy, the standard Gibbs free energy of formation ΔG^0 is applied.

To understand whether a reaction can thermodynamically occur or not, Ellingham/Richardson diagrams were reported. As shown in Fig. 2.11, the standard free energy for oxide formation as a function of partial pressure and temperature are summarized. As the value of ΔG^0 can represent the stability of oxides directly, it is clear that the stability of oxides increases from Cu_2O to CaO.

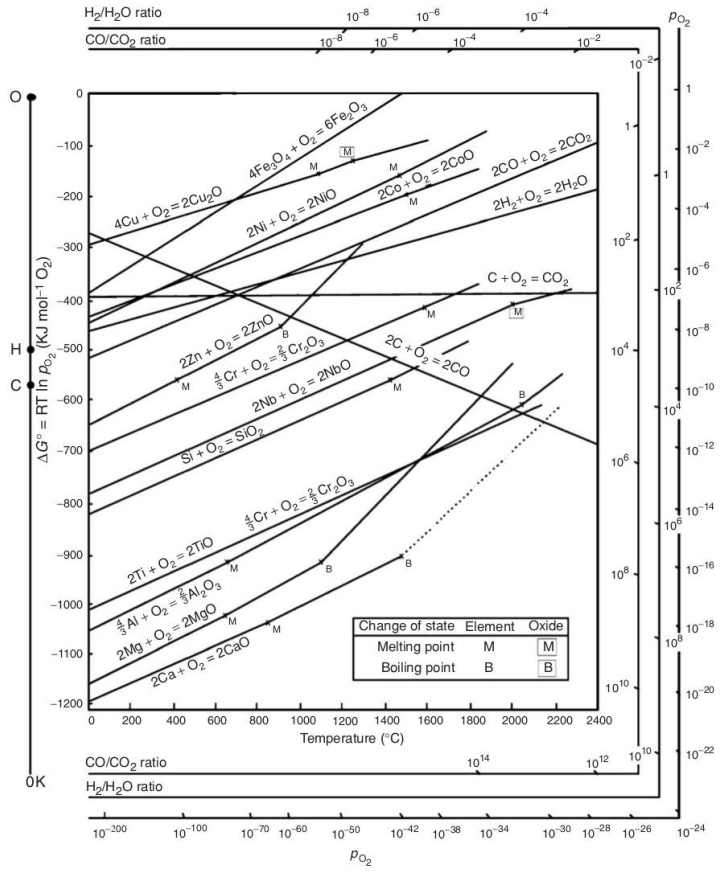

Figure 2.11 Ellingham/Richardson diagram of standard free energy of formation for some oxides as a function of temperature [22].

2.2.2.2 Kinetics of oxidation

Growth of oxide scales, reaction rates and kinetics are basis for elucidation of oxidation mechanism. In oxidation of metals, the following rate laws are commonly encountered: linear, parabolic and logarithmic laws [23-26].

Linear law

The oxidation proceeds with a constant reaction rate with some typical conditions, which can be described by the following linear rate equation [23]:

$$x = k_l t, \tag{2.2}$$

where k_l is linear rate constant, t is time and x usually refers to the oxide thickness or the amount of oxygen consumed per unit area of metal. The linear rate law can be observed when the oxide layer is very thin and the metal activity keeps in high level in phase interface [25].

Parabolic law

Most of metals follow parabolic law when exposure to above 400 °C with respect to time. The parabolic rate law can be described as the following equations [23]:

$$\frac{dx}{dt} = \frac{k_p}{x}, \tag{2.3}$$

or

$$x^2 = k_p \cdot t + C, \tag{2.4}$$

where k_p is the parabolic rate constant. The parabolic rate law is accompanied by diffusion-controlled scale growth [26].

Logarithmic law

At temperatures below 300-400 °C, the oxidation process was found to obey logarithmic law. The reaction rate is very fast at the beginning of oxidation

and drops to low rates when a thin oxide film forms with a thickness around 100 nm. The logarithmic law can be described with the following equations:

$$x = k_{log} \log(t + t_0) + A, \tag{2.5}$$

$$1/x = B - k_{il} log t, \tag{2.6}$$

where k_{log} is the logarithmic rate constant, k_{il} is rate constant and A, B are constants.

In practical applications, the oxidation of metals is a complex process and seldom obeys only one oxidation rate law. Some of the borderline cases are displayed in Fig. 2.12.

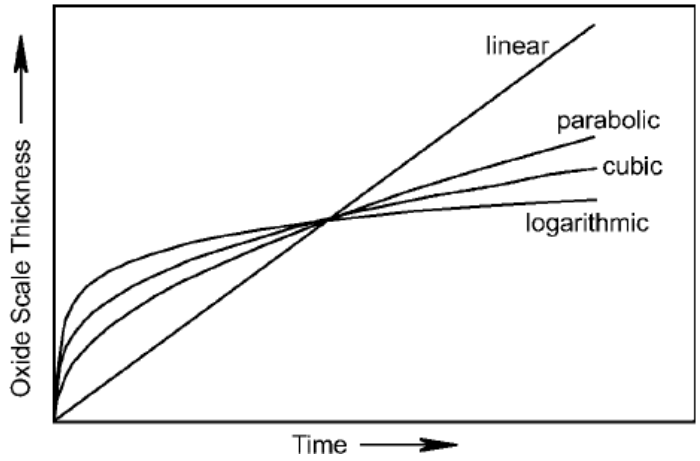

Figure 2.12 Schematic representation of rate laws for oxide formation [2].

Usually, the oxidation process obeys a combination of the basic three oxidation rate laws and can change from one to another with time and temperature. One example of combining rate laws is cubic rate law as shown in Fig. 2.12, which is a combination of logarithmic law and parabolic law and usually was found to be act at low temperature. At higher temperatures, a combination of parabolic and linear rate law can be observed. These rate laws or the change and

combination of rate laws closely relate to the formation and nature of oxide scales with respect to time and temperatures [23].

The classical analysis of oxidation kinetics is the thermogravimetric analysis, which involves the measurement of mass change of sample, or the atmosphere change. The determination of the oxidation reaction rate has been carried out by fitting the weight gain data with time into the following power law equation [27-29]:

$$\left(\frac{\Delta W}{A}\right)^n = k_n t \,, \tag{2.7}$$

where ΔW is the weight gain, A is the surface area, n is the reaction index, k_n is the reaction rate constant and t is time. The n values can be obtained by regression analysis of logarithmic plots of the weight gain per surface area vs. time from time dependent weight gain data. This method was adopted to evaluate the oxidation reaction rate of oxidation of a Ga-containing near-α titanium alloy at a temperature range of 650-750 °C in chapter 5.

2.2.3 Oxidation of titanium alloys

In this section, oxide growth process is described firstly and literature reviews of oxidation of titanium alloys and titanium aluminides as well as the effects of alloying elements, microstructure and temperature on oxidation behaviors are also carried out.

2.2.3.1 Oxide growth mechanism

Oxidation of metals involve the formation of an oxide scale that covers the metal surface uniformly. The formation of an oxide scale of a pure metal can be divided into the following four steps [2] as shown in Fig. 2.13:

a) oxygen adsorption
b) nucleation of oxide
c) lateral growth of oxide
d) formation of compact oxide

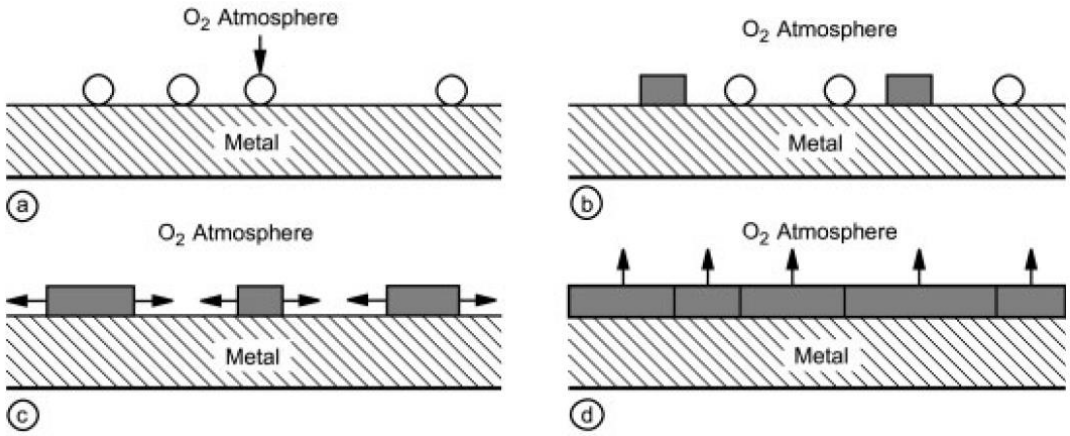

Figure 2.13 Schematic illustrations of 4 steps for oxide formation: a) oxygen adsorption, b) oxide nucleation, c) oxide lateral growth, and d) compact oxide formation [2].

The initial step of oxygen adsorption involves attachment of oxygen to metal surface by chemical adsorption or physical adsorption as shown in Fig. 2.13a. For physical adsorption, gases are bound to metal surface by van der Waals force while for chemical adsorption, it is bounded by chemical bonds [2, 23]. After metal surface saturated with adsorbed oxygen, oxide nuclei forms and growth laterally as shown in Fig. 2.13b and 2.13c. These adsorption, nuclei and

lateral growth occur rapidly at elevated temperatures and sufficiently high oxygen partial pressure. Once a thin, compact film has been formed as shown in Fig. 2.13d, further growth of oxide scale is controlled by mass transport through oxide scale. In this case, the type and morphology of oxide scale, cracks, voids in oxide scale, grain boundary and volume diffusion all affect the mass transport process, thus affecting oxide growth.

Oxides are compound with a high portion of ionic bounding. Oxygen ions and metal ions form cation and anion partial lattices, which form an electrically neutral lattice as a whole. The electronegativity of each element may play an important role for mass transformation. In addition, large numbers of imperfections such as metal ions located at the interstitial positions, non-metal ion vacancies, metal ion vacancies and non-metal ions located in the interstitial positions affect mass transformation in oxide scale significantly [30]. TiO_2 is the most commonly formed oxide during isothermal oxidation at high temperatures for titanium alloys. There are four polymorphs of TiO_2 found in nature, however, only rutile structure is commonly recognized during oxidation as it is the most thermodynamically stable polymorph at all temperatures [31]. Rutile is known as a non-stoichiometric compound and is often expressed as TiO_{2-x}. The defect structure in rutile involves both oxygen vacancies and tri- and tetra- valent interstitial Ti cations as described in reference [32], which can affect mass transfer electrically.

Titanium has a high chemical affinity to oxygen (indicated by Ti-O bond energy of 2.12 eV, comparable to the Ti-Ti bond energy of 2.56 eV) [12] and high solid solubility of oxygen approximate to 14.5 wt % in α titanium in Ti-O phase diagram [33]. The formation of an oxide scale during isothermal process in titanium alloy is directly influenced by thermodynamics, such as similar stabilities of TiO and Al_2O_3 as shown in Fig. 2.11 and kinetic aspects, such as the relative high growth rate of TiO_2 compared to Al_2O_3. Al is the most common alloying element in Ti alloy, as shown in Fig. 2.14 [2], a sketch of oxide scale and oxygen inter-diffusion zone of titanium-based alloys with different Al contents exposed to identical thermal conditions.

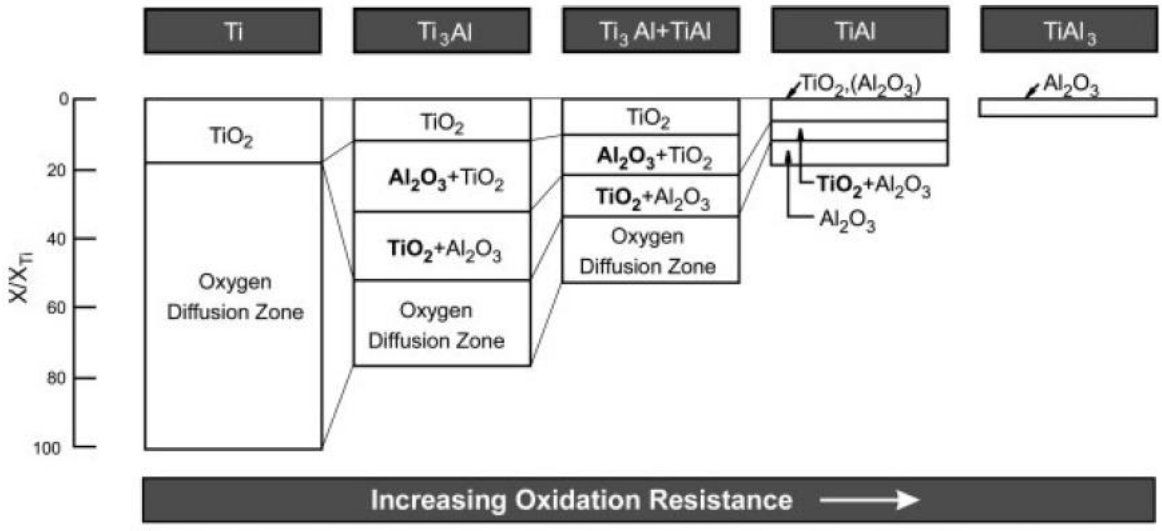

Figure 2.14 Schematic representation of oxide scales and oxygen inter-diffusion zone of titanium-based alloys [2].

Addition of more Al results in a reduction in oxide scale thickness. The stabilization and continuity layer of Al_2O_3 improve the oxidation resistance as can be seen in Fig. 2.14. The oxide scale typically has a multilayer microstructure consisting of a TiO_2 top layer and a heterogeneous mixture of TiO_2 and Al_2O_3 in

varying proportions [28,34]. The formation of a multilayered structure was presented in detail by Du et al. [28] and Fig. 2.15 shows a schematic process for the formation of multi-layered structure of oxide in Ti-6Al-4V alloy.

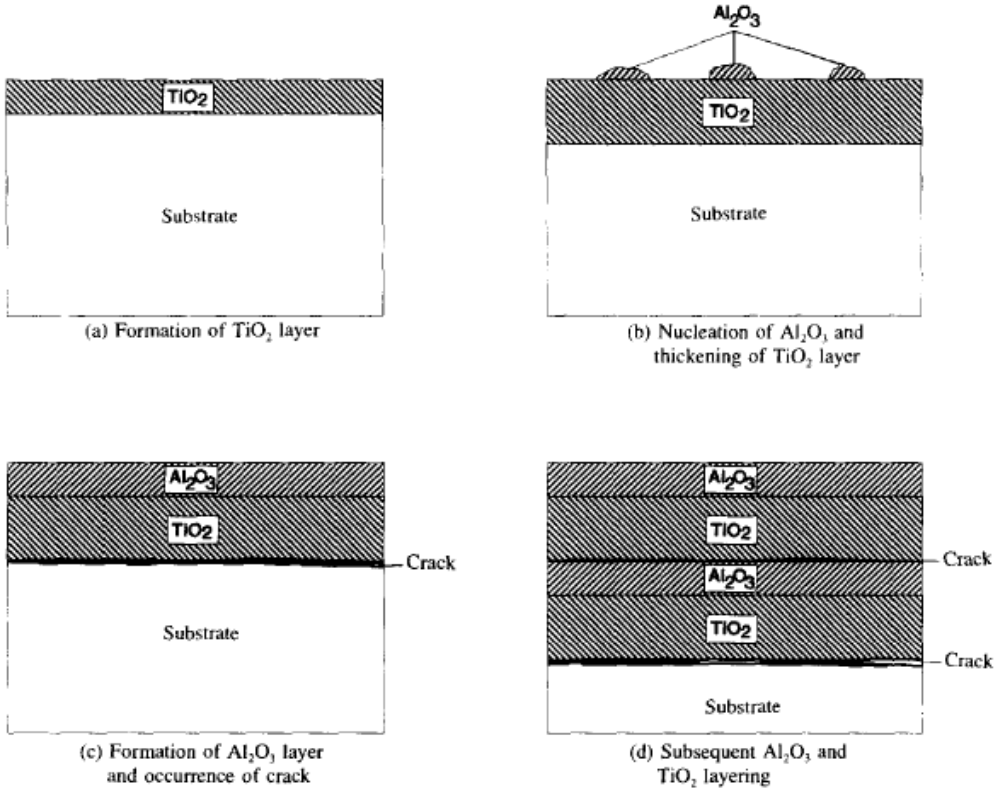

Figure 2.15 Schematic illustrating the mechanism controlling air oxidation of Ti-6Al-4V in temperature range of 650-860 °C [28].

A mechanism for the formation of multilayered oxides was proposed by Du et al. [28]. At first, TiO_2 preferentially developed on the alloy surface due to the relative high activity of Ti compared to Al. Once the thin TiO_2 layer is formed, the substrate was separated from its environment (Fig. 2.15a). The oxygen partial pressure at interface of substrate/oxide would decrease considerably to a value approaching that of the dissociation partial pressure of TiO_2. At such low oxygen partial pressure, the formation of Al_2O_3 at oxide/metal interface is difficult due to

the requirement of a relative higher minimum activities of Al. As oxygen diffuses inward to oxide/substrate interface and TiO_2 forms at this interface thus increasing oxide thickness, Ti would be trapped at the oxide/substrate interface. At the same time, the oxygen partial pressure is relative high at gas/oxide interface, and allows the formation of Al_2O_3 layer on top of the already formed TiO_2 oxide scale as shown in Fig. 2.15b. Once the double-layered oxide scale formed, a growth of such oxide scale would lead to cracks when oxide scale reached its plastic limit. The occurrence of the detachment at oxide/substrate interface would make outward diffusion of Al and Ti difficult and increase oxygen partial pressure to the level suitable for the formation of a second TiO_2 layer. As the oxidation continues, these process will repeat and result in the formation of multilayered oxide scales (Fig. 2.15d).

The alloying, microstructures, temperature and time affect oxide scale morphology, oxide composition, and oxidation kinetics such as oxide growth rate. These are discussed in the following three sections.

2.2.3.2 Effects of alloying elements on oxidation behavior

The addition of alloying elements is one of the methods to improve oxidation resistance as well as mechanical properties of titanium alloys.

Many researchers have examined the influence of certain elements on the oxidation behavior of Ti-based alloys [11, 28, 35-44] and also of TiAl-based intermetallics [45-51]. Based on the previous investigation, it was found that Cu,

Y, V, Cr, and Mn enhanced the weight gain of alloys; Sn, Zr, Hf, Ta, Ni, and Co had little effect on the weight gain of alloys; and Si, Nb, Mo, and W reduced the weight gain of alloys, where W and Mo showed the highest reduction of weight gain. It was also suggested that the enrichment of W and Mo in the metal side of the oxide/metal interface caused the formation of a Mo- or W-rich β-Ti and/or δ-Ti phase, which led to a more rapid supply of Al into the scale and/or formation of an Al_2O_3 layer along the interface. The main mechanisms for enhancing oxidation resistance are to suppress oxide growth or element diffusion by valence control rule [48, 49], and to form a discrete layer which works as a barrier layer to prevent oxidation [46]. However, there is few work about the effect of Ga addition on the oxidation behavior in Ti alloys during isothermal oxidation at high temperatures.

2.2.3.3 Effects of temperature on oxidation behavior

The oxidation of commercial pure titanium in different types of environments at a wide temperature range have been extensively investigated [52-63]. The most notable and important studies of oxidation on pure titanium at a temperature range of 300-1000 °C have been performed by Kofstad et al. [53]. The basic oxidation behaviors and kinetics based on temperature and time were analyzed by analyzing the weight gain profiles as a function of time and temperature (Fig. 2.16).

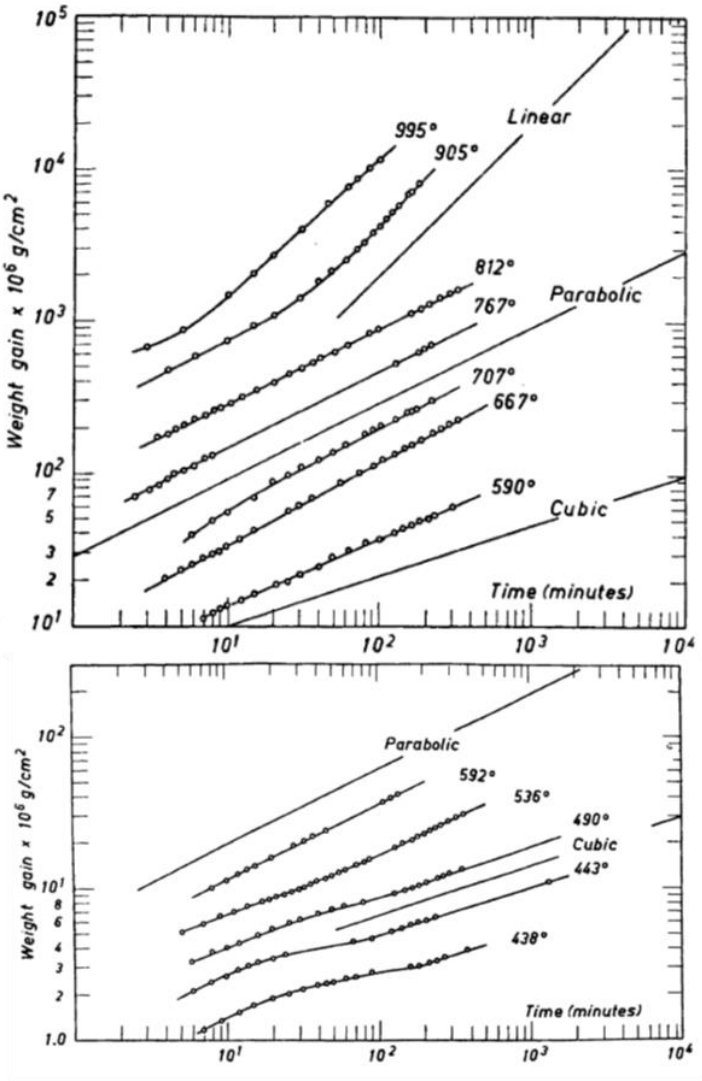

Figure 2.16 Oxidation of titanium in dry air at the temperature range of 400-1000 °C [53].

It was shown from Fig. 2.16 and with data from reference [53] that at temperatures below 300 °C the oxidation rate obeys logarithmic law, in the temperature range of 300-600 °C cubic law, in the temperature range of 600-850 °C parabolic law and above 850 °C linear law. The rate laws observed at high temperatures often were described as an initial parabolic rate law followed by a linear rate law, while in other cases the rate law was interpreted as a mixture of linear and parabolic rate laws. It should be pointed out that there are no definite

temperatures at which the oxidation changes rate law; rather there are temperature intervals where different rate laws may be observed depending upon the duration of the oxidation. According to the observation and discussion of oxidation behavior of titanium at low temperatures, it was suggested that the logarithmic rate law is associated with an oxide film formation [59]. The rate of dissolution and diffusion of oxygen in titanium is consequently very small compared to the rate of film formation during the logarithmic rate law period. For cubic rate law, it was suggested that the diffusion of oxygen through the outer layer of the oxygen-enriched titanium resulted in this cubic rate law based on the high solubility of oxygen in titanium [53]. The parabolic rate laws and linear rate laws were associate with oxide scale formation and oxygen diffusion into substrate forming brittle and hard oxygen enriched layer [27-29]. The linear rate of oxidation was regarded to be a result of the appearance of some cracks due to stress generated in oxides as well as in oxygen enriched layer and formation of porous oxide scales [32, 53].

The effects of temperature and time on oxidation behavior of conventional titanium alloys such as Ti-6Al-4V [27, 28, 34, 61, 62], Ti-6Al-2Sn-4Zr-2Mo [29, 63, 64], IMI 834 [35, 65, 67] and other titanium based alloys [17, 65, 66] have also been widely investigated. The oxidation kinetics, the oxidation reaction index as well as the oxidation reaction rate have strong relationship with temperature and time.

The Ga-containing near-α alloy showed less weight gain compared to IMI834 and TIME1100 and Ga dissolved in Al_2O_3 layer. The temperature dependencies of the oxidation behavior and the recrystallization in Ga-added titanium alloy were carried out in our study. Our results showed that oxidation follows a parabolic relationship at 650 °C and a parabolic-cubic relationship at 700 and 750 °C. The densification of oxide layers near the substrate was observed at 700 and 750 °C. Recrystallization at the oxide/metal interface occurred at 700 and 750 °C while the recrystallization was not observed at 650 °C. The abundance ratio of Al_2O_3 in oxide layers increased as temperature increasing, which may suppress oxide growth and suppress oxidation reaction rate. The details were given in chapter 5.

2.3 Diffusion

As discussed in section 2.2.3.4, diffusion of oxygen plays an important role in oxidation process of titanium alloys, the fundamentals of solid-state diffusion and diffusion in titanium alloys and also the formation of α-case in Ti alloys are presented.

2.3.1 Fundamentals of solid-state diffusion

Diffusion is the net movement of molecules or atoms from a region of high concentration (or high chemical potential) to a region of low concentration (or low chemical potential). The atoms movement usually takes place through vacancies and interstitial sites in solids known as volume diffusion or through

grain boundary and dislocations known as short-circuit diffusion [68-70]. For volume diffusion, the interstitial diffusion mechanism is typical for diffusion of atoms with small atomic radius such as hydrogen, carbon, nitrogen and oxygen, which are more mobile and go much faster in metals [70].

The diffusion phenomenon is governed by a Fourier type of law, and the mathematical equation can be represented as [69]:

$$J = -D\frac{\partial C}{\partial x}, \tag{2.8}$$

where J is the quantity of materials (e.g. flux), C is concentration, x is diffusion direction and D is the diffusion constant. This formulation is known as Fick's first law. By suitable mathematical manipulation Fick's second law can be derived:

$$\frac{\partial C}{\partial t} = \frac{\partial}{\partial x}(D\frac{\partial C}{\partial x}), \tag{2.9}$$

Adopting the boundary conditions, the solutions of the diffusion equation can be obtained. In a practical application, solids can be assumed as semi-infinite thickness and surface concentration is constant, then one solution can be described as [69]:

$$\frac{C_x - C_0}{C_s - C_0} = 1 - \mathrm{erf}(\frac{x}{2\sqrt{Dt}}), \tag{2.10}$$

where C_x is the concentration of diffused atoms at a distance of x after a diffusion time of t, C_0 is the initial concentration in bulk material and the concentration at infinite depth after diffusion time of t, C_s is the surface concentration constant. If

it is desired to achieve a specific C_x concentration in the calculation domain then the left and the right side of Eq. 2.10 becomes constant. This results in the following expression [69]:

$$\frac{x^2}{Dt} = \text{constnat} \tag{2.11}$$

Eq. 2.11 is a simplified approximate solution for Fick's second law and was applied to estimate diffusion coefficients for oxygen in Ga-containing titanium alloy (chapter 5). In addition, diffusion coefficients at various temperatures are related by Arrhenius-type equation [71]:

$$D = D_0 \exp(-\frac{Q}{RT}), \tag{2.12}$$

where D_0 is the frequency factor and Q the activation energy, R is the universal gas constant and T is absolute temperature. This equation is linear on a $\ln D$, reciprocal temperature plot. Thus D_0 and Q may be calculated by fitting with experimentally determined D values. Eq. 2.12 was used for determining diffusion activation energy in Ga-containing alloy which will be shown in chapter 5.

2.3.2 Diffusion in titanium alloys

The knowledge of oxygen diffusion is essential for understanding oxidation mechanism in titanium and its alloys. Many investigations have been carried out on oxygen diffusion phenomenon [72-75].

Diffusion of single oxygen atoms through HCP (α) Ti was initially proposed as atom-hopping between identical interstitial sites, following an

Arrhenius relationship with temperature. Oxygen prefers to occupy an octahedral interstitial site surrounded by six titanium atoms [12], so oxygen diffusion was assumed by some researchers as to either direct octahedral-to-octahedral transitions through tetrahedral transition states, or transport from octahedral to metastable tetrahedral sites [72]. However, some researchers found that tetrahedral site was unstable and all of the heterogeneous networks contribute to the diffusion of oxygen [73]. For determining the O diffusivity in Ti and Ti alloys, several experimental methods and simulations were carried out by many researchers [72-81]. Liu and Welsch [76] have published a comprehensive review about oxygen diffusivities in α and β titanium alloys in a temperature range of 250-1400 °C. The reported values of the diffusion coefficient shows a considerable scatter (Fig. 2.17) and hence in those for the activation energy, which may be related to the diversity in experimental methods. Some of the data have been obtained by radioactive tracer method of ^{18}O, microhardness measurements, vacuum fusion gas extraction methods, secondary ion mass spectrometry depth profiling method [76]. As volume diffusion and grain boundary diffusion occurred simultaneously in polycrystalline, the values of oxygen diffusivity were "effective diffusivity". It has been known that grain boundaries provide high diffusivity (short circuit) paths in metals for a few decades. A schematic of grain boundary diffusion model (Fisher model) and shape of a typical penetration profile of grain boundary diffusion are shown in Fig. 2.18a and b respectively. Katsman [81] estimated oxygen grain boundary

diffusivity to be 10^{-6} cm^2/s by computer simulation in β-NiAl system. In titanium alloy, Vykhodets [82] measured O volume diffusivity in α Ti single crystals in directions parallel ($D_{//}$) and perpendicular ($D_{\perp}$) to the C-axis using nuclear reaction $^{18}O(p, \alpha)^{15}N$ and $^{16}O(d, p_1)^{17}O$. The ratio of the diffusion coefficients $D_{//}/D_{\perp}$ was 0.87±0.01. Besides, Wu et al. [73] explained the near isotropy of oxygen diffusion as transitions occur between the three different interstitial sites with similar absolute rates.

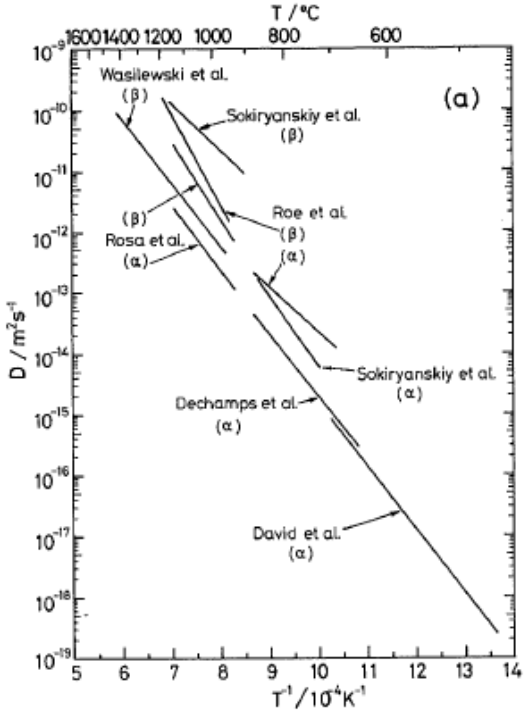

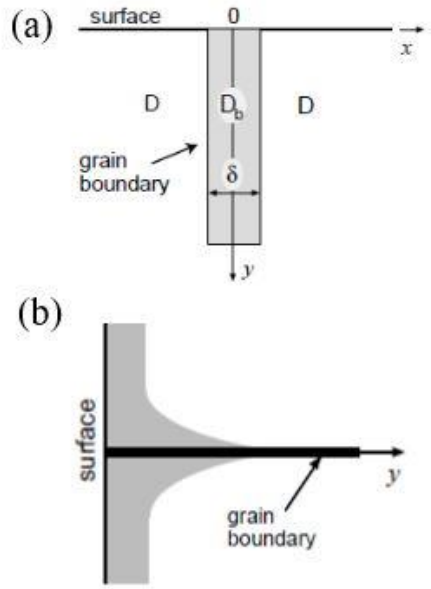

Figure 2.17 (left) Oxygen diffusivity in α and β titanium alloys [76].

Figure 2.18 (right) Schematic of (a) geometry of Fisher model, (b) shape of a typical grain boundary diffusion [83].

2.3.3 Alpha-case formation in titanium alloys

As described previously, the overall oxidation process includes oxide formation on the surface and oxygen diffusion in the substrate metal. The diffusion of O in Ti results in an O-enriched layer, commonly known as α-case layer, which is a hard and brittle layer that significantly reduces several important mechanical properties of titanium alloys. α-case thickness have been mainly evaluated by three methods: (1) optical observation after proper etching, (2) microhardness measurement and (3) direct oxygen concentration measurement. The dissolution of oxygen in Ti increases hardness by solid solution strengthening. The hardness value was almost proportional to oxygen concentration presented in titanium alloys [84-86]. Therefore, many researchers evaluated α-case in Ti alloys by hardness measurement [29,66,84]. Gaddam et. al [29] and Mcreynolds et al. [63]quantitatively compared those three methods and found that microhardness and oxygen concentration measurement(EPMA) gave similar results for alpha-case evaluation while optical measurement underestimated the α-case thickness evaluation. Fig. 2.19 shows oxide and α-case layer for a Ga-containing Ti alloy after exposed at 750 °C for 240 h. After polishing and proper etching, the α-case layer with brighter contrast can be observed as shown in Fig. 2.19a and b. We also evaluated α-case thickness by direct O concentration as shown in Fig. 2.20. Normalized O concentration was applied for α-case thickness evaluation. The O concentration relatively kept consistent as absolute oxygen concentration. The details were given in chapter 5.

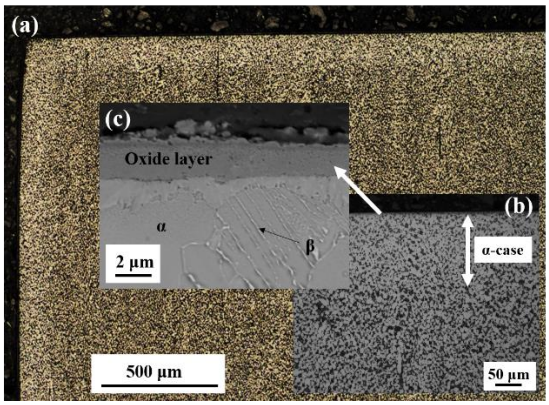

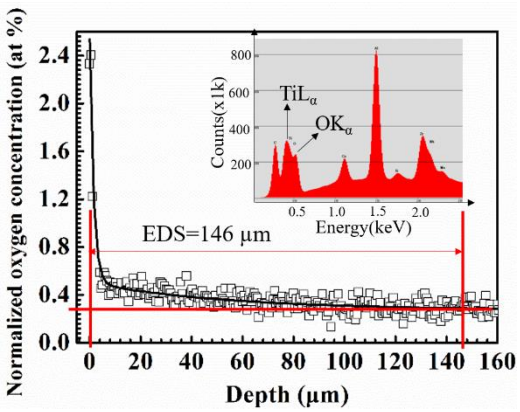

Figure 2.19 (left) Oxide and alpha-case by optical microscopy after etching.

Figure 2.20 (right) Alpha-case thickness determined by EDS.

2.4 Diffusion induced recrystallization (DIR)

In this section, a phenomenon known as diffusion induced recrystallization (DIR) is explained. The fundamentals of DIR and DIR in titanium alloys were discussed.

2.4.1 Fundamentals of DIR

When a crystalline solid comes in contact with solute source, its equilibrium composition changes. Equilibration has been observed to occur in many polycrystalline metals and ceramics through the migration of grain boundaries [87-89]. Compared with conventional recrystallization induced by plastic deformation, recrystallization by alloying has been called diffusion (or chemically) induced recrystallization (DIR or CIR), since it occurs under chemical inequilibrum.

DIR has been widely observed and investigated by many researchers in a variety of systems [87-97]. In previous studies of DIR, the nature and origin of

driving force for DIR and the mechanisms for DIR were proposed as follows: volume-Kirkendall stress [90], tensile stress resulting from the difference in grain boundary diffusivity between solvent and solute atoms [91], misfit dislocation [92, 93], and chemical-free energy arising from the chemical composition difference between parent and DIR grains [94]. It should be noted that each mechanism shown above is still not clear based on the current experiments. Liu et al. [96] investigated recrystallization during oxidation of a Ni-Cu alloy. Fig. 2.21a shows small recrystallized grains formed by oxidation induced recrystallization at a wavy metal/oxide interface after oxidation in air at 600 °C for 5.5 h in a Cu-Ni system. It was suggested that volume change between oxide and metal and diffusion Cu into Ni may have caused recrystallization beneath the metal/oxide interface during oxidation at higher temperatures [96]. A schematic of this process was shown in Fig. 2.21b. Chae et al. [97] elucidated the DIR in TiC system by the transmission electron microscopy as shown in Fig. 2.22. Subgrains were observed as a result of dislocation rearrangement, and the coalescence of subgrains was expected to lead to the generation of boundaries. The dislocations, which acted as a driving force for DIR, was suggested to be created by the diffusion of solute atoms, which resulted in the change of lattice parameters [97].

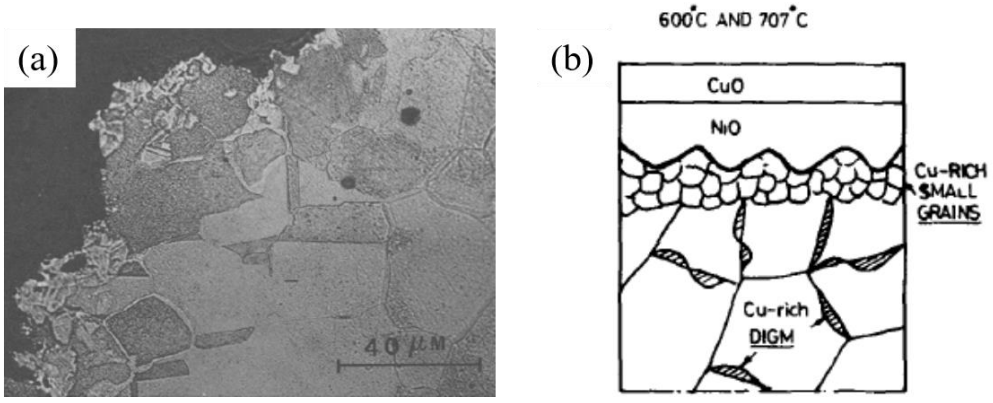

Figure 2.21 (a) Oxidation induced recrystallization (OIR), and (b) schematic representation of small OIR grains during oxidation in Cu-Ni system [96].

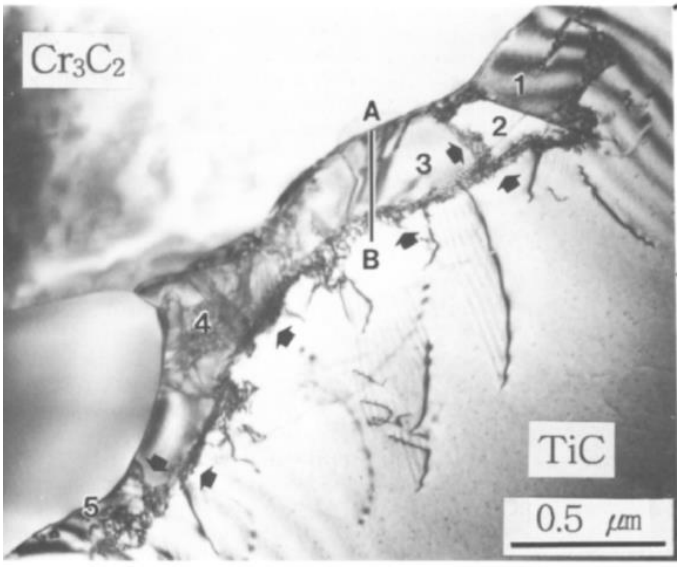

Figure 2.22 TEM micrographs of subgrains and sub-boundaries of dislocation networks in TiC system [97].

2.4.2 DIR in titanium alloys

As discussed before, DIR has been observed in many systems. However, to the author's knowledge, recrystallization at the oxide/metal interface for Ti alloys has not been reported. In my Ga-containing alloy, recrystallization during isothermal oxidation at 750 °C was observed as shown in Fig. 2.23. As Al, and Ga concentration was found to be higher beneath metal/oxide interface, a possible

mechanism for such recrystallization process was proposed and schematically shown in Fig. 2.24. The details will be given in chapter 4 and mechanism will be discussed in chapter 5.

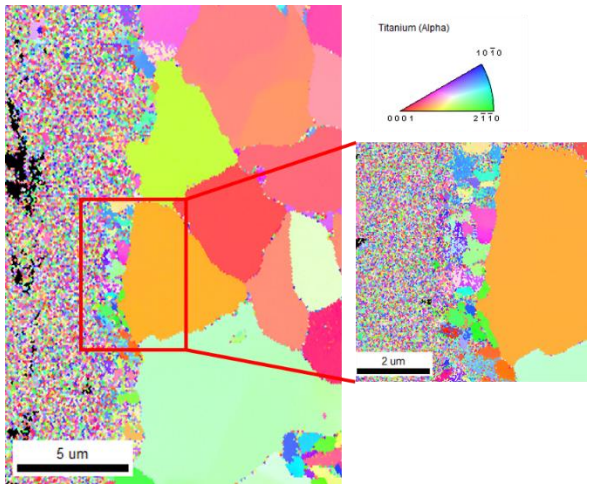

Figure 2.23 Recrystallization area detected by EBSD in a Ga-added Ti alloy [98].

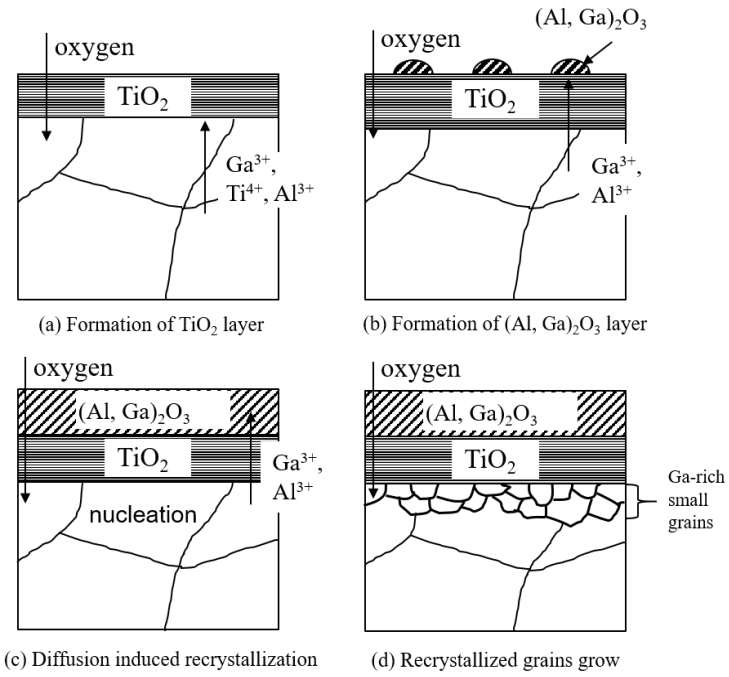

Figure 2.24. Schematic representations of DIR process in a Ga-added Ti alloy [98].

2.5 References

[1] G. Lutjering, and J. C. Williams, Titanium, Berlin: Springer-Verlag, 2007.

[2] C. Leyens, and M. Peters, Titanium and Titanium Alloys, Weinheim: Wiley, 2003.

[3] C. E. Shamblen, and T. K. Redden, Creep resistance and high-temperature metallurgical stability of titanium alloys containing gallium, Metallurgical and Metearials Transactions B, 3 (1972) 1299-1305.

[4] G. Welsch, R. Boyer, and E. W. Collings, Materials properties handbook: titanium alloys, ASM international, 1993.

[5] V. T. Witusiewicz, A. A. Bondar, U. Hecht, S. Rex, and T. Y. Velikanova, The Al-B-Nb-Ti system III - Thermodynamic re-evaluation of the constituent binary system Al-Ti, Journal of Alloys and Compounds, 465 (2008) 64-77.

[6] M. Peters, J. Kumpfert, C. H. Ward and C. Leyens, Titanium alloys for aerospace applications, Advanced Engineering Materials, 5-6 (2003) 419-427.

[7] H. W. Rosenberg, Titanium alloying in theory and practice, in: the Science, Technology and Application of Titanium, (1970) 851-859.

[8] S. Saal, L. Wagner, G. Lutjering, H. Pillhofer, and M. A. Daeubler: Zeitschrift Fur Metallukunde, 90 (1990) 535-539.

[9] D. F. Neal, S. P. Fox, The influence of silicon and silicides on the properties of near-α titanium alloys: in Titanium'92, Science and Technology, F. H. Froes and I. L. Caplan (Eds.), TMS, Warrendale, PA (1993) 287-294.

[10] C. Ramachandra, A. K. Singh, and G. M. K. Sarma, Microstructural characterisation of near-α titanium alloy Ti-6Al-4Sn-4Zr-0.70 Nb-0.50 Mo-0.40 Si, Metallurgical and Materials Transactions A, 24 (1993) 1273-1280.

[11] T. Kitashima, Y. Yamabe-Mitarai, S. Iwasaki, and S. Kuroda, Effects of alloying elements on the tensile and oxidation properties of α and near-α Ti alloys, in: Proceedings of the 13th World Conference on Titanium, Wiley, California, USA, (2015) 479-485.

[12] H. Conrad, Effect of interstitial solutes on the strength and ductility of titanium, Progress in Materials Science, 26 (1981) 138-143.

[13] W. R. Tyson, Strengthening of hcp Zr, Ti and Hf by interstitial solutes–a review, Canadian Metallurgical Quarterly, 6 (1967) 301-332.

[14] G. Welsch, W. Bunk, Deformation modes of the α-phase of Ti-6Al-4V as a function of oxygen concentration and aging temperature, Metallurgical Transactions A, 13 (1982) 889-899.

[15] H. Dong, X. Y. Li, Oxygen boost diffusion for the deep-case hardening of titanium alloys, Materials Science and Engineering A, 280(2000) 303-310.

[16] A. R. Ebrahimi, F. Zarei, and R. A. Khosroshahi, Effect of thermal oxidation process on fatigue behavior of Ti-4Al-2V alloy, Surface and Coatings Technology, 203 (2008) 199-203.

[17] C. Leyens, M. Peters, D. Weinem, and W. A. Kaysser, Influence of long-term annealing on tensile properties and fracture of near-α titanium alloy Ti-6Al-2.75Sn-4Zr-0.4Mo-0.45Si, Metallurgical and Materials Transactions A, 27 (1996) 1709-1717.

[18] W. Jia, W. Zeng, X. Zhang, Y. Zhou, J. Liu, and Q. Wang, Oxidation behavior and effect of oxidation on tensile properties of Ti60 alloy, Journal of Materials Science, 46 (2011) 1351-1358.

[19] Z. Liu, and G. Welsch, Effects of oxygen and heat treatment on the mechanical properties of alpha and beta titanium alloys, Metallurgical Transactions A, 19 (1988) 527-542.

[20] A. Madsen, E. Andrieu, H. Ghonem, Microstructural changes during aging of a near-α titanium alloy, Materials Science and Engineering A, 171 (1993) 191-197.

[21] H. Fukai, H. Iizumi, K. Minakawa, and O. Ouchi, The Effects of the oxygen-enriched surface layer on mechanical properties of α+ β type titanium alloys, ISIJ International, 45 (2005) 133-141.

[22] N. Birks, G. H. Meier, and F. S. Pettit, Introduction to the High Temperature Oxidation of Metals, Cambridge University Press, 2006.

[23] P. Kofstad, High Temperature Corrosion, Elsevier, 1988.

[24] U. R. Evans, The Corrosion and Oxidation of Metals, Edward Arnold, London, 1960.

[25] K. Hauffe, Oxidation of Metals, Plenum, New York, 1966.

[26] A. T. Fromhold, Jr., Theory of Metal Oxidation, vol. I- fundamentals, North-Holland, Amsterdam, 1976.

[27] S. Frangini, and A. Mignone, Various aspects of the air oxidation behaviour of a Ti-6Al-4V alloy at temperatures in the range 600–700 °C, Journal of Materials Science, 29 (1994) 714-720.

[28] H. L. Du, P. K. Datta, D. B. Lewis, and J. S. Burnell-Gray, Air oxidation behaviour of Ti-6Al-4V alloy between 650 and 850 °C, Corrosion Science, 36 (1994) 631-642.

[29] R. Gaddam, B. Sefer, R. Pederson, and M. Antti, Oxidation and alpha-case formation in Ti–6Al–2Sn–4Zr–2Mo alloy, Materials Characterization, 99 (2015) 166-174.

[30] P. Kofstad, Defects and transport properties of metal oxides, Oxidation of Metals, 44 (1995) 3-27.

[31] R. A. Spurr, and H. Myers, Quantitative analysis of anatase-rutile mixtures with an X-ray diffractometer, Analytical Chemistry, 29 (1957) 760-762.

[32] P. Kofstad, High temperature oxidation of titanium, Journal of Less Common Metals, 12 (1967) 339-464.

[33] J. L. Murray, and H. A. Wriedt, in Binary Alloy Phase Diagrams, T. B. Massalski, ed., ASM INTERNATIONAL, Materials Park OH, (1990) 2924-2926.

[34] H. L. Du, P. K. Datta, D. B. Lewis, and J. S. Burnel-Gray, High-temperature corrosion of Ti and Ti-6Al-4V alloy, Oxidation of Metals, 45 (1996) 507-527.

[35] T. J. Johnson, M. H. Loretto, and M. W. Kearns, Oxidation of high temperature titanium alloys, in: Proceedings of the Seventh World Titanium Conference, Warrendale, PA, TMS, (1992) 2035-2042.

[36] A. M. Chaze, G. Beranger, and C. Coddet, A comparison of the influence of Si, Al, and Cr additions on the high temperature oxidation behavior of titanium, in Titanium: Science and Technology, G. Lutjering, U. Zwicker, and W. Bunk, Editors, DGM: Oberursel, (1985) 2665-2672.

[37] A. M. Chaze and C. Coddet, Influence of alloying elements on the dissolution of oxygen in the metallic phase during the oxidation of titanium alloys, Journal of Materials Science, 22 (1987) 1206-1214.

[38] T. J. Johnson, M. H. Loreto, C. M. Younes and M. W. Kearns, A study of the role of alloying additions during the high temperature oxidation of IMI834, in: Second International Conference on the Microscopy of Oxidation, Cambridge, London, England, (1993) 1-10.

[39] A. M. Chaze and C. Coddet, Influence of the nature of alloying elements on the adherence of oxide films formed on titanium alloys, Oxidation of Metals**,** 28 (1987) 61-71.

[40] H. Chuanxi and L. Bingnan, Effects of Nb and W on mechanical properties and oxidation resistance of high temperature titanium alloys, in: Titanium ’92: Science and Technology, Proceedings of the Seventh World Titanium Conference, Warrendale, PA, TMS, (1992) 1891-1899.

[41] A. M. Chaze, C. Coddet, and G. Beranger, Dissolution of oxygen in the metallic phase during high temperature oxidation of titanium and some alloys, in : Sixth World Conference on Titanium IV, (1988) 1765-1770.

[42] S. Z. Zhang, B. Zhou, N. Liu, and L. Q. Chen, Effects of Microstructure and Rare-Earth Constituent on the Oxidation Behavior of Ti–5.6 Al–4.8 Sn–2Zr–1Mo–0.35 Si–0.7 Nd Titanium Alloy, Oxidation of Metals, 81 (2014) 373-382.

[43] T. Kitashima, Y. Yamabe-Mitarai, S. Iwasaki, and S. Kuroda, Effects of Ga and Sn Additions on the Creep Strength and Oxidation Resistance of Near-α Ti Alloys, Metallurgical and Material Transactions A, 47 (2016) 6394-6403.

[44] T. Kitashima and T. Kawamura, Prediction of oxidation behavior of near-α titanium alloys, Scripta Materialia, 124 (2016) 56-58.

[45] S. Becker, A. Rahmel, M. Schorr, and M. Schutze, Mechanism of isothermal oxidation of the intel-metallic TiAl and of TiAl alloys, Oxidation of Metals, 38 (1992) 425-464.

[46] Y. Shida and H. Anada, The influence of ternary element addition on the oxidation behaviour of TiAl intermetallic compound in high temperature air, Corrosion Science, 35 (1993) 945-953.

[47] Y. Shida and H. Anada, Oxidation behavior of binary Ti–Al alloys in high temperature air environment, Materials Transactions, 34 (1993) 236-242.

[48] M. Yoshihara and Y. W. Kim, Oxidation behavior of gamma alloys designed for high temperature applications, Intermetallics, 13 (2005) 952-958.

[49] M. Yoshihara and K. Miura, Effects of Nb addition on oxidation behavior of TiAl, Intermetallics, 3 (1995) 357-363.

[50] S. Taniguchi and T. Shibata, Influence of additional elements on the oxidation behaviour of TiAl, Intermetallics, 4 (1996) S85-S93.

[51] C. Z. Wagner, Electrochemistry, Reaction Types in the Oxidation of Alloys, 63 (1959) 772-782.

[52] H. L. Gegel, and S. Fujishiro, Titanium Science, Technology and Application of Titanium, R. I. Jaffee and H. M. Burte, Ed., PlenumPress, NY, (1973) 2179-2194.

[53] P. Kofstad, K. Hanffe, and H. Kjollesdal, Investigation on the oxidation mechanism of titanium, Acta Chemical Scandinavica, 12 (1958) 239-266.

[54] E. A. Gulbransen, and K. F. Andrew, Kinetics of the reactions of titanium with O_2, N_2, and H_2, Journal of metals transactions, 185 (1949) 741-748.

[55] J. W. Hickman, E. A. Gulbransen, Oxide films formed on titanium, zirconium, and their alloys with nickel, copper, and cobalt, Analytical Chemistry, 20 (1948) 158-165.

[56] M. H. Davies, and C. E. Birchenall, Oxidation of titanium, Journal of Metals, 3 (1951) 877-880.

[57] J. T. Waber, On the Cubic Law of Oxidation, The Journal of Chemical Physics, 20 (1952) 734-735.

[58] E. Gemelli, and N. H. A. Camargo, Oxidation kinetics of commercially pure titanium, Revista Materia, 12 (2007) 525-531.

[59] N. Carera, N. F. Mott, Theory of the oxidation of metals, Reports on Progress in Physics, 12 (1949) 163-184.

[60] U. R. Evans, The oxidation of metals, Reviews of Pure and Applied Chemistry, 5 (1955) 1-20.

[61] H. Guleryuz, and H. Cimenoglu, Oxidation of Ti–6Al–4V alloy, Journal of Alloys and Compounds, 472 (2009) 241-246.

[62] D. Poquillon, C. Armand, and J. Huez, Oxidation and oxygen diffusion in Ti–6Al–4V alloy: improving measurements during sims analysis by rotating the sample, Oxidation of Metals, 79 (2013) 249-259.

[63] K. S. Mcreynolds, and S. Tamirisakandala, A study on alpha-case depth in Ti-6Al-2Sn-4Zr-2Mo, Metallurgical and Materials Transaction A, 42 (2011) 1732 -1736.

[64] R. N. Shenoy, J. Unnam, and R. K. Clark, Oxidation and embrittlement of Ti-6Al-2Sn-4Zr-2Mo alloy, Oxidation of Metals, 26 (1986) 105-124.

[65] C. Leyens, M. Peters, and W. A Kaysser, Oxidation behavior of near-α titanium alloys and their protection by coatings, in the Titanium ’95: Science and Technology, Proceedings of the 8th World Conference on Titanium, London: Institute of Materials, Birmingham, England, (1996) 1935-1942.

[66] T. Kitashima, Y. Yamabe-Mitarai, S. Iwasaki, and S. Kuroda, Effects of Ga and Sn additions on the creep strength and oxidation resistance of near-α Ti alloys, Metallurgical and Materials Transactions A, 47 (2016) 6394-6403.

[67] R. W. Evans, R. J. Hull, and B. Wilshire, The effects of alpha-case formation on the creep fracture properties of the high-temperature titanium alloy IMI834, Journal of materials processing technology, 56 (1996) 492-501.

[68] P. Shewmon, Diffusion in solids, Warrendale, Paris, Minnerals, Metals and Materials Society, 2nd Ed., 1989.

[69] C. Wagner, Diffusion in Solids, Liquids, Gases, W. Jost, Ed. Academic Press, New York, 1952.

[70] W. D. Callister, Materials Science and Engineering – an Introduction, Wiley, New York, 2007.

[71] J. Crank, The Mathematics of Diffusion, Oxford Clarendon Press, 2nd Ed., 1979.

[72] V. B. Vykhodets, T. Y. Kurennyk, The mechanism of oxygen jumps during diffusion in alpha-Ti, Physics of Metals and Metallography, 78 (1994) 325-329.

[73] H. H. Wu, and D. R. Trinkle, Direct diffusion through interpenetrating networks: oxygen in titanium, Physical review Letters, 107 (2011) 045504(1)-045504(4).

[74] D. David, G. Beranger, A Study of the Diffusion of Oxygen in α-Titanium Oxidized in the Temperature Range 460°–700° C, Journal of the Electrochemical Society, 130 (1983) 1423-1426.

[75] V. B. Vykhodeets, S. M. Klotsman, T. Ye. Kurennykh, A. D. Levin, V. A. Pavlov, Diffusion of oxygen in α-Ti (V. Temperature dependence coefficients of oxygen diffusion), The Physics of Metals and Metallography, 68 (1989) 94-97.

[76] Z. Liu, and G. Welsch, Literature survey on diffusivities of oxygen, aluminum, and vanadium in alpha titanium, beta titanium, and in rutile, Metallurgical transactions A, 19 (1988) 1121-1125.

[77] M. H. Song, S. M. Han, D. J. Min, G. S. Choi, and J. H. Park, Diffusion of oxygen in β-titanium, Scripta Materialia, 59 (2008) 623-626.

[78] H. Nakajima, and M. Koiwa, Diffusion in titanium, ISIJ International, 31 (1991) 757-766.

[79] F. L. Bregolin, M. Behar, and F. Dyment, Diffusion study of ^{18}O implanted into α-Ti using the nuclear resonance technique, Applied Physics A: Materials Science and Processing, 86 (2007) 481-484.

[80] V. B. Vykhodets, T. E. Kurennykh, A. S. Lakhtin, and A. Ya. Fishman, Diffusion of light elements in BCC, FCC and HCP metals, Solid State Phenomena, 138 (2008) 119-132.

[81] A. Katsman, H. J. Grabke, and L. Levin, Penetration of oxygen along grain boundaries during oxidation of alloys and intermetallics, Oxidation of Metals, 46 (1996) 313-331.

[82] V. B. Vykhodets, S. M. Klotsman , T. Ye. Kurennykh , L. D. Kurmayeva et al., A. D. Levin, V. A. Pavlov, M. A. Plekhanov, L.V. Smirnov, Oxygen diffusion in α-Ti (I. Anisotropy), The Physics of Metals and Metallography, 63 (1987) 127-133.

[83] C. Herzig, and Y. Mishin, Grain boundary diffusion in metals, in: Diffusion in Condensed Matter, J. Karger, P. Heitjans, and R. Haberlandt, eds. Braunschweg, Vieweg, (1998) 337-366.

[84] W. R. Tyson, Solution hardening of titanium by oxygen, Scripta Materialia, 12 (1969) 917-921.

[85] C. J. Rosa, Oxygen diffusion in alpha and beta titanium in the temperature range of 932 to 1142 °C, Metallurgical and Materials Transactions A, 1 (1970) 2517-2522.

[86] F. M. Guclu, H. Cimenoglu, and E. S. Kayali, The recrystallization and thermal oxidation behaviour of CP-titanium, Materials Science Engineering C, 26 (2006) 1367-1372.

[87] A. H. King, Diffusion induced grain boundary migration, International Materials Reviews, 32 (1987) 173-189.

[88] D. Y. Yoon, Theories and observations of chemically induced interface migration, International Materials Reviews, 40 (1995) 149-179.

[89] D. Liu, W. A. Miller, and K. T. Aust, Diffusion induced grain boundary migration in Ni-Cu Diffusion couples, Acta Metallurgica, 37 (1989) 3367-3378.

[90] V. Y. Doo, and R. W. Balluffi, Structural changes in single crystal copper-alpha brass diffusion couples, Acta Metallurgica, 6 (1958) 428-438.

[91] T. A. Parthasarathy, and P. G. Shewmon, Vapor transport and DIGM in the Ni-Fe system, Metallurgical Transactions A, 14 (1983) 2560-2563.

[92] J. W. Matthews, and J. L. Crawford, Formation of grain boundaries during diffusion between single crystal films of gold and palladium, Philosophical Magazine, 11 (1965) 977-991.

[93] J. W. Matthews, and W. A. Jesser, Formation of grain boundaries during diffusion between single-crystal films, Journal of Vacuum Science and Technology, 6 (1969) 641-644.

[94] E. T. Mittemeijer, and A. M. Beers, Recrystallization and interdiffusion in thin bimetallic films, Thin Solid Films, 65 (1980) 125-135.

[95] Y. K. Paek, H. Y. Lee, and S. J. L. Kang, Diffusion induced recrystallization in alumina, Journal of the European Ceramic Society, 24 (2004) 613-618.

[96] D. Liu, W. A. Miller, and K. T. Aust, Diffusion induced grain boundary migration and recrystallization during oxidation of a Ni-48.5 Pet Cu alloy, Metallurgical and Materials Transactions A, 19 (1988) 1667-1675.

[97] K. W. Chae, C. S. Hwang, D. Y. Kim, and S. J. Cho, Diffusion induced recrystallization of TiC, Acta Materialia, 44 (1996) 1793-1799.

[98] Y. Yang, T. Kitashima, T. Hara, Y. Hara, Y. Yamabe-Mitarai, M. Hagiwara, and S. Iwasaki, Effects of Ga, Sn addition and microstructure on oxidation behavior of near-α Ti alloy, Oxidation of Metals, (2017). doi:10.1007/s11085-017-9741-5.

Chapter 3 Materials and experimental procedures

In this chapter, the basic information of investigated alloys, the examining methods for sample observations, and the experimental techniques are described.

3.1 Materials

The materials in this thesis are TKT39, TKT41, unalloyed Ti, Ti-4Al, Ti-8Al and Ti-8Ga. TKT-series Ti alloys are developed in NIMS. The nominal chemical compositions of TKT39, TKT41 in wt. %, the equivalent Al values, and β transus temperatures are shown in Table 3.1. The equivalent Al values of alloy TKT39 and TKT41 are calculated based on: $[Al]_{eq}$= [Al]+1/6[Zr]+1/2[Ga]+1/3[Sn]+10[O] as discussed in session 2.1.2. Table 3.2 shows the chemical composition of the rest alloys.

Table 3.1 Chemical composition in wt. % for TKT39 and TKT41.

Alloy	Ti	Al	Sn	Ga	Zr	Nb	Mo	Si	O	Al Eq.	T_β /°C
TKT39	80.3	7	4.5	-	6	1	1	0.2	0.053	10.0	985±5
TKT41	81.8	7	-	3	6	1	1	0.2	0.093	10.4	995±5

Table 3.2 Chemical compostion in wt. % for unalloyed Ti, Ti-4Al, Ti-8Al and Ti-8Ga.

Alloy	Ti	Al	Ga
Unalloyed Ti	100.0	-	-
Ti-4Al	97.7	2.3	-
Ti-8Al	95.0	5.0	-
Ti-8Ga	88.8	-	11.2

The materials in this thesis are all prepared by a cold crucible levitation melting method. Each ingot was double-melted to enhance the compositional

homogeneity. After forging and grooving-rolled as shown in Fig. 3.1a and 3.1b, proper heat treatment was carried out to obtain specific microstructures.

A procedure consisting of three steps was used to evaluate oxidation behaviors, i.e., preparation of tested samples after thermomechanical treatment, oxidation test, and finally evaluation and observation processes.

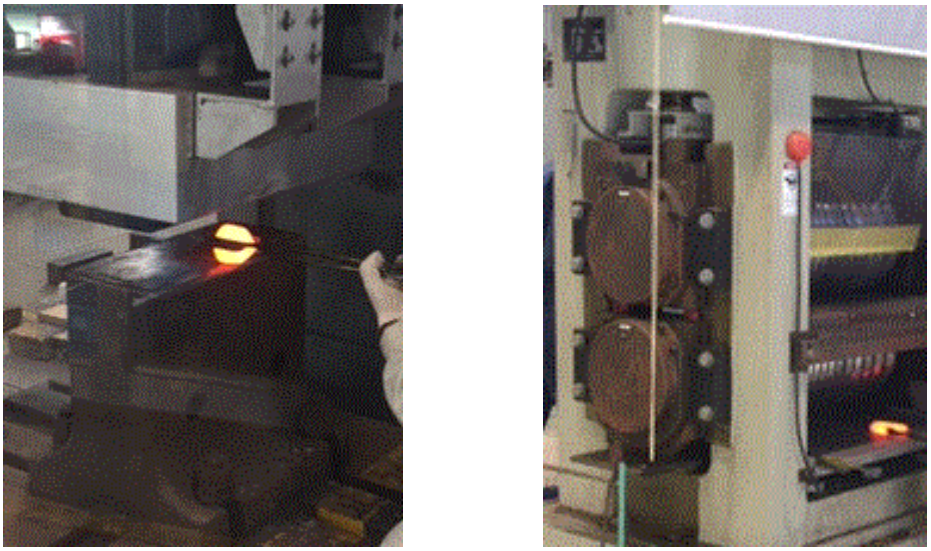

(a) Forging **(b) Rolling**

Figure 3.1 (a) forging (b) rolling.

In first step, the samples were cut into cylindrical shape with a diameter of 8 mm and a height of 4 mm as shown in Fig. 3.2 by wire electrical discharge machining. After cutting, the samples were manually polished using #800 SiC papers, followed by ultrasonic cleaning in acetone for 10 mins. In second step, oxidation tests were carried out in an electric furnace in air at atmosphere pressure. Test samples were placed into Al_2O_3 crucibles in a vertical position and introduced into the furnaces. A thermal-couple was placed inside the furnace close to samples to follow a test temperature during isothermal oxidation process.

Before isothermal oxidation, the furnace was kept for more than 24 h to maintain at a steady state. Isothermal oxidation tests were carried out at 650, 700, 750 °C. Additionally, all samples were scaled using analytical microbalance with an accuracy of ±0.0001 g after 20, 45, 70, 90, 110, 240, 340, and 500 h exposure.

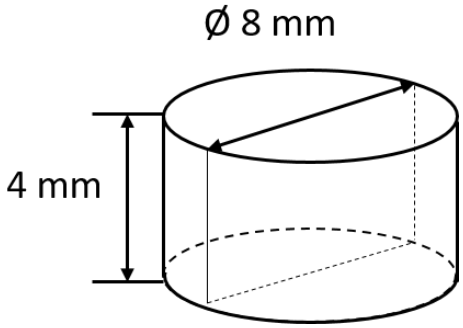

Figure 3.2 Geometry of tested samples.

After different exposure time at each tested temperatures, sample were prepared to determine the α-case thickness, oxide thickness and also the time dependent recrystallization. To avoid oxide layer spallation due to mechanical cutting, all tested samples were put perpendicular to the face placed on the crucible and mounted. After mounting, the sample with a thickness of 4 mm were cut to observe the half surface as shown in Fig. 3.2. The samples were mounted using a STRUERS CitoPress-10 mounting machine. After mounting, samples were polished to ~0.06 μm with colloidal silica using a BUEHLER polishing machine followed by cleaning in steam water with a VS-D100 ultrasonic cleaning machine.

3.2 Experimental techniques

In this section the experimental techniques used to investigate the oxide scale, α-case layer and recrystallization are described.

Hardness measurement

O content in Ti almost is proportional to hardness in Ti and can be estimated by microhardness measurements. As oxygen concentration decreases along diffusion direction from surface and tends to be steady, hardness also decreases from surface and tends to be constant accordingly. Thus, α-case thickness were measured based on the hardness values. In the current work, two methods were conducted out for α-case thickness measurement: hardness and EDS for direct oxygen concentration measurement. The hardness measurement was performed by the MMT-7 Matsuzawa Vickers Microhardness Tester with a load of 10 g during 15 s.

X-ray Diffraction

X-ray diffraction (XRD) is a technique used to determine the molecular and atomic structure of a crystal. To determine the composition of oxides formed on the surface of different alloys under different conditions, an XRD on a RINT2500 X-ray diffractometer using Cu Kα radiation, operated at 50 kV and 300 mA was applied. The scans were performed with 0.02 ° step size in the 2-theta range of 20°- 80°.

Scanning Electron Microscope

The scanning electron microscope is widely used for observation and analysis of oxide layer morphology. Oxide layer, alpha-case layer and recrystallization layer were all evaluated using field-emission-gun scanning electron microscopy (SEM, ZEISS Auriga) at accelerating voltages of 2kV, 5 kV and 15 kV. The micrographs were obtained using secondary electrons (SE) and back scattered electrons (BSE) mode.

Energy-dispersive X-ray Spectroscopy

Chemical analyses were performed using energy-dispersive X-ray spectroscopy (EDS) attached to the SEM equipment at an accelerating voltage of 15 kV with the detector AMETEK Octane Super 60 mm^2. By comparing the results of α-case thickness measured by EDS and hardness, EDS results were selected as alpha-case thickness values for all samples due to the direct results of oxygen concentration and it reliability and accuracy.

Transition Electron Microscope

The JEM-2100 is a multipurpose, 200 kV field emission analytical electron microscope. The FE electron gun (FEG) produces highly stable and bright electron probe. TEM was mainly used in the current work to detect the formation, the size and distribution of α_2 phase in two alloys and also to observe the recrystallization areas at higher magnification with enough resolution.

Chapter 4 Effect of alloying elements on oxidation behaviour

4.1 Abstract

We investigated the effects of adding Ga or Sn, with almost the same Al equivalent, on the oxidation behaviors of near-α Ti alloy with the bimodal structure and lamellar structure. The replacement of Sn with Ga decreased the weight gain of the oxidation sample during oxidation, suppressed oxide growth, and improved adherence between the oxide and substrate. The lamellar structure showed a lower weight gain of the oxidation sample compared to the bimodal structure in both alloys. Unlike conventional near-α Ti alloys, recrystallization occurred near the oxide/substrate interface in Ga-added alloy, which may contribute to the release of stress, improvement of the adherence between the oxide and substrate, and prevention of the spallation of oxides in the Ga-added alloy. A possible mechanism for the recrystallization in the Ga-added alloy was also discussed.

4.2 Introduction

The reduction of aircraft weight and enhancement of gas-turbine working temperature are two important aspects of future aircraft engine development, as they could contribute to kerosene savings due to the improvement of jet-engine working efficiency [1, 2]. Near-α Ti alloys are attractive structural materials with a high strength-to-density ratio and excellent corrosion resistance, and they have been applied to jet-engine components operating at high temperature [3].

However, when exposed to gaseous environments containing oxygen, especially at elevated temperatures, the mechanical properties of Ti alloy components degrade, limiting the high-temperature capability during service and hindering commercial application. The interaction of Ti alloys with oxygen not only results in the oxygen embrittlement of the substrate surface of the components due to the high solubility of oxygen [4-7], but also causes a loss of ductile metallic material due to the formation of oxides on the surface [8, 9]. The oxidation behavior of Ti alloys is strongly affected by alloying additions, microstructure, and the oxidizing environment [10].

Many researchers have examined the influence of certain elements on the oxidation behavior of Ti-based alloys [8, 11-21]. Chaze et al. [11, 12, 14, 16] found that Al and Si caused a significant reduction in the amount of oxygen dissolved in the metallic phase during oxidation, whereas the effect of Cr was negligible. They also found that low amounts of Al and Si slightly decreased the adherence of the oxide layer to the metal substrate, while high amounts of Al and Si increased it; furthermore, Cr improved the adherence of the oxide layer. Johnson et al. [8, 13] and Chuanxi and Bingnan [15] found that the addition of Nb and W improved surface stability and suppressed oxide-scale formation, while the addition of V enhanced oxide-scale formation. Kitashima et al. [19, 20, 21] systematically investigated the oxidation behavior of near-α Ti alloys with the addition of a variety of elements and found that Sn and Ge segregate at the

oxide/substrate interface while Mo, Nb, W, Ga, Zr, and Hf dissolve in the internal TiO_2 scale without segregating at the oxide/substrate interface. The authors also demonstrated the role of each element by regression analysis and found a good correlation with alloy compositions, where the squared multiple correlation coefficient was 0.93 [21]. The oxidation behavior of α-Ti alloys and α-β Ti alloys is mainly dominated by the TiO_2 kinetics because the amount of Al is not sufficient to form a continuous Al_2O_3 layer [22].

There have also been reports on the effect of alloying elements on the formation of TiO_2 and Al_2O_3 in TiAl-based intermetallics [23-28]. Yoshihara et al. [25, 26] systematically investigated the effects of Nb addition on the oxidation behavior of TiAl and found that Nb remarkably suppressed TiO_2 growth. Taniguchi and Shibata [27] found that a relatively low addition of Zr or Hf resulted in the formation of highly protective alumina scales. Some mechanisms have been previously discussed as follows: (1) The valence-control rule: additional elements that can decrease the oxygen vacancies in TiO_2 effectively decrease the overall oxidation rate such as Nb [26]; (2) The formation of a barrier layer: a discrete layer aggregates in the scale near the oxide/substrate interface, working as a barrier to some extent for Si [23]; (3) Wagner's scaling model: internal oxidation changes to external oxidation to form a continuous alumina layer [28].

It should be noted that the oxidation behavior is also affected by the microstructure morphology [29-31]. Perez [29], Pitt and Ramulu [30], and Yang et al. [31] investigated the effects of grain size on the oxidation behavior of Ti alloys and pure Ti by both experiment and simulation and suggested that a higher grain size resulted in a lower weight gain of both Ti alloys and pure Ti during oxidation, mainly because of the lower grain boundary/grain ratio. Tiley et al. [32] demonstrated that the lath orientations in Ti-6242S affected oxygen diffusivity, in turn affecting the depth of oxygen ingress in this alloy. Leyens et al. [33, 34] investigated the effects of microstructures of IMI834 and TIMETAL1100 on the oxidation behavior and showed that, in both alloys, the fully lamellar structure gained less weight than the bimodal structure, which may mainly be due to the relatively lower grain boundary/grain ratio as explained by the authors. Zhang et al. [17] also reported similar results for the bimodal and fully lamellar microstructure, and the reason for its phenomenon was suggested to be the fact that the primary α phase in the bimodal structure promoted the fast growth of TiO_2. However, there have been few reports on the combined effects of alloying elements and microstructure on the oxidation behavior of Ti alloys.

α-stabilizing elements, Al, Ga, and Sn, promote high-temperature strength in Ti alloys by solid solution strengthening [35]. In addition, the addition of these elements promotes the precipitation of the α_2 phase with the D019 structure, which results in dispersion strengthening and low ductility [35]. The Al

equivalence, which is calculated as Al+1/2×Ga+1/3×Sn+1/6×Zr+10×O in wt% [21], has been used to evaluate ductility after creep exposure. To avoid embrittlement, the Al equivalences of previous near-α Ti alloys have been set to be lower than 9. Sn, which is conventionally added in near-α Ti alloys, accelerates the oxide growth of TiO_2 and causes the spallation of oxides [19, 20, 36], while added Ga was found to dissolve in the oxide scale without segregation at the oxide/substrate interface in near-α Ti alloys [20]. Therefore, the replacement of Sn with Ga may be effective to design a new oxidation-resistant alloy. In this study, the oxidation behaviors of two near-α Ti alloys containing Ga or Sn with the same Al equivalence were investigated, and the effect of microstructure in both alloys was examined.

4.3 Experimental procedures

Near-α Ti alloy ingots TKT39 with added Sn and TKT41 with added Ga were produced by the cold crucible levitation melting method. The nominal chemical composition of the ingots is listed in Table 4.1. The Al-equivalence values, calculated as Al+1/2×Ga+1/3×Sn+1/6×Zr+10×O in wt% [21], were designed to be 9.5 for both TKT39 (Sn) and TKT41 (Ga). Each ingot was double-melted to enhance the compositional homogeneity. The cast ingots were β-forged at 1130 °C and then groove-rolled to 50% reduction at 980 °C in the α+β region to form square rods with sides of 14 mm. The β transus temperatures for TKT39 (Sn) and TKT41 (Ga) were 985±5 °C and 995±5°C, respectively, as determined

through microstructure observations after heat treatment at different temperatures. To obtain two different microstructures for each alloy, TKT39 (Sn) was heat treated at two different temperatures, 965°C (bimodal) or 1005°C (fully lamellar), for 1 h, followed by air cooling, and TKT41 (Ga) was heat treated at 970°C (bimodal) or 1010°C (fully lamellar) for 1 h, followed by air cooling. Subsequently, both alloys were aged at 700°C for 2 h and air cooled.

Table 4.1. Chemical compositions (wt. %), Al equivalence values, and β transus temperatures in TKT39 (Sn) and TKT41 (Ga).

Alloy	Ti	Al	Sn	Ga	Zr	Nb	Mo	Si	O	Al Eq.	T_β /°C
TKT39	80.3	7	4.5	-	6	1	1	0.2	0.053	10.0	985±5
TKT41	81.8	7	-	3	6	1	1	0.2	0.093	10.4	995±5

Cylindrical samples for oxidation tests were cut from the center of as-aged samples with a diameter of 8 mm and a height of 4 mm by wire electrical discharge machining. The surfaces of the specimens were finally polished using #800 SiC papers, followed by ultrasonic cleaning in acetone. Isothermal oxidation tests were performed at 750°C in laboratory air. Each sample was placed in an alumina crucible, and the weight change was measured together with the weight of the crucible; therefore, spalled oxides scattered in the crucible were considered in the weight measurement. The samples in alumina crucibles were removed from the furnace after 20, 45, 70, 90, 110, 140, 240, 340, and 500 h of exposure. The mass change of each sample was measured using a microbalance with an accuracy of ±0.0001 g.

Microstructural characterizations of aged samples were performed using field-emission-gun scanning electron microscopy (SEM, ZEISS Auriga) at accelerating voltages of 5 kV and 15 kV. Samples for SEM observation were embedded in resin and polished using polishing papers and SiO_2. The volume fraction of the primary α-phase was determined using the software ImageJ.

After the oxidation test, the constituent oxide phases were identified by X-ray diffraction (XRD) on a RINT2500 X-ray diffractometer using Cu Kα radiation, operated at 50 kV and 300 mA. Before microstructural characterization, the oxidized samples were cold mounted, cut, and metallographically polished by polishing papers and SiO_2. The cross-sectional microstructures of the oxidized samples were analyzed by SEM and electron backscatter diffraction (EBSD) attached to the SEM equipment at an accelerating voltage of 15 kV with the detector Ametek Digiview 5. Chemical analyses were performed using energy-dispersive X-ray spectroscopy (EDS) attached to the SEM equipment at an accelerating voltage of 15 kV with the detector Ametek Octane Super 60 mm^2.

The specimens for transmission electron microscope (TEM) observation were prepared by electrolytic polishing of thin discs of 3 mm in diameter, punched from thin sections of ~50 μm thickness. Electrochemical polishing was carried out in an electrolyte containing 6% perchloric acid, 35% n-butyl alcohol and 59% methanol at 20 V, using a twin jet polisher. The temperature of the electrolyte was maintained at -20 °C, using liquid nitrogen, throughout the

process of electrochemical thinning. The samples were observed by TEM of JEOL-2100 with an accelerating voltage of 200 kV.

4.4 Results and discussion

The microstructure of as-heat-treated TKT39 (Sn) was bimodal with an equiaxed fine-grained primary α phase because the solution heat treatment at 965°C is close to the β transus temperature (Fig. 4.1a). Solution heat treatment at 1005°C, which is higher than the β transus temperature, produced a fully lamellar microstructure (Fig. 4.1b). The microstructure of TKT41 (Ga) was bimodal after solution heat treatment at 970°C (Fig. 4.1c) and fully lamellar (Fig. 4.1d) after a solution heat treatment at 1010°C. The volume fractions of the primary α-phase in bimodal TKT39 (Sn) and bimodal TKT41 (Ga) were 66.1% and 62.9%, respectively. The replacement of Sn with Ga increased the β transus temperature from 985±5 °C to 995±5 °C. Silicide precipitates can be observed as bright spots in Fig. 4.1a and 4.1c.

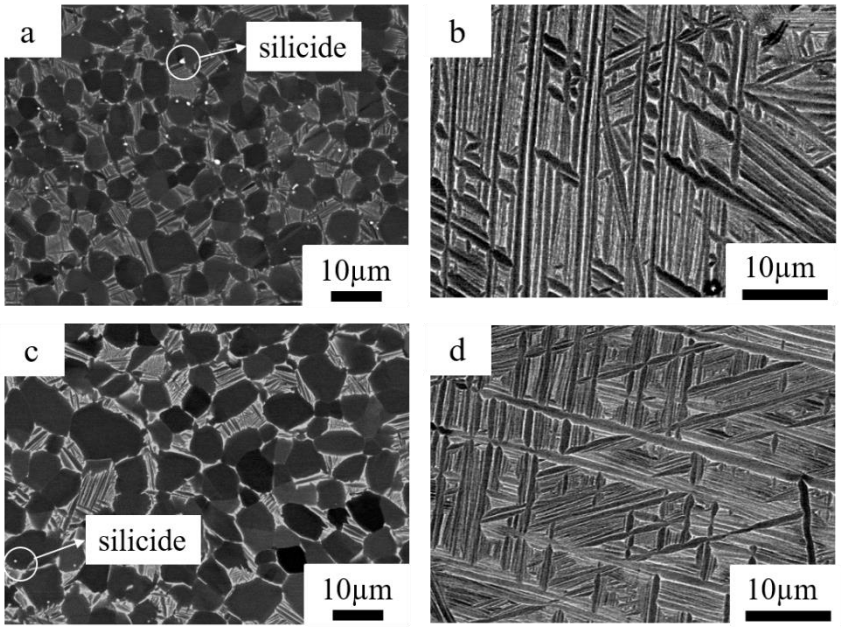

Figure 4.1. Backscattered electron images of heat-treated alloys: (a) TKT39 (Sn)-bimodal, (b) TKT39 (Sn)-lamellar, (c) TKT41 (Ga)-bimodal, and (d) TKT41 (Ga)-lamellar.

As described before, the addition of alloying elements affected the precipitation of α_2 phase, it is necessary to check whether α_2 phase exist or not in our designed alloys. Fig. 4.2 shows the bright field TEM microstructure, electron diffraction pattern and dark field TEM micrograph using super-lattice reflection of as heat-treated TKT39(Sn) alloy and TKT41(Ga) alloy. As shown in Fig. 4.2, clear α_2 super-lattice reflections in selected area diffraction pattern together with the fundamental α reflections were observed in both alloys. The dark filed images using super-lattice reflection from α_2 phase, as indicated by small white circle shown in middle image of Fig. 4.2, indicated the uniform precipitation of α_2 phase in both alloys. The size of α_2 precipitation was around 10 nm.

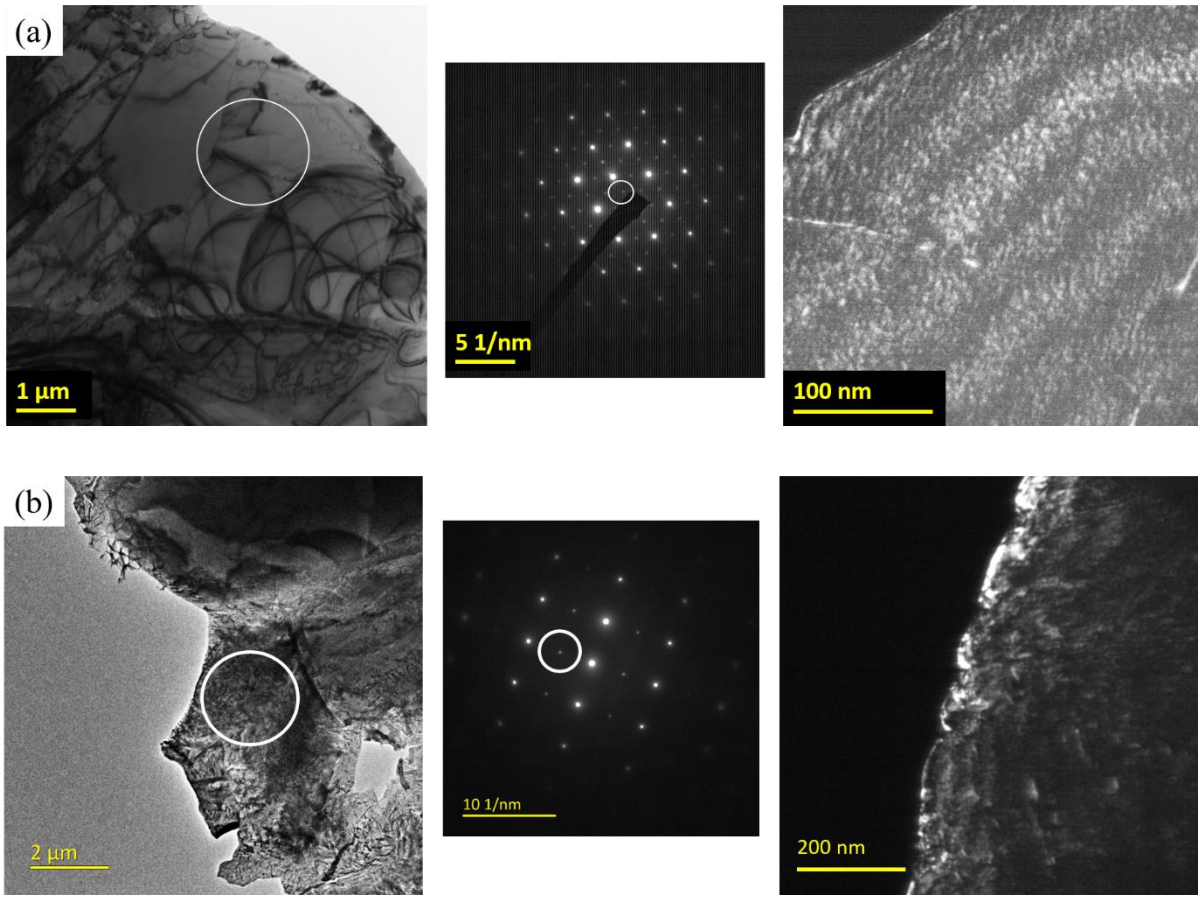

Figure 4.2. Bright field TEM microstructures (left image) and electron diffraction patterns (middle image) taken from white circled region (left image) and dark field images (right image) using α2 super-lattice reflection highlighted in white circle of middle image for (a) TKT39-Sn alloy with beam direction on[0001] and (b) TKT41-Ga alloy with beam direction on [01$\bar{1}$0], respectively.

Fig. 4.3 shows the weight gain of a sample per unit area for TKT39 (Sn) and TKT41 (Ga) alloys with bimodal and fully lamellar microstructures oxidized in laboratory air for up to 500 h at 750 °C. The overall weight gains of TKT39 (Sn)-bimodal, TKT39 (Sn)-lamellar, TKT41 (Ga)-bimodal, and TKT41 (Ga)-lamellar were 5.55, 4.78, 1.92, and 1.72 mg/cm^2, respectively, after oxidation for 500 h at 750 °C. The weight gain of TKT39 (Sn) was considerably greater than that of TKT41 (Ga) in both bimodal and fully lamellar microstructures, and the weight-gain difference between these two alloys increased with increase in

exposure time. The weight gain during isothermal oxidation is due to oxide formation and oxygen dissolution, which depend on the alloy composition and microstructure [8, 34]. In both alloys, the bimodal structure gained more weight than the fully lamellar structure, which is consistent with previous studies [16, 33, 34]. In addition, the TKT41 (Ga) alloy with bimodal structure showed significantly lower weight gain (1.92 mg/cm^2) compared to the TKT39 (Sn) alloy (4.78 mg/cm^2) with fully lamellar microstructure, which indicated that Ga plays a more important role in oxidation behavior than microstructure in this study. The spallation of oxides on the surface of TKT39 (Sn) with both microstructures was observed after the oxidation test, as shown in Fig. 4.4a and 4.4b. The replacement of Sn with Ga clearly suppressed the spallation of oxides, as shown in Fig. 4.4c and 4.4d.

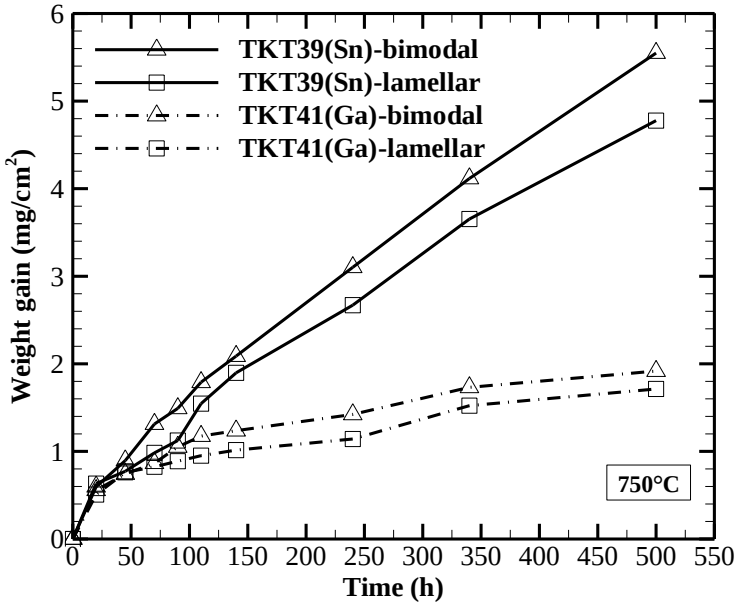

Figure 4.3. Weight gains for specimens of TKT39 (Sn) and TKT41 (Ga) with bimodal and lamellar structures oxidized at 750°C for up to 500 h.

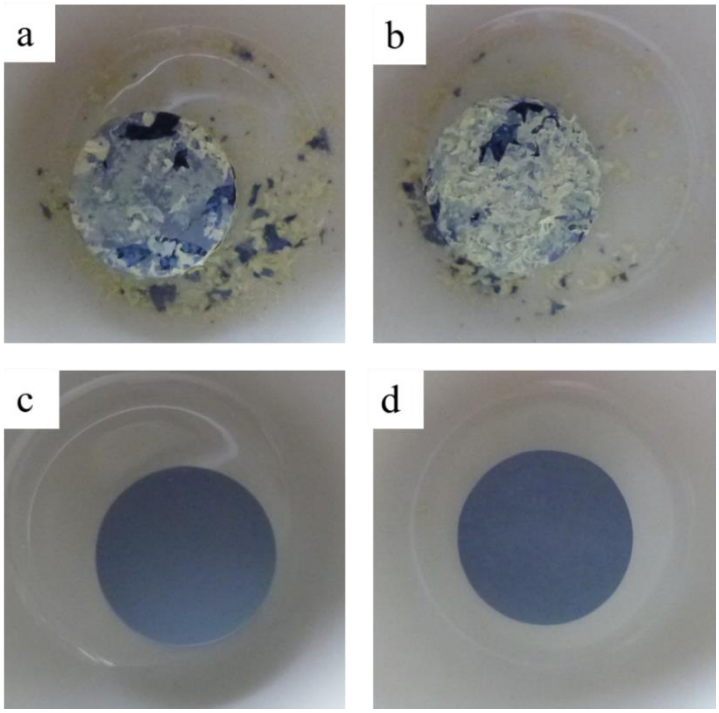

Figure 4.4. Surfaces of (a) TKT39 (Sn)-bimodal, (b) TKT39 (Sn)-lamellar, (c) TKT41 (Ga)-bimodal and (d) TKT41 (Ga)-lamellar in crucibles after oxidation at 750°C for 500 h.

The surfaces of oxidized specimens were analyzed by XRD. Three different phases were distinguished after the oxidation of TKT39 (Sn), and four different phases were distinguished in TKT41 (Ga), as shown in Fig. 4.5. The main oxide phases were TiO_2 (rutile) and α-Al_2O_3 for both alloys. Reflections of α-Ti were also detected from the matrix material in both alloys, which indicated that the X-rays penetrated the oxide scales during measurement. $(Ga, Al)_2TiO_5$ was confirmed on the surfaces of Ga-added TKT41 alloy, as suggested in [20]. The intensity ratios of TiO_2/Al_2O_3 at diffraction angel of 27.4°/37.8° for TKT39 (Sn) were 1.97 and 1.53 with the bimodal and lamellar microstructure, respectively. For TKT41 (Ga), the intensity ratios of TiO_2/Al_2O_3 at diffraction angel of 27.4°/37.8° were 0.73 and 0.34 with the bimodal and lamellar

microstructure, respectively. These results indicated that the replacement of Sn with Ga suppressed TiO_2 (rutile) formation or promoted Al_2O_3 formation on the surface.

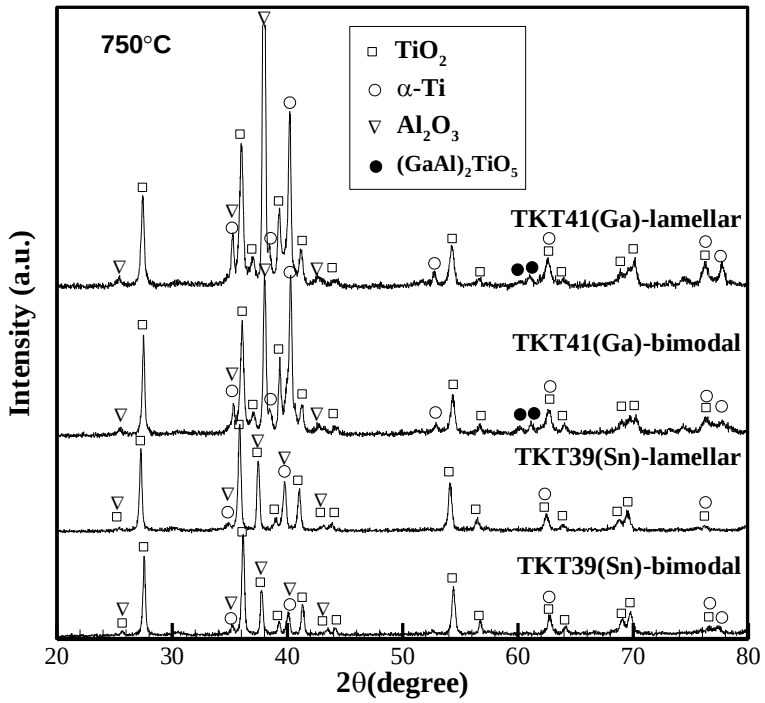

Figure 4.5. XRD patterns of TKT39 (Sn)-bimodal, TKT39 (Sn)-lamellar, TKT41 (Ga)-bimodal and TKT41 (Ga)-lamellar oxidize at 750°C.

The distributions of elements within the oxide layer and substrate after the oxidation of both alloys with different microstructures were examined by EDS measurements. Fig. 4.6 shows the concentration profiles of Al, Sn, Ga, Ti, and O in TKT39 (Sn) and TKT41 (Ga) along the red lines shown in backscattered electron (BSE) images. As shown in Fig. 4.6a and 4.6b, in the TKT39 (Sn) alloy, the thicknesses of the oxide scales were 14 μm and 11 μm for the bimodal and fully lamellar microstructure, respectively. Both oxides had a multilayer microstructure consisting of a heterogeneous mixture of TiO_2 and Al_2O_3. Sn was segregated in the substrate near the oxide/substrate interface in both TKT39

samples with different microstructures. In TKT41 (Ga), as shown in Fig. 4.6c and 4.6d, the thickness of the oxide scales consisting of external Al_2O_3 and internal TiO_2 was 2.7 μm and 2.5 μm for the bimodal and fully lamellar microstructure, respectively. The oxide layer in the Ga-added alloy was thinner owing to the suppression of oxide growth by the replacement of Sn with Ga. Unlike Sn, no segregation of Ga was observed at the oxide/substrate interface in TKT41 (Ga) for both microstructures. Ga was found to be enriched in the external Al_2O_3 layer in TKT41 (Ga) for both the bimodal and fully lamellar microstructures.

Oxide formation in Ti alloys has been well studied [18, 37], and an oxide multilayer consisting of TiO_2 and Al_2O_3 were formed in near-α Ti alloys. Similar multilayers consisting of several alternating TiO_2 and Al_2O_3 layers were observed in TKT39 alloy with added Sn, while in TKT41 alloy with added Ga, only a single outer Al_2O_3 layer and inner TiO_2 layer were observed. Similar results were obtained in [20]. Spallation occurred in Sn-added samples, and a clear segregation was observed at the oxide scale/substrate interface, while in Ga-added samples, no spallation nor segregation was observed. These results are consistent with previous studies [20]. Adherent oxides can provide acceptably low oxidation rates. In addition, the loss of the protective oxide by spallation will lead to high local oxidation rates of the alloy substrate [34]. $(Ga, Al)_2TiO_5$ [20] and a Ga-enriched layer corresponding to the Al-enriched layer near the oxide surface were detected in TKT41, and there was no evidence of the formation of nitrides, as described

by Becker et al. [22, 33]. Kitashima et al. [20] demonstrated that (Ga, Al)$_2$TiO$_5$ may form near or in Al_2O_3 because gallium oxide may dissolve in Al_2O_3, which is based on the Ga_2O_3-Al_2O_3-TiO_2 phase system [38], and Ga addition may promote Al_2O_3 formation according to the decrease in the intensity ratios of TiO_2/ Al_2O_3, which may act as a barrier that reduces the oxygen transfer flux, thereby decreasing the oxide growth rate [20].

Fig. 4.7 shows the microstructure characteristics of TKT41 (Ga)-bimodal after oxidation for 500 h at 750 °C. In Fig. 4.7a, a wavy layer was observed in the substrate beneath the oxide layer. The compositions were determined by EDS, and the average Ga concentration in this wavy layer was approximately 5.23 wt. %, which is greater than that in bulk (3.81 wt. %). Such slight enrichment near the oxide can be also observed in Fig. 4.6(c), which we will discuss later.

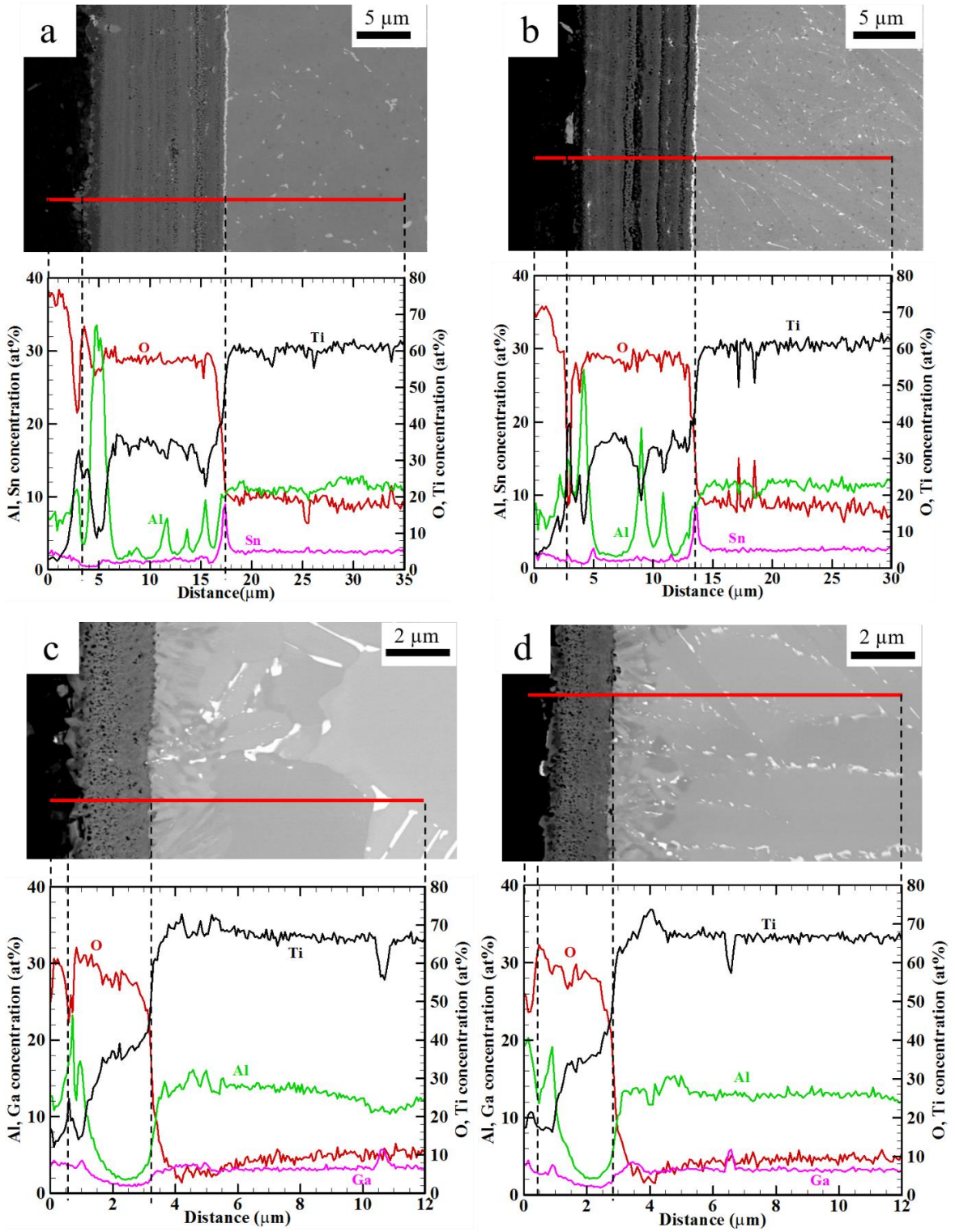

Figure 4.6. Concentration profiles of Al, Sn, Ga, Ti and O obtained in the oxide and substrate along the lines for (a) TKT39 (Sn)-bimodal, (b) TKT39 (Sn)-lamellar, (c) TKT41 (Ga)-bimodal and (d) TKT41 (Ga)-lamellar after oxidation at 750°C for 500 h.

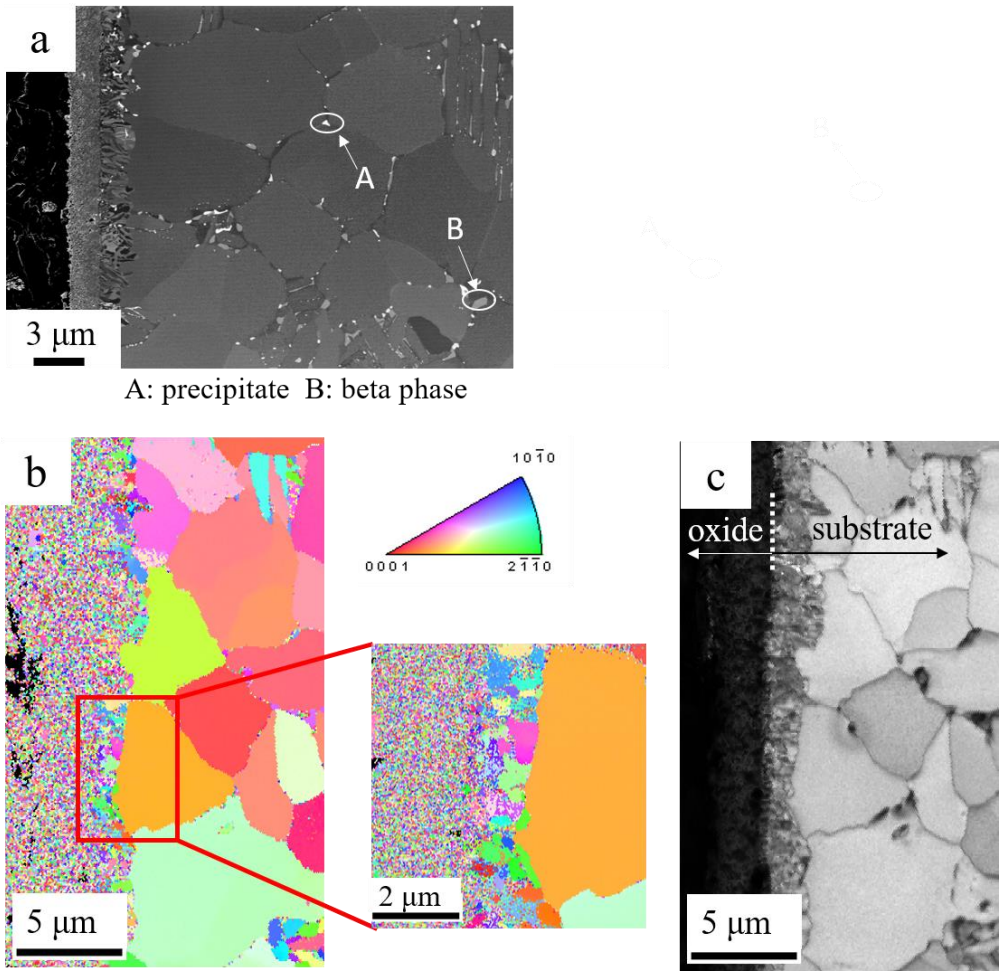

Figure 4.7. Microstructure characteristics of TKT41 (Ga)-bimodal after oxidation for 500 h at 750 °C. (a) BSE image (b) IPF map, and (c) IQ map near the surface.

Fig. 4.7b and 4.7c show EBSD results near the surface, including the oxide layer and the wavy layer beneath oxide layer in the substrate. As shown in the inverse pole figure (IPF) map of Fig. 4.7b, the wavy layer consisted of small grains with distinct orientation, and the grain size was approximately 0.5 μm, which is much less than substrate grain size of 5 μm. The image quality map (IQ map) EBSD data (Fig. 4.6c) also shows distinct lines between the oxide layer and wavy layer as well as between the wavy layer and substrate. For comparison, the microstructure characteristics of TKT39-bimodal (Sn) after oxidation for 500 h

at 750 °C is shown in Fig. 4.8. A clear boundary between the oxide layer and substrate was observed in both the IPF map (a) and IQ map (b). No small grains near the oxide scale were observed for TKT39 (Sn)-bimodal. The replacement of Sn with Ga promoted the formation of small grains.

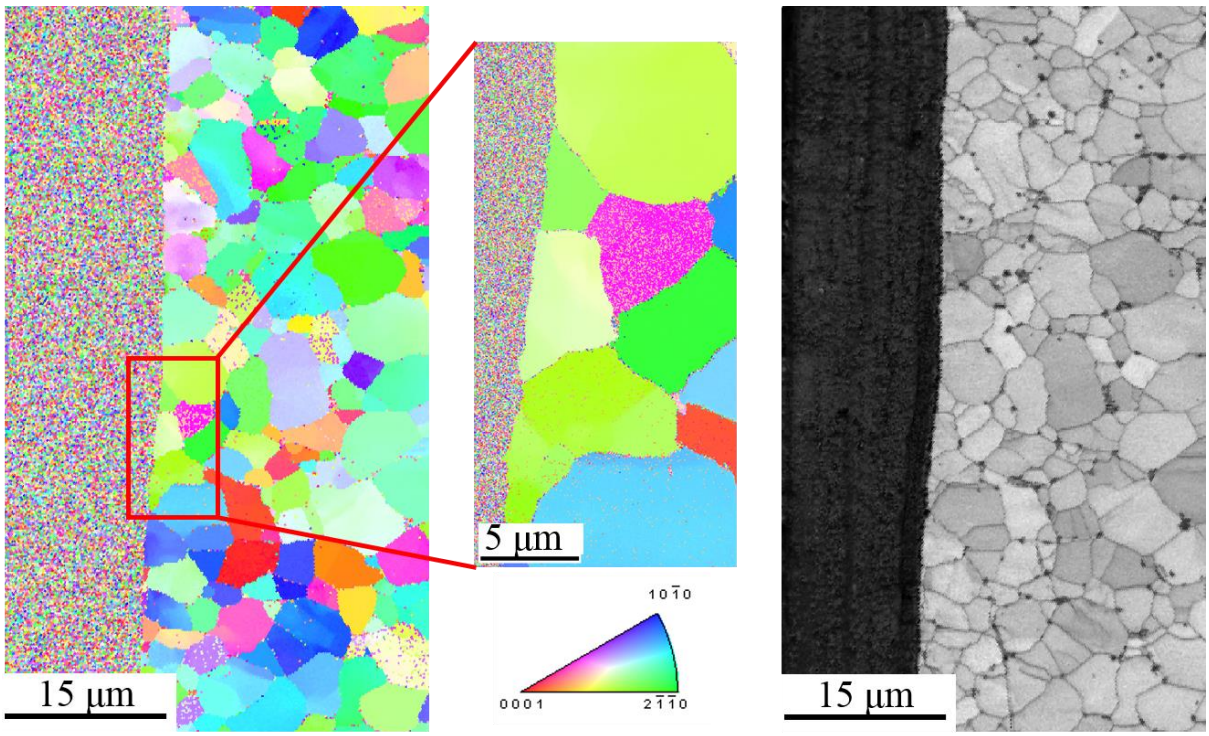

Figure 4.8. Microstructure characteristics of TKT39 (Sn)-bimodal after oxidation for 500 h at 750 °C. IPF map (left) and IQ map (right).

There have been reports on recrystallization at the oxide/substrate interface during oxidation. In Ni-Cu alloy [39], the recrystallization may have occurred because of the diffusion of elements in the alloy, a phenomenon termed diffusion-induced recrystallization (DIR). A similar DIR phenomenon was observed in other systems such as Cu-Ni system [39], Ni-Fe system [40], Al_2O_3 [41], and TiC [42]. However, to the authors' knowledge, the recrystallization process in Ti alloy has not yet been reported. To investigate the recrystallization process during

oxidation, four TKT41 (Ga)-bimodal samples were prepared. Fig. 4.9 shows the recrystallization process of TKT41 (Ga)-bimodal after exposure at 750 °C for (a) 20 h, (b) 45 h, (c) 90 h, and (d) 140 h, respectively.

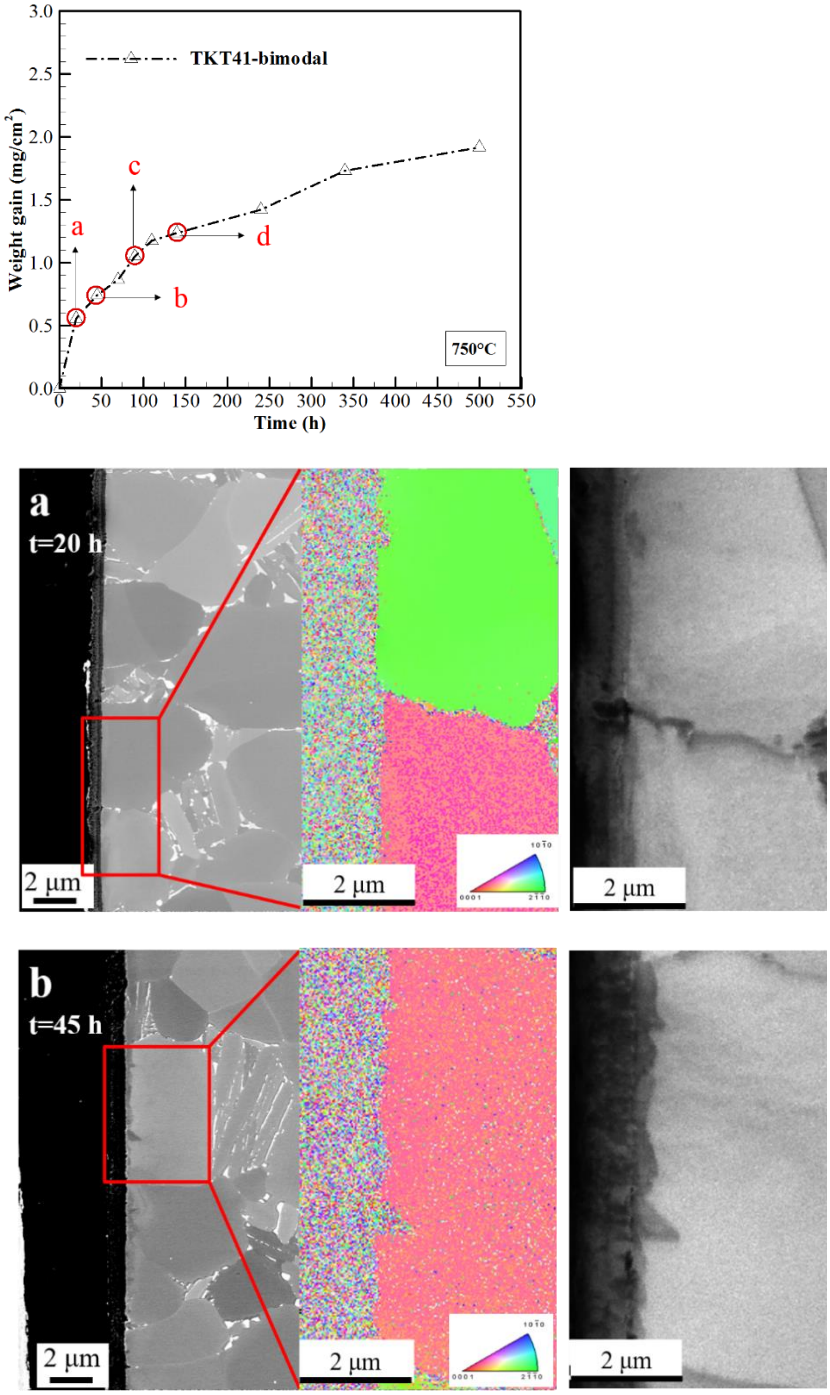

Figure 4.9. Recrystallization process of TKT41 (Ga)-bimodal after oxidation for (a) 20 h, (b) 45 h, (c) 90 h, and (d) 140 h at 750 °C. IPF map (left) and IQ map (right).

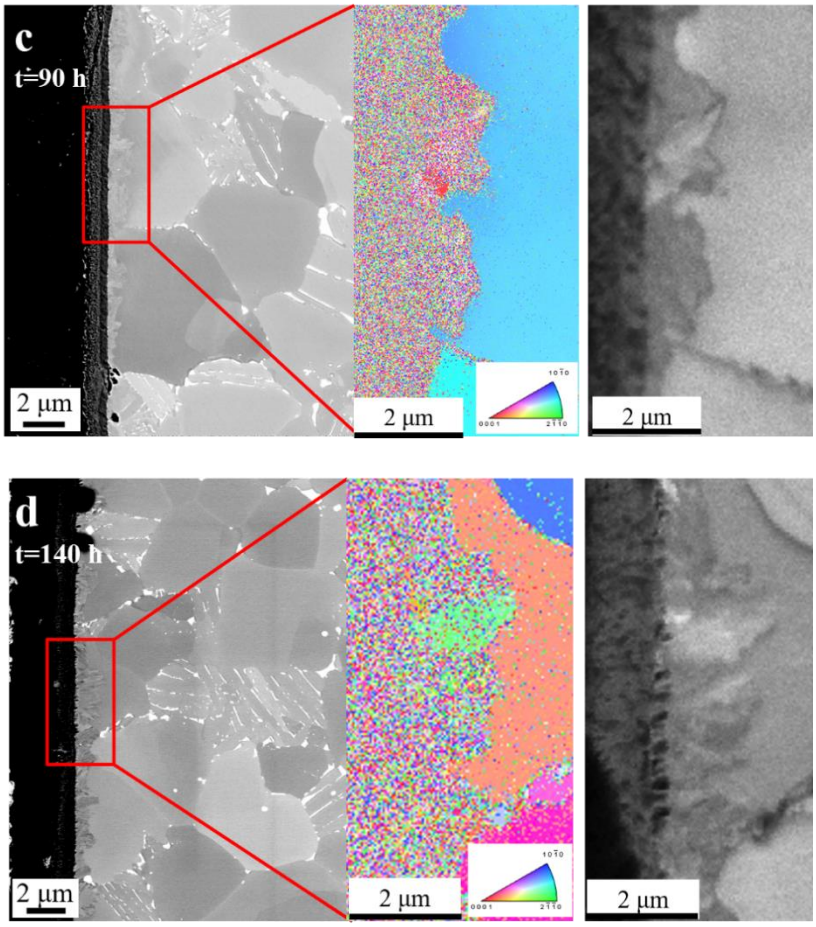

Figure 4.9. Recrystallization process of TKT41 (Ga)-bimodal after oxidation for (a) 20 h, (b) 45 h, (c) 90 h, and (d) 140 h at 750 °C. IPF map (left) and IQ map (right). (Continued)

In Fig. 4.9a to Fig. 4.9d, the BSE image, EBSD IPF map, and EBSD IQ map are shown from left to right. As shown in Fig. 4.9a and 4.9b, at the beginning of the oxidation process, no distinct recrystallized grains were detected after exposure to air for 20 h or 45 h at 750 °C. As the exposure time increased, the oxide layer as well as the recrystallized layer grew thicker and recrystallized grains grew larger; consequently, some small recrystallized grains with random orientations were observed, as shown in Fig. 4.9c and Fig. 4.9d.

To observe recrystallized grains more clearly and to confirm whether α_2 phase significantly changed during isothermal oxidation, TEM observation was

carried out. Fig. 4.10 shows the bright field images near oxide region after 20 h and 500 h exposure at 750 °C for TKT41(Ga)-bimodal alloy. From Fig. 4.10, it is obvious that no recrystallized grains after 20 h exposure while after 500 h exposure, grains with the average grain size of ~400 nm were observed just beneath oxide layer as shown in Fig. 4.10b, which is consistent with EBSD results as shown in Fig. 4.7b and Fig. 4.9a.

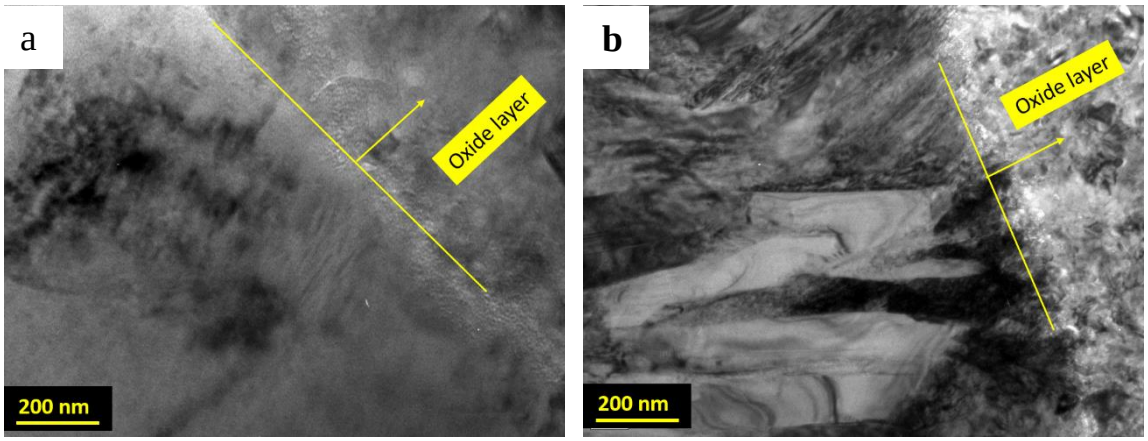

Figure 4.10. Bright field images of TKT41(Ga)-bimodal after oxidized at 750 °C for (a) 20 h and (b) 500 h.

It is well known that the precipitation of ordered α_2 phase can improve strength by precipitation strengthening but decrease ductility [35]. The size and distributions of the temporal evolution of α_2 precipitation during isothermal oxidation strongly affects the properties such as creep or fatigue. Fig. 4.11 shows the dark field images of α_2 precipitation at the beginning of oxidation (20 h exposure) and after long time exposure (500 h exposure) of TKT41. As shown in Fig. 4.11, clear α_2 super-lattice reflections in selected area diffraction pattern together with the fundamental α reflections were shown after 20 h and 500 h

exposure at 750 °C. The dark filed images using super-lattice reflection from α_2 phase, as indicated by small white circle shown in electron diffraction pattern, indicated the uniform precipitation of α_2 phase. In addition, the precipitation of α_2 phase was estimated to be around 10 nm in diameter after 20 h exposure and kept almost same during isothermal oxidation up to 500 h.

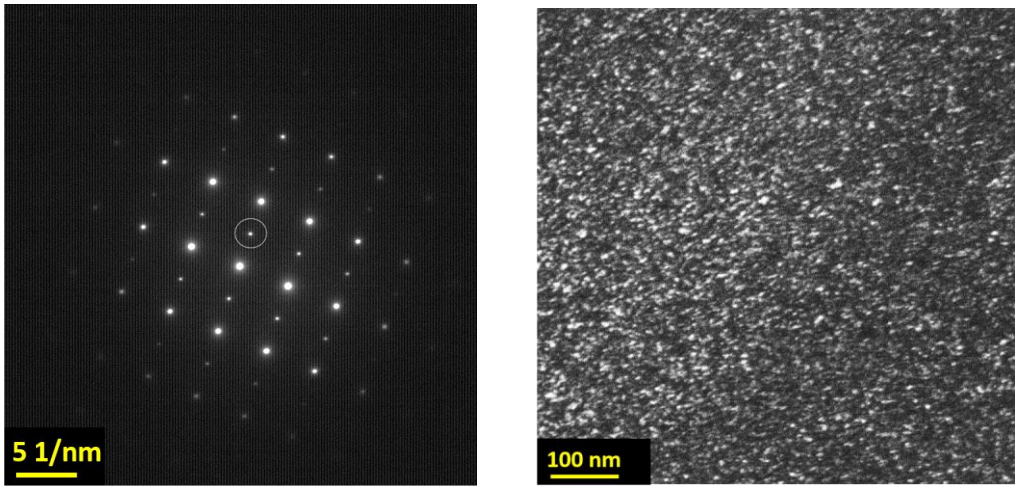

(a) 20 h exposure at 750 °C (left: DP, right: DF image)

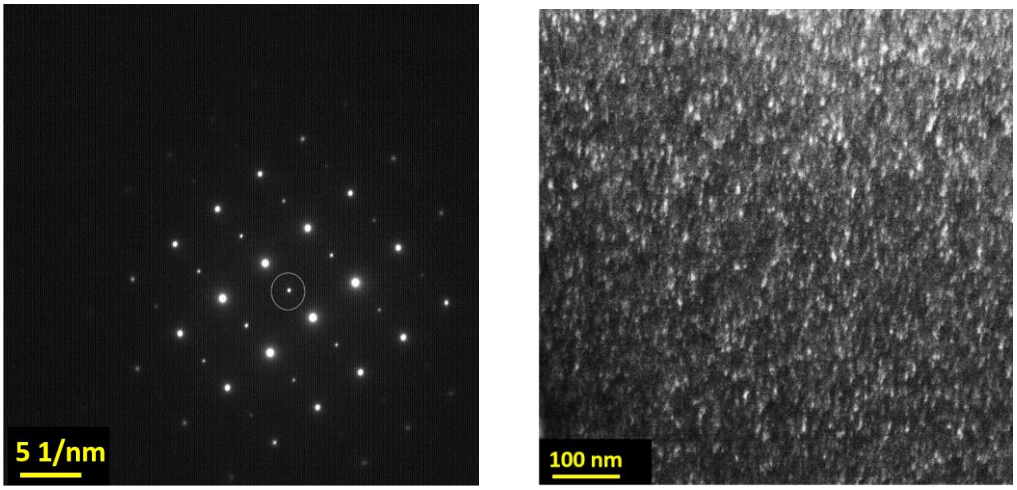

(b) 500 h exposure at 750 °C (left: DP, right: DF image)

Figure 4.11. Electron diffraction pattern (DP) and dark field (DF) images of α2 phase after exposure at 750 °C for (a) 20 h and (b) 500 h of TKT41.

Based on our previous discussion and results, it is suggested that DIR may occur in the Ga-added Ti alloy during oxidation, as schematically shown in Fig. 4.12. We propose the following mechanism for the DIR. Initially, owing to the relatively higher activity of Ti compared to Al, TiO_2 is preferentially formed on the surface of Ti alloy [18]. Subsequently, Al^{3+} and Ga^{3+} cations diffuse outward through TiO_2 to form $(Al, Ga)_2O_3$ outside, and Ti^{4+} combines with the inward diffusion oxygen to form TiO_2 at the oxide/substrate interface. As the Ga^{3+} cation diffuses outward and Ga is enriched near the oxide/substrate interface, as shown in Fig. 4.6c, stress at the interface increased owing to plastic deformation with lattice distortion. This was suggested by TEM analysis in Cu-Zn alloy [43]. Subsequently, dislocation sub-boundaries are formed, resulting in the generation of recrystallized grains. Recrystallized grains grow larger with higher Ga concentration. This recrystallization process could release a part of the oxide/substrate interface stress, as suggested in Refs [44, 45], improving the adherence between the oxides and substrate and suppressing the oxide spallation in Ga-added Ti alloy. The temperature dependency of the recrystallization and the effect of the recrystallization on mechanical properties are the subjects of a future study.

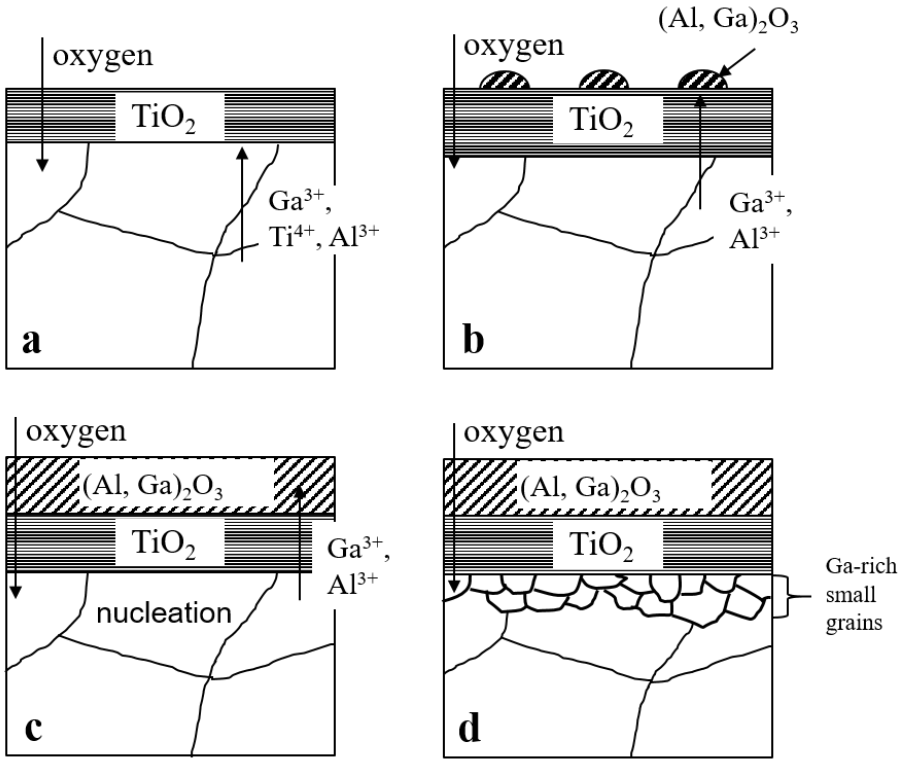

Figure 4.12. Schematic representation of oxidation process of Ga-added Ti-alloy: (a) Formation of TiO_2 layer, (b) Formation of $(Al, Ga)_2O_3$ layer, (c) Diffusion induced recrystallization and (d) Recrystallized grains grow larger.

4.5 Conclusions

The oxidation behaviors of two near-α Ti alloys containing Ga or Sn with bimodal structure and lamellar structure were investigated. Sn and Ga were set to have approximately equal Al equivalent values. The present study led to the following conclusions:

(1) The replacement of Sn with Ga decreased the weight gain of the oxidation sample during oxidation, suppressed oxide growth, and improved adherence between the oxide and substrate. In Ga-added alloy, there was no Ga

segregation at the oxide/substrate interface, and the formation of $(Al, Ga)_2O_3$ and $(Ga, Al)_2TiO_5$ was suggested.

(2) The lamellar structure showed a smaller weight gain of the oxidation sample compared to the bimodal structure in both alloys. In addition, the Ga-added alloy with bimodal microstructure showed a smaller weight gain compared to the Sn-added alloy with lamellar structure.

(3) In the Ga-added alloy, recrystallization occurred near the oxide/substrate interface, which may contribute to the release of stress, improvement of the adherence between the oxide and substrate, and prevention of the spallation of oxides.

(4) α_2 precipitated in both alloys with bimodal microstructure and α_2 precipitation had a diameter of 10 nm; in TKT41(Ga) alloy with bimodal microstructure, the diameter α_2 precipitates has little change during isothermal oxidation up to 500 h at 750 °C.

4.6 References

[1] T. Kitashima, K. S. Suresh, and Y. Yamabe-Mitarai, Present stage and future prospects of development of compressor material, Crystal Research and Technology, 50 (2015) 28-37.

[2] J. H. Perepezko, The hotter the engine, the better, Science, 326 (2009) 1068-1069.

[3] G. Lütjering, and J. C. Williams, Titanium, 2nd ed, Springer, Berlin, 2003.

[4] R. N. Shenoy, J. Unnam, and R. K. Clark, Oxidation and embrittlement of Ti-6Al-2Sn-4Zr-2Mo alloy, Oxidation of Metals, 26 (1986) 105-124.

[5] Z. Liu, and G. Welsch, Effects of oxygen and heat treatment on the mechanical properties of alpha and beta titanium alloys, Metallurgical Transactions A, 19 (1988) 527-542.

[6] T. Kitashima, L. J. Liu, and H. Murakami, Numerical analysis of oxygen transport in alpha titanium during isothermal oxidation, Journal of The Electrochemical Society, 160 (2013) C441-C444.

[7] D. A. P. Reis, C. R. M. Silva, M. C. A. Nono, M. J. R. Barboza, F. Piorino Neto, and E. A. C. Perez, Effect of environment on the creep behavior of the Ti-6Al-4V alloy, Materials Science and Engineering A, 399 (2005) 276-280.

[8] T. J. Johnson, M. H. Loretto, and M. W. Kearns, Oxidation of high temperature titanium alloys, in: Proceedings of the Seventh World Titanium Conference, Warrendale, PA, TMS, (1992) 2035-2042.

[9] K. S. Mcreynolds, and S. Tamirisakandala, A study on alpha-case depth in Ti-6Al-2Sn-4Zr-2Mo, Metallurgical and Materials Transactions A, 42 (2011) 1732-1736.

[10] C. Leyens, and M. Peters, Titanium and Titanium Alloys, Wiley-VCH, Weinheim, 2003.

[11] A. M. Chaze, G. Beranger, and C. Coddet, A comparison of the influence of Si, Al, and Cr additions on the high temperature oxidation behavior of titanium,

in Titanium: Science and Technology, G. Lutjering, U. Zwicker, and W. Bunk, Editors, DGM: Oberursel, (1985) 2665-2672.

[12] A. M. Chaze, and C. Coddet, Influence of alloying elements on the dissolution of oxygen in the metallic phase during the oxidation of titanium alloys, Journal of Materials Science, 22 (1987) 1206-1214.

[13] T. J. Johnson, M. H. Loreto, C. M. Younes and M. W. Kearns, A study of the role of alloying additions during the high temperature oxidation of IMI834, in: Second International Conference on the Microscopy of Oxidation, Cambridge, London, England, (1993) 1-10.

[14] A. M. Chaze, and C. Coddet, Influence of the nature of alloying elements on the adherence of oxide films formed on titanium alloys, Oxidation of Metals, 28 (1987) 61-71.

[15] H. Chuanxi and L. Bingnan, Effects of Nb and W on mechanical properties and oxidation resistance of high temperature titanium alloys, in: Titanium ’92: Science and Technology, Proceedings of the Seventh World Titanium Conference, Warrendale, PA, TMS, (1992) 1891-1899.

[16] A. M. Chaze, C. Coddet, and G. Beranger, Dissolution of oxygen in the metallic phase during high temperature oxidation of titanium and some alloys, in : Sixth World Conference on Titanium IV, (1988) 1765-1770.

[17] S. Z. Zhang, B. Zhou, N. Liu, and L. Q. Chen, Effects of microstructure and rare-earth constituent on the oxidation behavior of Ti-5.6 Al-4.8 Sn-2Zr-1Mo-0.35 Si-0.7 Nd titanium alloy, Oxidation of Metals, 81 (2014) 373-382.

[18] H. L. Du, P. K. Datta, D. B. Lewis, and J. S. Burnell-Gray, Air oxidation behaviour of Ti-6Al-4V alloy between 650 and 850 °C, Corrosion Science, 36 (1994) 631-642.

[19] T. Kitashima, Y. Yamabe-Mitarai, S. Iwasaki, and S. Kuroda, Effects of alloying elements on the tensile and oxidation properties of α and near-α Ti alloys, in: Proceedings of the 13th World Conference on Titanium, Wiley, California, USA, (2015) 479-485.

[20] T. Kitashima, Y. Yamabe-Mitarai, S. Iwasaki, and S. Kuroda, Effects of Ga and Sn additions on the creep strength and oxidation resistance of near-α Ti alloys, Metallurgical and Material Transactions A, 47 (2016) 6394-6403.

[21] T. Kitashima, and T. Kawamura, Prediction of oxidation behavior of near-α titanium alloys, Scripta Materialia, 124 (2016) 56-58.

[22] S. Becker, A. Rahmel, M. Schorr, and M. Schutze, Mechanism of isothermal oxidation of the intel-metallic TiAl and of TiAl alloys, Oxidation of Metals, 38 (1992) 425-464.

[23] Y. Shida, and H. Anada, The influence of ternary element addition on the oxidation behaviour of TiAl intermetallic compound in high temperature air, Corrosion Science, 35 (1993) 945-953.

[24] Y. Shida, and H. Anada, Oxidation behavior of binary Ti-Al alloys in high temperature air environment, Materials Transactions, 34 (1993) 236-242.

[25] M. Yoshihara, and Y. W. Kim, Oxidation behavior of gamma alloys designed for high temperature applications, Intermetallics, 13 (2005) 952-958.

[26] M. Yoshihara, and K. Miura, Effects of Nb addition on oxidation behavior of TiAl, Intermetallics, 3 (1995) 357-363.

[27] S. Taniguchi, and T. Shibata, Influence of additional elements on the oxidation behaviour of TiAl, Intermetallics, 4 (1996) S85-S93.

[28] C. Z. Wagner, Electrochemistry, Reaction Types in the Oxidation of Alloys, 63 (1959) 772-782.

[29] P. Perez, Influence of the alloy grain size on the oxidation behaviour of PM2000 alloy, Corrosion Science, 44 (2002) 1793-1808.

[30] F. Pitt, and M. Ramulu, Influence of grain size and microstructure on oxidation rates in titanium alloy Ti-6Al-4V under superplastic forming conditions, Journal of Materials Engineering and Performance, 13 (2004) 727-734.

[31] Y. Yang, T. Kitashima, T. Hara, Y. Hara, Y. Yamabe-Mitarai, M. Hagiwara, and L. J. Liu, Effect of grain size on oxidation resistance of unalloyed titanium, Materials Science Forum, 879 (2016) 2187-2192.

[32] J. Tiley, J. Shaffer, A. Shiveley, A. Pilchak, and A. Salem, The effect of lath orientations on oxygen ingress in titanium alloys, Metallurgical and Materials Transactions A, 45 (2014) 1041-1048.

[33] C. Leyens, M. Peters, and W. A. Kaysser, Influence of microstructure on oxidation behaviour of near-α titanium alloys, Materials Science and Technology, 12 (1996) 213-218.

[34] C. Leyens, M. Peters, and W. A Kaysser, Oxidation behavior of near-α titanium alloys and their protection by coatings, in the Titanium ’95: Science and

Technology, Proceedings of the 8th World Conference on Titanium, London: Institute of Materials, Birmingham, England, (1996) 1935-1942.

[35] C. E. Shamblen, and T. K. Redden, Creep resistance and high-temperature metallurgical stability of titanium alloys containing gallium, Metallurgical and Materials Transactions B, 3 (1972) 1299-1305.

[36] E. M. Kenina, I. I. Kornilov, and V. V. Vanilova, Effect of oxygen on the scale resistance of titanium-tin alloys, Metal Science and Heat Treatment, 14 (1972) 396-398.

[37] T. Kitashima, and Y. Yamabe-Mitarai, Oxidation behavior of germanium- and/or silicon-bearing near-α titanium alloys in air, Metallurgical and Materials Transactions A, 46 (2015) 2758-2767.

[38] A. L. Jaromin, and D. D. Edwards, Subsolidus phase relationships in the Ga_2O_3-Al_2O_3-TiO_2 system, Journal of American Ceramic Society, 88 (2005) 2573-2577.

[39] D. Liu, W. A. Miller, and K. T. Aust, Diffusion induced grain boundary migration and recrystallization during oxidation of a Ni-48.5 Pet Cu alloy, Metallurgical Transactions A, 19 (1988) 1667-1675.

[40] T. A. Parthasarathy, and P. G. Shewmon, Vapor transport and DIGM in the Ni-Fe system, Metallurgical Transactions A, 14 (1983) 2560-2563.

[41] Y. K. Paek, H. Y. Lee, and S. J. L. Kang, Diffusion induced recrystallization in alumina, Journal of the European Ceramic Society, 24 (2004) 613-618.

[42] K. W. Chae, C. S. Hwang, D. Y. Kim, and S. J. Cho, Diffusion induced recrystallization of TiC, Acta Materialia, 44 (1996) 1793-1799.

[43] S. A. Hackney, F. S. Biancaniello, D. N. Yoon, and C. A. Handwerker, Observations on crystal defects associated with diffusion induced grain boundary migration in Cu-Zn, Scripta Metallurgica, 20 (1986) 937-942.

[44] C. Coddet, A. M. Chaze, and G. Beranger, Measurements of the adhesion of thermal oxide films: application to the oxidation of titanium, Journal of Materials Science, 22 (1987) 2969-2974.

[45] J. Stringer, Stress generation and relief in growingoxide films, Corrosion Science, 10 (1970) 513-543.

Chapter 5 Effect of temperature on oxidation behaviour

5.1 Abstract

Isothermal oxidation testing of Ga-containing near-α Ti alloy was performed in air at temperatures of 650, 700, and 750 °C for up to 500 h. Results revealed that the alloy oxidation kinetics followed a parabolic law at 650 °C and a parabolic-cubic law at 700 and 750 °C, while the abundance of Al_2O_3 in oxide layers increased with temperature after the dissolution of Ga_2O_3 species in the Al_2O_3 phase. The activation energy of the α-case formation was close to the magnitudes obtained for conventional titanium alloys despite its temperature-dependent recrystallization observed near the oxide/metal interface at 700 and 750 °C.

5.2 Introduction

Near-α Ti alloys are attractive structural materials, which are used in high-temperature components in gas turbine engines due to their high strength-to-density ratio and excellent corrosion resistance [1]. Although increasing the service temperature of a gas turbine can improve its working efficiency and save kerosene, it also leads to the degradation of titanium alloy components with time due to the oxygen-containing gaseous environment [2,3]. The related degradation mechanisms involve the formation of rapidly growing non-protective oxide layers caused by the high chemical affinity of titanium to oxygen [4,5] and embrittlement of the substrate zone due to the high solubility of oxygen molecules

(such an oxygen-enriched substrate zone is commonly called α-case) [6-9]. The presence of α-case results in the deterioration of important mechanical properties of Ti alloys such as ductility, fracture toughness, and fatigue life.

The oxidation behaviour of Ti and Ti alloys at high temperatures has been studied by many researchers [10-21]. Kofstad et al. [10,11] systematically investigated the oxidation behaviour of pure titanium at various temperatures in different types of environments and found that its oxidation rate depended on temperature and time. In particular, the oxidation rate of Ti followed a logarithmic law at temperatures below 300 °C, a cubic law in the temperature range of 300–600 °C, and a parabolic law in the temperature range of 600–850 °C (which ultimately became a linear law after a prolonged time). The effects of temperature and time on the oxidation behaviour of conventional Ti alloys such as Ti–6Al–4V [12-16], Ti–6Al–2Sn–4Zr–2Mo [5,6,17], IMI 834 [4,18,19], and other titanium-based alloys [18,20,21] have also been examined in detail. Thus, Frangini et al. [12] found that the oxidation rate of Ti–6Al–4V mainly followed a parabolic law between 600 and 700 °C, but started to exhibit a linear behaviour after 50 h of treatment at a temperature of 700 °C (similar observations were reported by Guleryuz et al. [13]). Du et al. [14] reported the formation of a multilayered oxide-scale structure in Ti–6Al–4V alloy between 650 and 850 °C and proposed its possible mechanism based on the reactivity of Ti and Al species towards O as well as the O partial pressure. Shenoy et al. [6] studied the oxidation

behaviour of Ti–6242 alloy in the temperature range of 593–760 °C and found that its oxidation rate mainly followed a parabolic law up to 650 °C. Gaddam et al. [17] reported a transition from the parabolic to the linear behaviour of the oxidation rate of Ti–6242 alloy at 700 °C. McReynolds et al. [5] and Gaddam et al. [17] quantitatively studied the α-case formation in Ti–6Al–2Sn–4Zr–2Mo alloy and found that the thickness of the α-case layer was a function of both temperature and time (in particular, its time dependence corresponded to a parabolic relationship). The oxidation behaviours of IMI834 [4,19], IMI125 [4], TIME1100 [18], and Ti60 [20] alloys were similar to that of Ti6242 alloy.

The addition of α-stabilizing elements, (such as Al, Ga, and Sn) in Ti alloys enhances their high-temperature strength via solid solution strengthening [22,23] and promotes the precipitation of the α_2 phase with the $D0_{19}$ structure, which results in dispersion strengthening and low ductility [22]. The Al equivalent (expressed in wt.%), which can be calculated using the formula Al+1/2×Ga+1/3×Sn+1/6×Zr+10×O [21], has been utilized to evaluate the alloy ductility after creep exposure (thus, to avoid the embrittlement of previously studied near-α Ti alloys, their Al equivalents were below 9). Sn, which is conventionally added to near-α Ti alloys, accelerates the growth of a TiO_2 layer and causes the spallation of oxides [21,24,25], while the replacement of Sn with Ga led to the dissolution of Ga in oxide scales without their segregation at the oxide/substrate interface [21]. In our previous study , the replacement of Sn with

Ga resulted in a smaller weight gain as compared to those observed for IMI834 and TIME1100 alloys, owing to the dissolution of Ga atoms in the Al_2O_3 layer, which might act as a barrier for oxygen diffusion. In addition, unlike conventional near-α Ti alloys, recrystallization was observed near the oxide/substrate interface of Ga-containing Ti alloy during its isothermal oxidation at a temperature of 750 °C after 500-h exposure. However, the temperature dependencies of the oxidation behaviour and recrystallization of Ga-containing titanium alloys have not been elucidated in sufficient detail. In this study, the effects of temperature and time on the oxidation behaviour (especially on the oxidation reaction rate and α-case formation) of a Ga-containing near-α Ti alloy and the temperature dependence of its recrystallization process were examined.

5.3 Experimental procedures

A 1-kg ingot of Ga-containing near-α TKT41 Ti alloy was produced via cold crucible levitation melting (its nominal chemical composition is listed in Table 5.1). The Al equivalent calculated using the formula Al+1/2×Ga+1/3×Sn+1/6×Zr+10×O [21] was set to 9.5, and the obtained ingot was melted twice to enhance its compositional homogeneity. The cast ingot was β-forged at a temperature of 1130 °C and then groove-rolled to a 90% reduction in the α+β region at 980 °C to form square rods with side lengths of 14 mm. The β transus temperature of TKT41 alloy determined through the microstructural observations conducted after heat treatment at different temperatures was equal

to 995±5 °C. After the heat treatment at 970 °C for 1 h with air cooling followed by the ageing at 700 °C for 2 h and subsequent air cooling, a bimodal microstructure containing silicide precipitates was obtained (see Fig. 5.1). The volume fraction of the equiaxed α phase estimated using the ImageJ software was equal to 62.9%.

Table 5.1. Chemical composition (wt. %), Al equivalence value, and β transus temperature of TKT41 alloy.

Alloy	Ti	Al	Ga	Zr	Nb	Mo	Si	O	Al Eq.	T_β /°C
TKT41	81.8	7	3	6	1	1	0.2	0.093	10.4	995±5

Cylindrical samples for oxidation testing with diameters of 8 mm and heights of 4 mm were cut from the centres of the as-aged samples via wire electrical discharge machining. The surfaces of the specimens were finally polished using #800 SiC paper followed by ultrasonic cleaning in acetone. Isothermal oxidation testing was performed in air at temperatures of 650 °C, 700 °C, and 750 °C by removing the sample-containing alumina crucibles from the furnace after 20, 45, 70, 90, 110, 140, 240, 340, and 500 h of exposure. The mass change of each sample was measured with an accuracy of ±0.0001 g using a microbalance.

Microstructural characterizations of the aged samples were performed using a field emission gun scanning electron microscope (SEM, ZEISS Auriga) at accelerating voltages of 5 kV and 15 kV. Samples for SEM observations were embedded in resin and polished with polishing paper and colloidal silica.

After oxidation testing, the constituent oxide phases were identified via X-ray diffraction (XRD) using a Rigaku X-ray diffractometer with Cu Kα radiation operated at a voltage of 50 kV and current of 300 mA. Before microstructural characterization, the oxidized samples were cold mounted, cut, and metallographically polished with polishing paper and colloidal silica. Hardness measurements were performed using a MMT−7 Matsuzawa Vickers microhardness tester at a load of 10 g and duration of 15 s. The cross-sectional microstructures of the oxidized samples were analysed via SEM and electron backscatter diffraction (EBSD) observations (performed with the EBSD module attached to the SEM equipment) at an accelerating voltage of 15 kV using an AMETEK Digiview 5 detector.

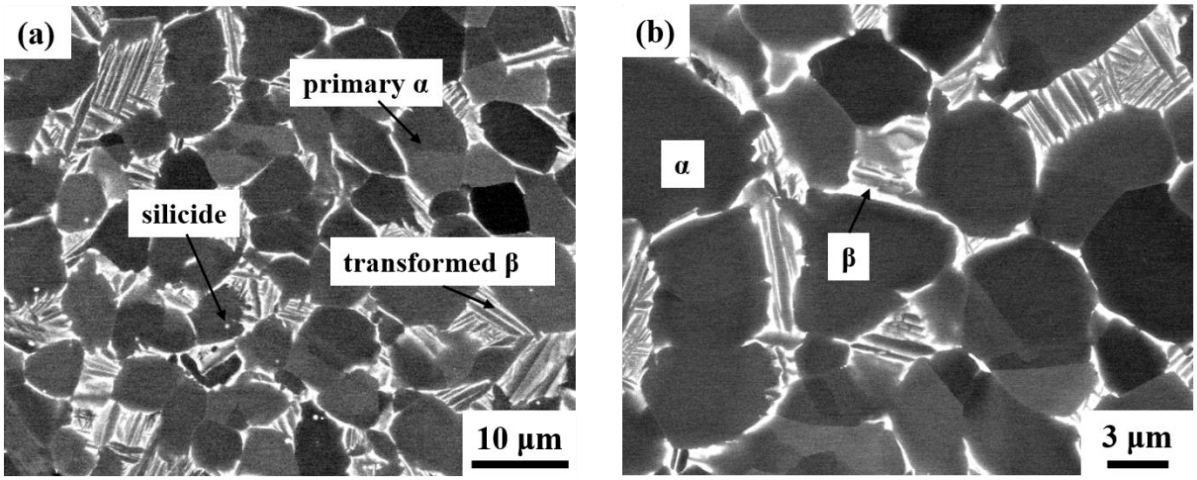

Figure 5.1. Backscattered electron images of microstructure of heat-treated TKT41 alloy.

5.4 Results and discussion

Fig. 5.2 shows the weight gains per surface area ($\Delta W/A$) measured for the alloy samples oxidized at 650, 700, and 750 °C in air for up to 500 h, which were

equal to 0.72, 1.39, and 1.91 mg/cm^2, respectively. The obtained results indicate that the overall weight gain increased with both time and temperature. To compare the oxidation behaviour of the studied Ga-containing alloy with those of conventional alloys, it was assumed that the oxidation behaviour followed a parabolic law, which corresponded to equation (1) below and was used to fit the data presented in Fig. 5.2:

$$\left(\frac{\Delta W}{A}\right) = \sqrt{k_p t}, \quad (1)$$

where k_p is the parabolic rate constant in g^{2}cm^{-4}s^{-1}. The k_p values of our alloy as shown in Table 5.2 were compared with those in other alloys as shown in Fig. 5.3 [16,17,26]. The calculation method of the value D in Table 5.2 will be described later.

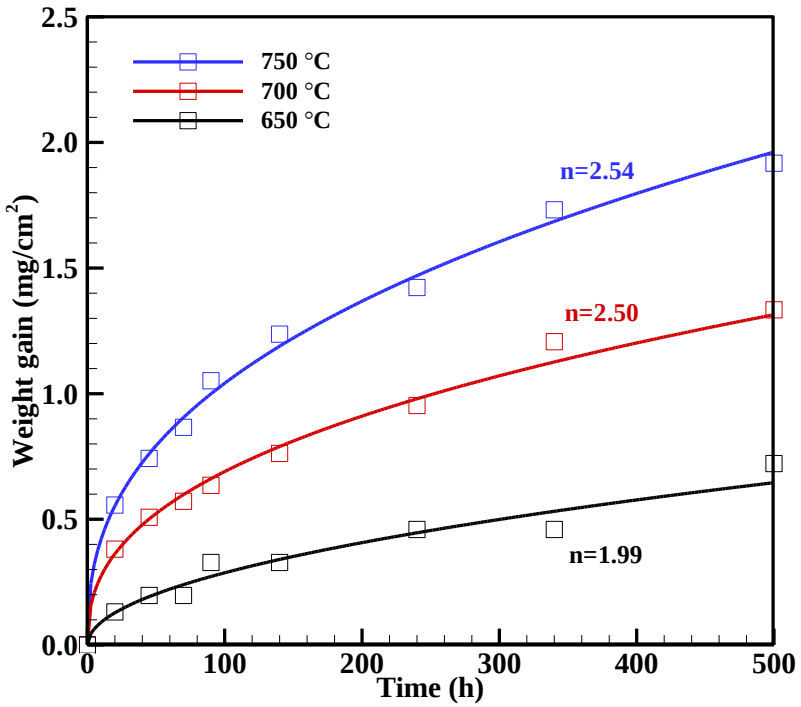

Figure 5.2. Weight gains of TKT41 during oxidation in air at 650°C, 700°C and 750°C for up to 500 h.

The magnitudes of k_p calculated for the Ga-containing alloy were smaller than those obtained for other conventional titanium alloys, indicating that the former exhibited a lower oxidation rate. It is well known that the oxidation behaviour of titanium and titanium alloys depends on the oxidation temperature; hence, the obtained weight gain data was fitted using the following power law equation [12,14,17]:

$$\left(\frac{\Delta W}{A}\right)^n = k_n t \,, \tag{2}$$

where n is the reaction index, k_n is the reaction rate constant, and t is the time. Therefore, the values of n values can be obtained by performing the regression analysis of the logarithmic plots of the weight gain per surface area versus time constructed using the data depicted in Fig. 5.2. The value of n gradually decreased with increasing temperature, thus changing the dependence described by equation (2) from a parabolic to a parabolic-cubic one (a similar trend was observed for IMI 834 alloy [4], although some other alloy systems such as Ti–6Al–4V [15] and unalloyed titanium [10,27] exhibited a decrease in *n* with increasing temperature). Such a transition of the oxidation kinetics of titanium alloys is associated with the oxide formation during the oxidation process.

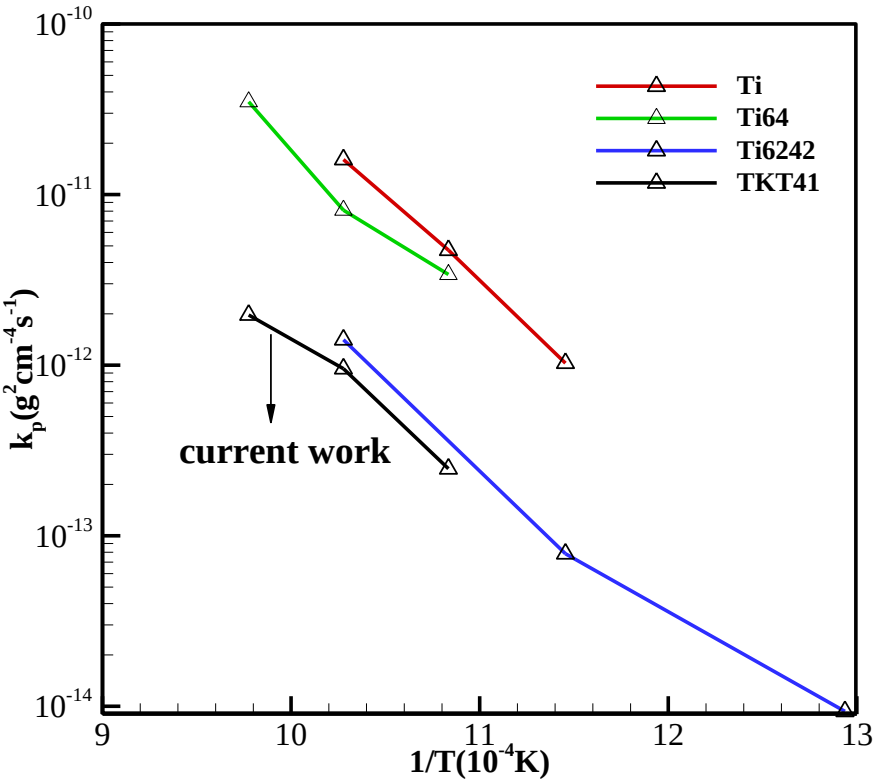

Figure 5.3. Parabolic rate constants of TKT41a, Ti-6Al-4V [16], Ti-6Al-2Sn-4Zr-2Mo [17], and Ti [26].

Fig. 5.4 displays the back-scattered SEM micrographs of the oxide scales formed after 20 and 500 h of exposure, which show that their thickness increased with temperature and exposure time, reaching the values of 0.45, 1.47, and 2.49 μm after 500 h of exposure at 650, 700, and 750 °C, respectively. In addition, porous oxide scales were formed after 500 h of exposure at 650 °C, whereas a dense oxide layer near the metal substrate containing an outer porous surface layer was observed after 500 h at temperatures of 700 °C and 750 °C. While the similar porous oxide layer was also formed after 20 h of exposure at 700 °C, the densification of oxide scales near the metal substrate that occurred after 500 h at 700 °C and 750 °C could be attributed to the change in the oxidation kinetics from the parabolic (at 600 °C) to the parabolic-cubic one (at 700–750 °C) caused by

the suppression of oxygen diffusion through oxide scales [4]. It should be noted that the oxidation kinetics of IMI 125 alloy underwent the transformation from a parabolic relationship at low temperatures to a linear kinetic at intermediate temperatures to a parabolic relationship at higher temperatures (here the linear kinetics described the diffusion of oxygen species along microcracks and pores) [4]. In the present study, the adherence of the oxide layer to the metal substrate was not significantly affected by the increased exposure time at all temperatures, although its spallation was observed for Ti–6242 alloy at 700 °C [17] as well as for Ti–6Al–4V alloy in the temperature range between 650 and 850 °C [14].

Table 5.2. Parabolic rate constants and oxygen diffusion coefficients in TKT41 at tested temperatures.

Temperature/°C	k_p/ $g^2cm^{-4}s^{-1}$	D/ m^2s^{-1}
650	2.47×10^{-13}	3.49×10^{-15}
700	9.54×10^{-13}	1.17×10^{-14}
750	1.97×10^{-12}	2.53×10^{-14}

In order to describe the formation of TiO_2 and Al_2O_3, the surfaces of the alloy specimens oxidized at various temperatures were analysed by XRD. According to the results presented in Fig. 5.5, four different phases can be distinguished after oxidation. The main oxide phases obtained at all temperatures were the TiO_2 (rutile) and α-Al_2O_3 ones, and the observed reflections of α-Ti from the alloy matrix indicated the penetration of X-rays through the oxide scales during measurements (the peaks corresponding to $(Ga, Al)_2TiO_5$ species on the alloy surface were also reported in Refs. [21]). The distributions of Al, Ga, Ti,

and O elements along the red lines in the backscattered electron images (Fig. 5.6) were examined by EDS after 500-h exposure at 650, 700, and 750 °C. Regardless of the temperature, the produced oxide species exhibited multilayer microstructures consisting of inner TiO_2 and outer Al_2O_3 layers (the former also contained inner dense and outer porous layers, which are depicted in Figs. 5.6(b) and (c) obtained at temperatures of 700 and 750 °C, respectively). A Ga-enriched layer corresponding to the Al-enriched layer near the oxide surface was detected at all temperatures, which suggested the dissolution of Ga_2O_3 in the Al_2O_3 phase [21]. The estimated Al concentration on the surface of the oxide layers was around 10 at.% at 650 °C, 15 at.% at 700 °C, and 20 at.% at 750 °C. The Al concentration on the surface increased with temperature. The obtained EDS results indicate that the formation of the Al_2O_3 phase on the surface of sample was promoted by the temperature increase of Ga-containing Ti alloy. It has been reported previously that in contrast to Sn addition, Ga addition promotes the formation of Al_2O_3 because of the dissolution of Ga_2O_3 in the Al_2O_3 matrix [21]. In the studied Ga-containing titanium alloy, the concentration of Al in outer oxide layer increased with temperature, indicating that the role of the diffusion barriers of Al, Ga, and O ions became more significant at higher temperatures.

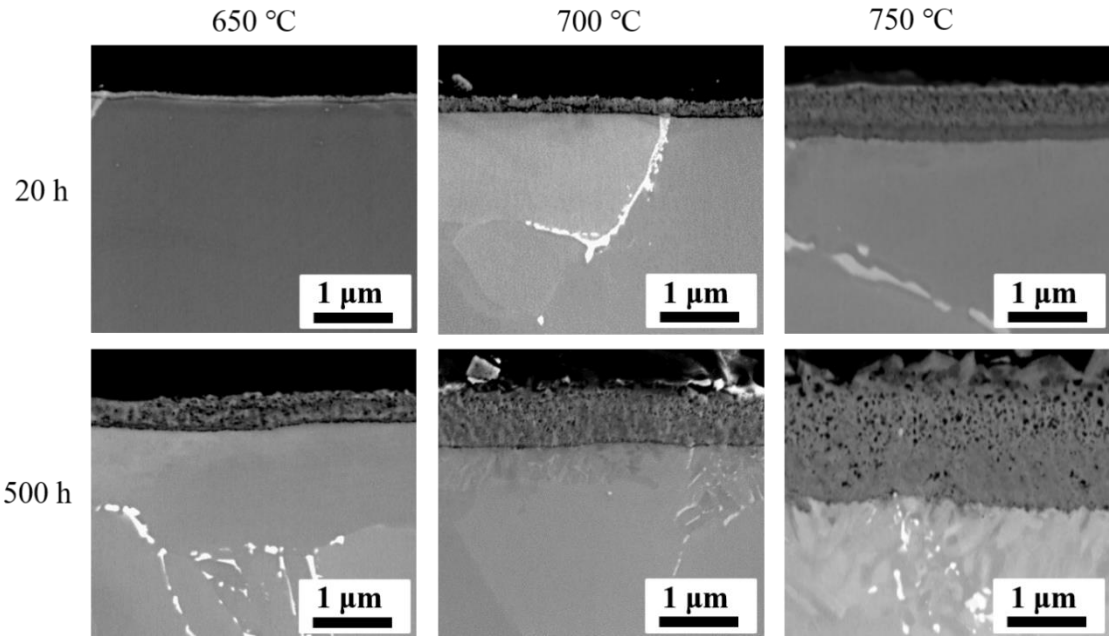

Figure 5.4. SEM micrographs (back-scattered electron images) of oxide scale after 20 h and 500 h exposure at 650, 700 and 750 °C.

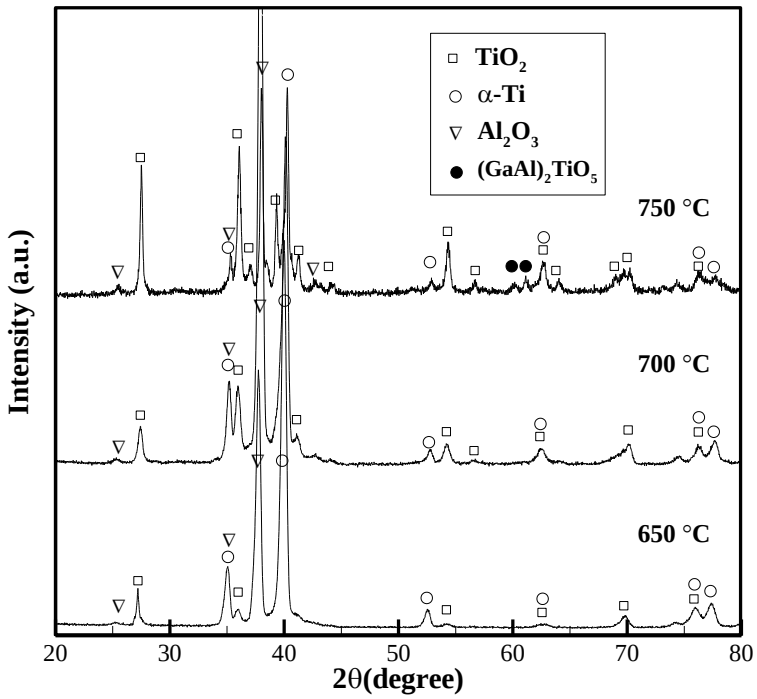

Figure 5.5. XRD patterns of TKT41 oxidized at 650°C, 700°C and 750°C for up to 500 h.

It is well known that the overall parabolic rate constant corresponding to the first oxidation stage of titanium can be expressed as the sum of parabolic rate constants for the growth of scales and formation of the oxygen solid solution layer

[8,28]. It has been also reported that the growth of α-case in Ti–6242 alloy follows a parabolic law [5,17]. In our previous study on Ga-containing Ti alloy, the recrystallization at the interface between the oxide layer and the alloy substrate was observed at 750 °C. The results obtained in this work suggest that similar to Cu–Ni [29] and Ni–Fe [30] alloys, the diffusion-induced recrystallization of the Ga-containing titanium alloy during its oxidation at high temperatures was accompanied by the lattice strain at the alloy interface. It is obvious that this recrystallization process was temperature-dependent, as indicated by the EBSD images depicted in Fig. 5.7 (here the left part of each panel shows an inverse pole figure, and the right part displays an image quality map) for the oxidized samples after 500-h exposure at (a) 750 °C, (b) 700 °C, and (c) 650 °C. As shown in Fig. 5.7, alloy recrystallization was observed at 750 °C and 700 °C, but not at 650 °C. The estimated thickness of the recrystallized layer was around 2 μm at 750 °C and less than 1 μm at 700 °C, which suggested that higher temperatures accelerated the recrystallization of the studied Ga-containing titanium alloy.

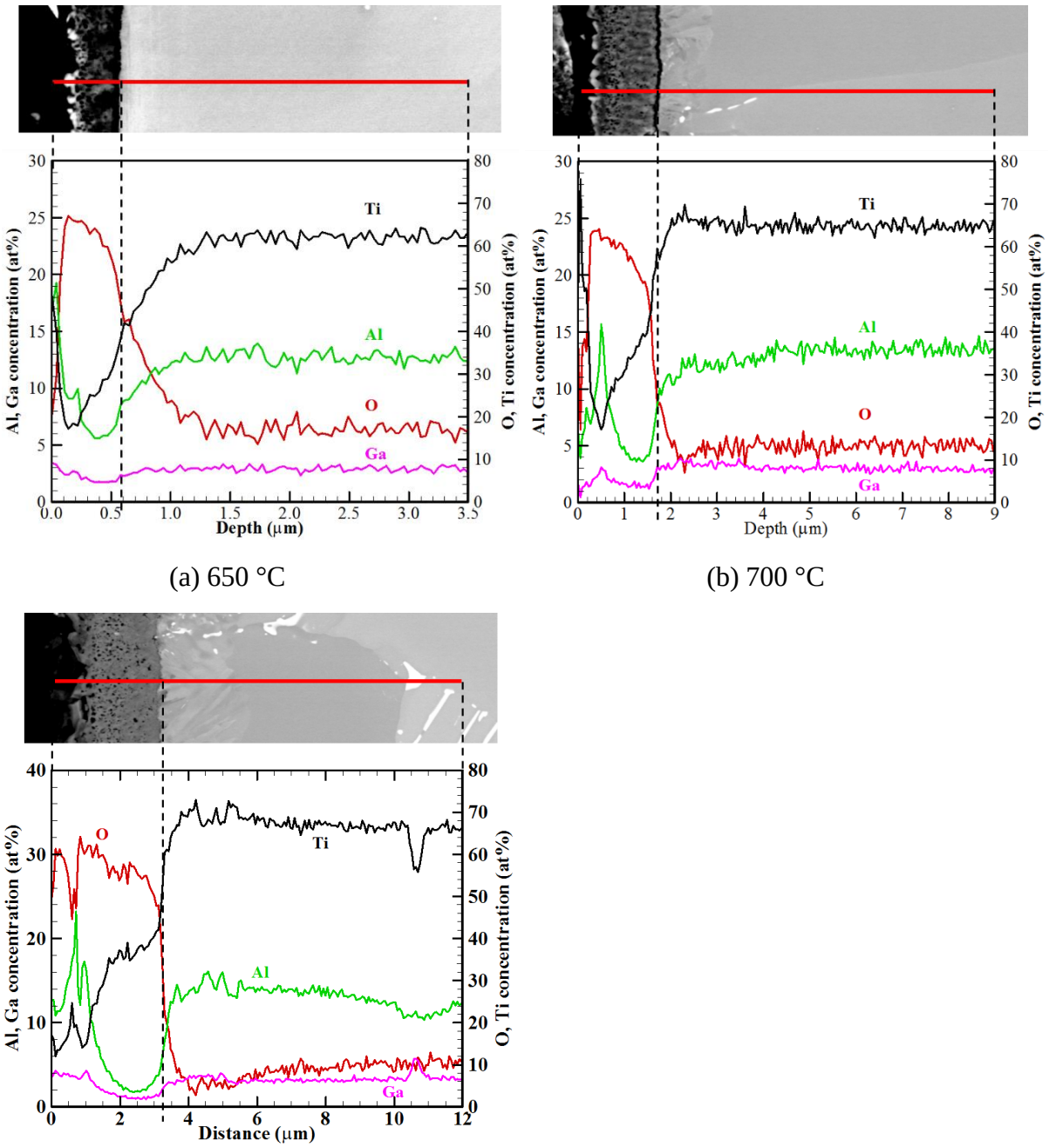

(a) 650 °C

(b) 700 °C

(c) 750 °C

Figure 5.6. Concentration profiles of Ti, Al, Ga and O obtained in the oxide and substrate along the lines for TKT41 at (a) 650 °C, (b) 700 °C and (c) 750 °C for 500 h.

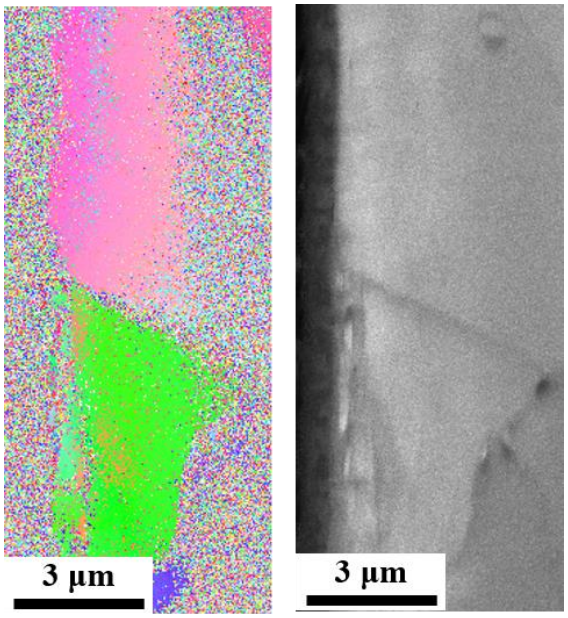

(a) 650 °C

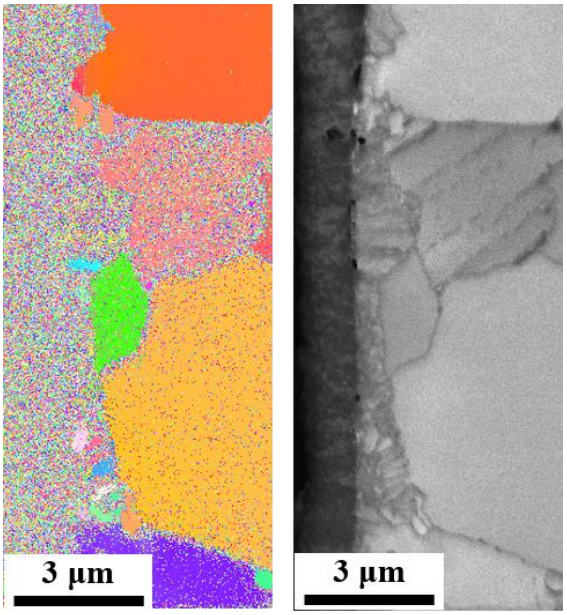

(b) 700 °C

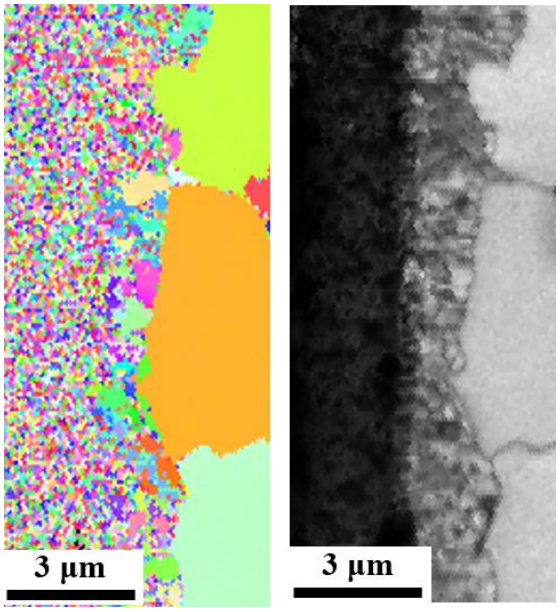

(c) 750 °C

Figure 5.7. EBSD results (left: inverse pole figure, right: image quality) of TT41a after 500 h exposure at (a) 650 °C, (b) 700 °C and (c) 750 °C, respectively.

To investigate the effect of the alloy recrystallization on the oxygen diffusion into the substrate, the thickness of the formed α-case was evaluated via optical observations after proper etching, microhardness measurements, and oxygen concentration measurements. Since oxygen dissolution increases alloy's

hardness due to solid solution strengthening, the hardness values obtained for titanium alloys were directly proportional to oxygen concentration [31,32,33]. Gaddam et al. [17] and McReynolds et al. [5] quantitatively compared the described three methods and found that the microhardness and oxygen concentration measurements by electron probe microanalysis (EPMA) produced similar results for the α-case evaluation, while the optical measurements underestimated the α-case thickness. Fig. 5.8 shows the α-case thicknesses obtained via oxygen concentration (EDS) and microhardenss measurements for the alloy sample heat-treated at 700 °C for 500 h (the normalized oxygen concentration was determined using the method described by Gaddam et al. [17]). Although the oxygen concentration discussed in this section was not equal to the absolute oxygen concentration inside the sample, it could still be used for evaluating the α-case thickness since the relative oxygen concentration along the sample thickness was kept consistent. Fig. 5.8b shows a typical EDS spectrum obtained for the cross-section of the oxidized sample, which contains distinct peaks corresponding to TiL_{α} and OK_{α} species. The α-case thicknesses determined by microhardness and EDS measurements were equal to 182 and 146 μm and the result by EDS measurement was comparable to the magnitudes of 154 μm obtained by Gaddam et al. [17] for Ti–6242 alloy after 500-h exposure at 700 °C via microhardness and EPMA measurements, respectively (in this work, EDS was selected for the alpha-case examination mainly due to its directness and reliability).

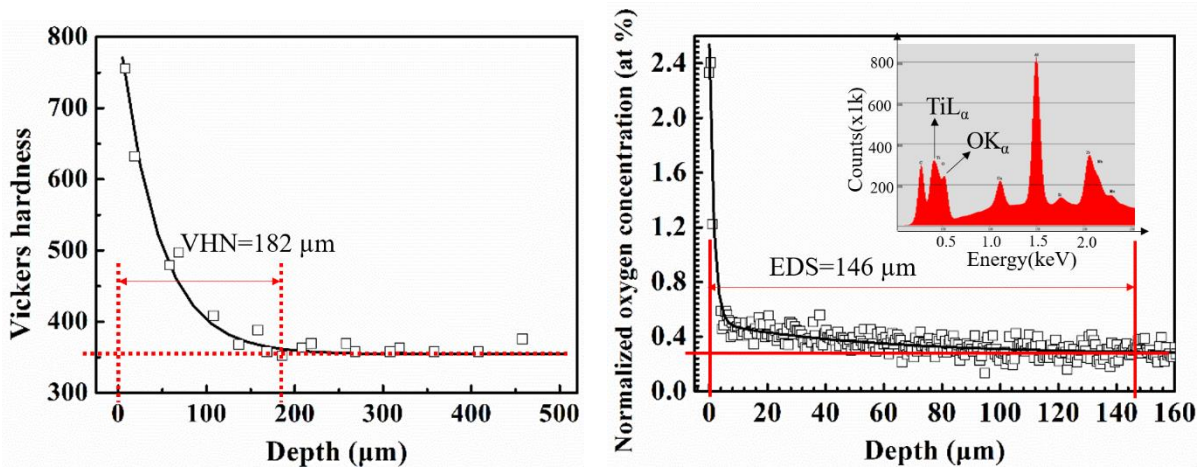

(a) (b)

Figure 5.8. Alpha-case thickness measured by (a) microhardness and (b) oxygen concentration.

To estimate the time-dependent α-case thickness, it is reasonable to assume that the studied alloy specimens have a semi-infinite thickness. In this case, the approximate solution for Fick's second law of diffusion can be expressed as follows [5]:

$$x = \sqrt{Dt}, \tag{3}$$

where x is the α-case thickness, D is the oxygen diffusion coefficient, and t is the exposure time. According to the results presented in Fig. 5.9, the α-case thickness increases with increasing temperature and exposure time in the temperature range of 650–750 °C. A good fit obtained for the α-case thickness using the square root function suggested that the formation of α-case followed Fick's second law of diffusion, which was consistent with the data reported for other conventional titanium alloys [5,17]. The values of D estimated via linear regression analysis are listed in Table 5.2. It is important to note that the oxygen diffusivity calculated

in this work represented a combination of the volume diffusion and the grain boundary diffusion.

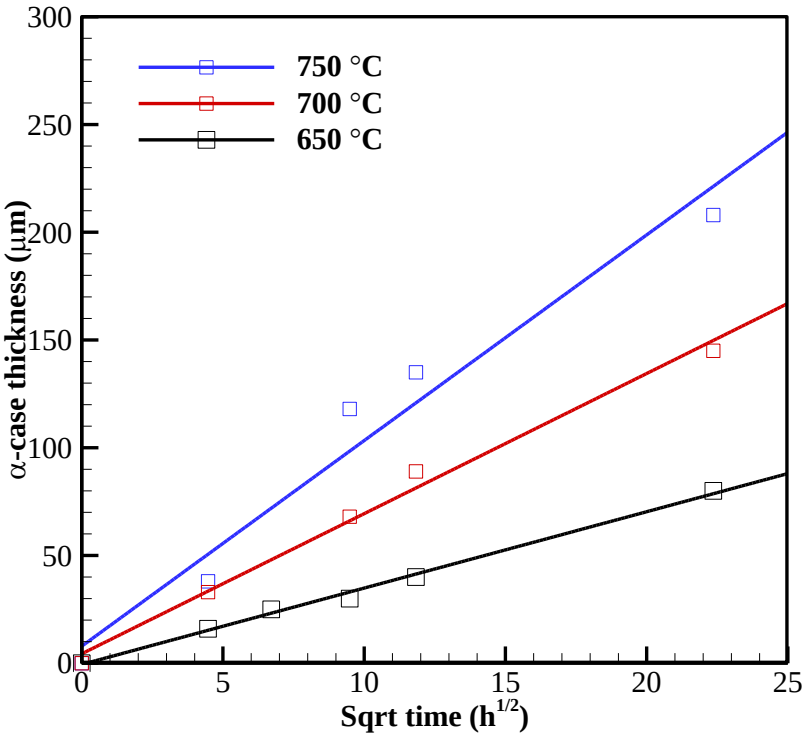

Figure 5.9. Alpha-case thicknesses measured by EDS as a function of time at 650, 700 and 750 °C.

The temperature dependence of D can be obtained using the following Arrhenius-type relationship:

$$D = D_0 \exp\left(\frac{-Q_{diff}}{RT}\right), \quad (4)$$

where D_0 is the pre-exponential factor, Q_{diff} is the activation energy of the oxygen diffusion in the α-case layer, R is the gas constant (8.3143 J/(mol K)), and T is the reaction temperature (K). As shown in Fig. 5.10, the value of Q_{diff} can be calculated from the plot of $\log D$ versus $1/T$, whose slope is equal to $Q_{diff}/2.303\,R$. The estimated Q_{diff} value was equal to 156 kJ/mol, which was

comparable to the magnitudes of 155 kJ/mol (for IMI125 alloy [4]), 153 kJ/mol (for Ti6242 alloy [17]), and 160 kJ/mol (for IMI834 alloy [19]). The obtained results suggest that the α-case formation in the studied alloy was mainly caused by the inward diffusion of oxygen with an activation energy not significantly different from the values estimated for conventional titanium alloys despite the observed recrystallization (since the expansion of the recrystallized region was much slower than the oxygen diffusion, the resulting oxygen-rich zone was larger than the recrystallized region).

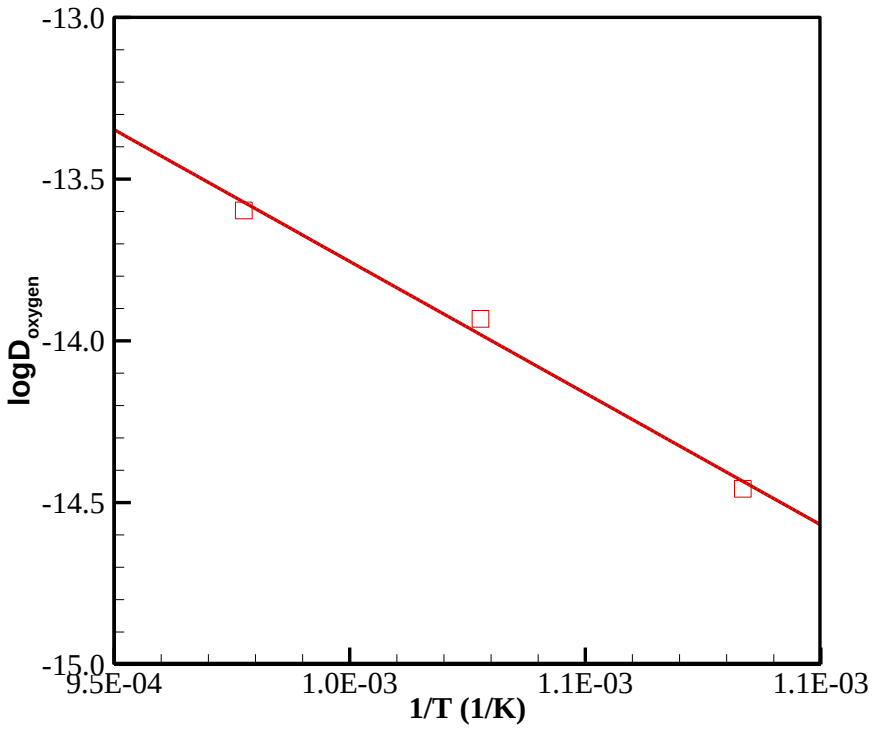

Figure 5.10. Arrhenius plot of the rate constant values calculated by utilizing alpha-case thickness values presented in Fig. 9.

The oxidation of the studied Ga-containing titanium alloy exhibited parabolic kinetics at 650 °C, which transformed into parabolic-cubic kinetics in the temperature region of 700–750 °C. However, similar to other conventional

titanium alloys, the measured growth rate of α-case followed a parabolic law despite the temperature-dependent recrystallization that occurred at the interface between the oxide and substrate layers. For the studied Ga-containing alloy, the reaction rate constant of around 2.5 measured at elevated temperatures likely resulted from the densification of the TiO_2 layer, while the fraction of Al_2O_3 in the oxide layers increased with the dissolution of Ga_2O_3 in the Al_2O_3 phase at high temperatures.

Based on our previous work, recrystallization was observed in Ga-added near-α titanium alloys and O concentration was found to be lower at recrystallization area after 500 h oxidation at 750 °C as shown in Fig. 5.6c. The elemental mapping analysis with the consideration of N were conducted in Ga-containing alloys.

Fig. 5.11 shows the elemental mapping images and also the element concentration profiles of N, O, Al, Ga, and Ti along a yellow line as suggested in second electron image (SEI) in Ga-containing Ti alloy after oxidation at 750 °C for 20 h. Based on the elemental mapping images and concentration profiles, it is obvious that a thin nitrogen-rich layer formed at the interface after 20 h exposure. From the EBSD result of Fig. 4.9a, the recrystallization was not observed at the interface.

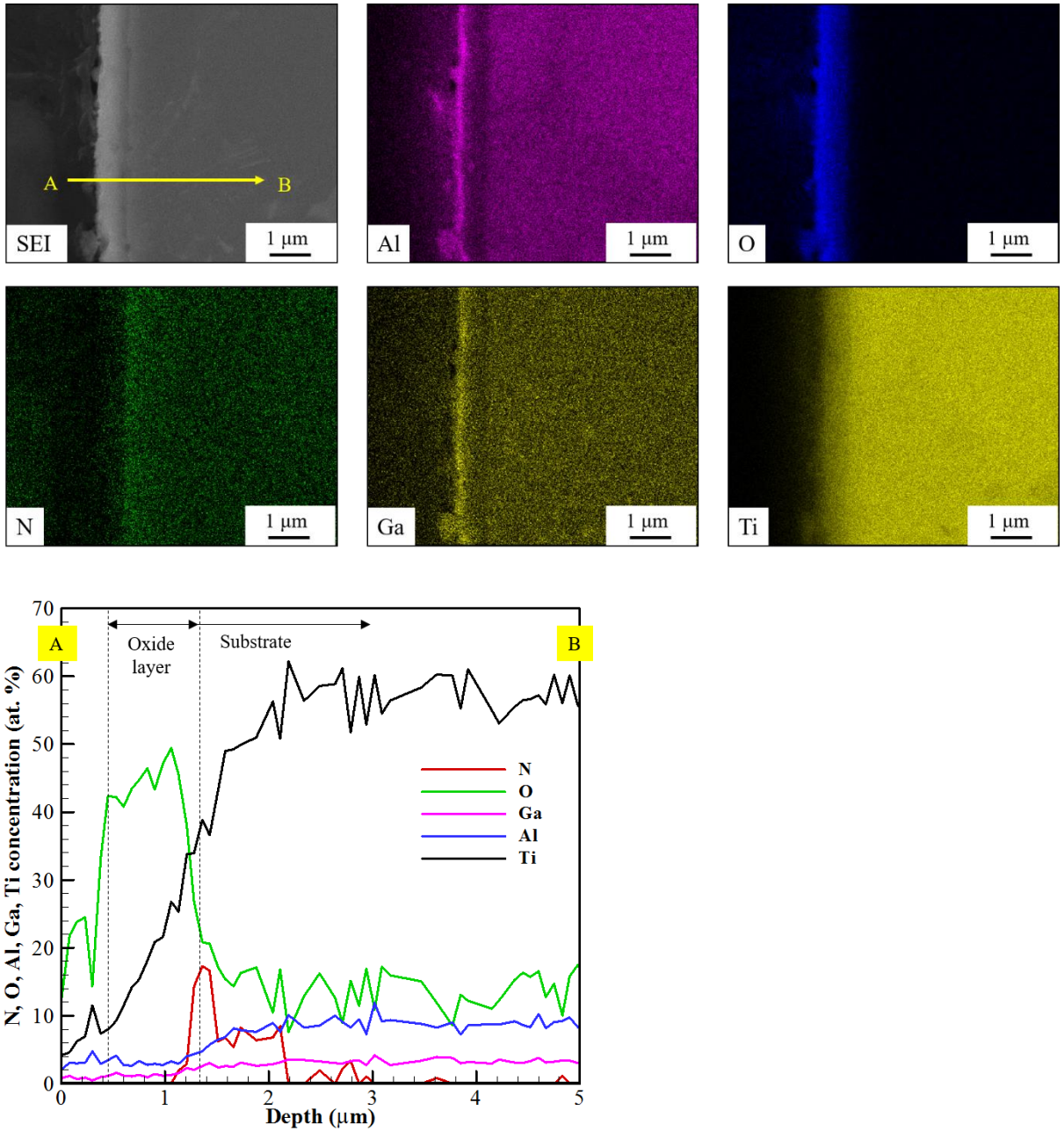

Figure 5.11 Elemental mapping images and concentration profiles of N, O, Al, Ga, and Ti for TKT41 at 750 °C for 20 h.

Fig. 5.12 shows the elemental mapping images and the element concentration profiles of N, O, Al, Ga, and Ti along a yellow line A-B in Ga-containing Ti alloy after oxidation at 750 °C for 500 h.

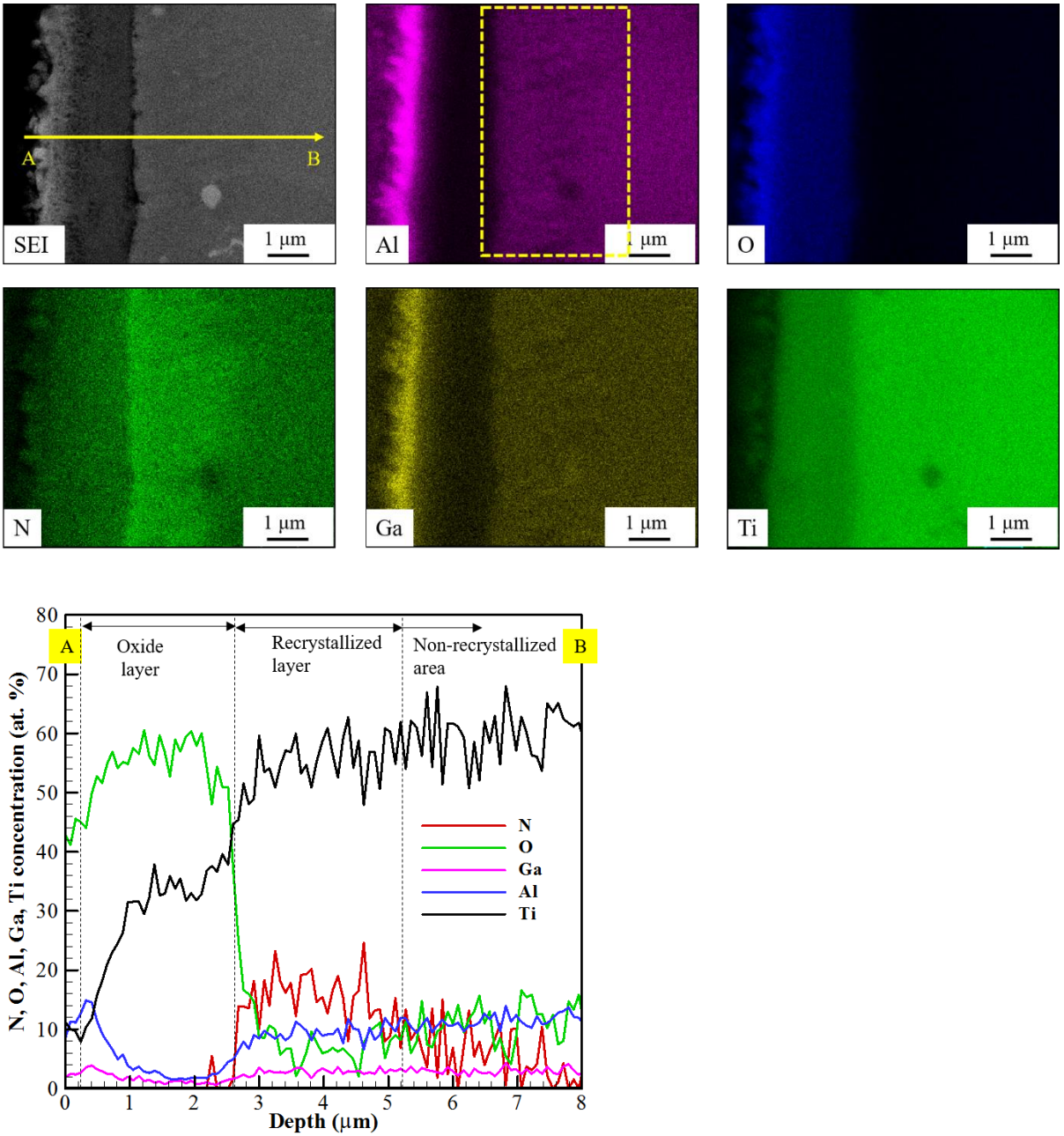

Figure 5.12 Elemental mapping images and concentration profiles of N, O, Al, Ga, and Ti for TKT41 (Ga-containing) at 750 °C for 500 h.

After 500 h exposure at 750 °C, recrystallized fine grains were observed near the interface in TKT41 as shown in Fig. 5.7c. As shown in Fig. 5.12, the concentration of Al was not homogeneous in the recrystallized area as suggested by a yellow rectangle dot line in the elemental mapping of Al. From the element concentration profiles, N concentration was very high near the interface while O

concentration was low. The higher concentration of N and the fluctuated concentration of Al in recrystallized area suggested that the formation of nitrides in the recrystallized grains. To discuss the growth of recrystallized grains, I analyzed two binary alloys: Ti-4Al and Ti-8Al after isothermally oxidized in laboratory air for up to 240 h at 700 °C.

Fig. 5.13 shows the SEM micrographs of Ti-4Al (a, b) and Ti-8Al (c, d) after exposed at 700 °C for 240 h. Top images are second electron images and bottom ones are back scattered diffraction images for each alloy in Fig. 5.13. Fig. 5.14 shows the EBSD result: the left figure is inverse pole figure map (IPF) and the right one is image quality (IQ) map.

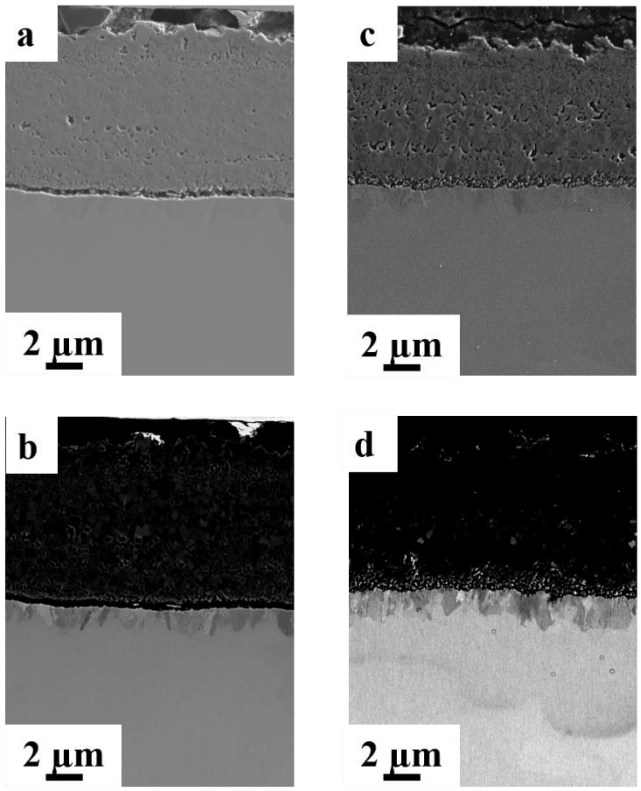

Figure 5.13. SEM micrographs of Ti-4Al (a, b) and Ti-8Al (c, d) after oxidation at 700 °C for 240 h. (top: second electron images, down: back scattered diffraction images)

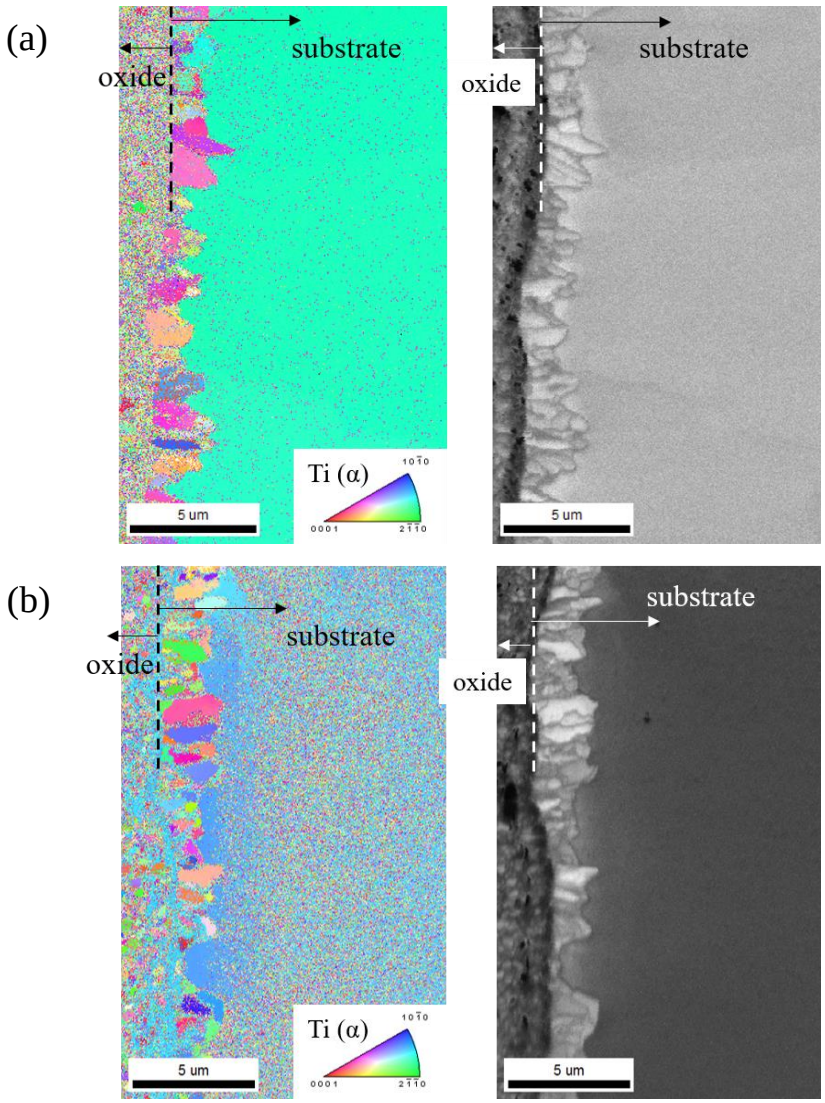

Figure 5.14. EBSD results of (a) Ti-4Al, and (b) Ti-8Al after 240 h exposure at 700 °C. (left: inverse pole figure map, right: image quality map)

As shown in Fig. 5.13 and Fig. 5.14, recrystallized grains were observed in both binary systems. The size of the small recrystallized grains in Ti-4Al and Ti-8Al were similar although the Al equivalent value of Ti-8Al was almost twice as that in Ti-4Al, which suggested that the Al equivalent value was not the main trigger for recrystallization in my study.

Fig. 5.15 shows the elemental mapping images and also the element concentration profiles of N, O, Al, and Ti along yellow lines as suggested in SEI in Ti-8Al alloy after oxidation at 700 °C for 240 h.

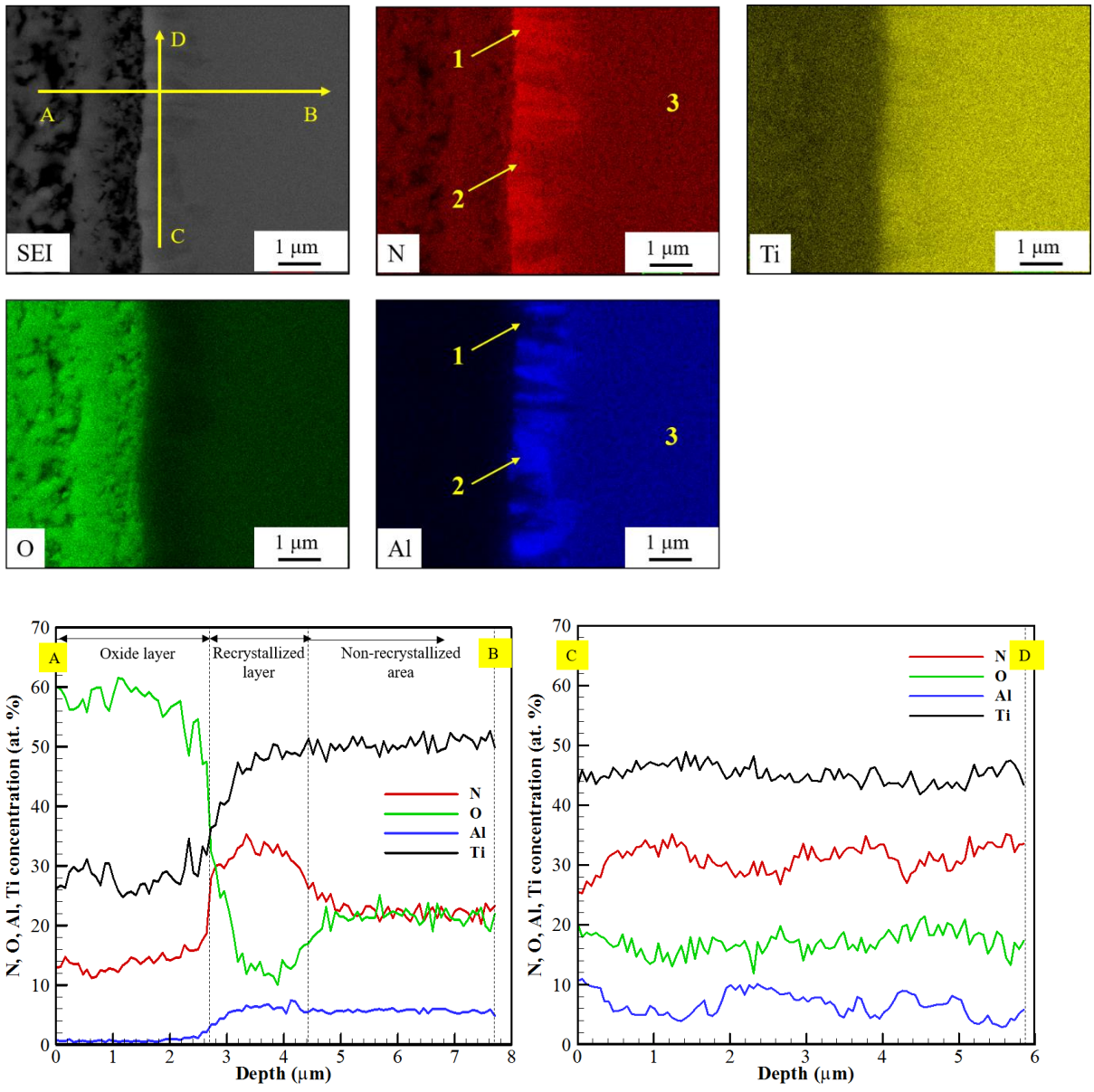

Figure 5.15. Elemental mapping images and concentration profiles of N, O, Al, and Ti for Ti-8Al at 700 °C for 240 h.

, However, the N concentration was high at recrystallized area as shown in element concentration profile of line A-B in Fig. 5.15. The elemental mapping images of Al and N showed that the Al content in N-rich part (as suggested by an

arrow 1 in Fig. 5.15) was smaller than that in the non-recrystallized grain (as suggested by an arrow 3). In addition, the Al content in Al-rich part (as suggested by an arrow 2) was higher than that in the non-recrystallized grain (as suggested by an arrow 3). It also can be seen the relatively high and low Al concentration by Al concentration profile of line C-D in recrystallized area. Leyens et al. [34] suggested the formation of Ti_3AlN in IMI834 and TIMETAL 1100, however, the location of such nitride was unclear. From the element concentration profile line-AB in Fig. 5.15, the N and Al concentration were approximately 30 at. % and 8 at. % in the recrystallized area, and from line C-D in Fig. 5.15, the N concentration can reach to 35 at. % in N-rich area. According to a phase diagram of Ti-Al-N system [35], grains with Ti_3AlN (Al-rich area) and Ti_2N (N-rich area), may have grown from the oxide/metal interface. The formation of Ti_3AlN grains and Ti_2N grains at the interface promotes the strains introduced by the precipitation of these phases resulting in the growth of recrystallized grains. Thus, an increase in N concentration at the oxide/metal interface strongly triggered the recrystallization.

Fig. 5.16 shows the elemental mapping images and also the element concentration profiles of N, O, Al, Sn, and Ti along a yellow line A-B in TKT39 (Sn-containing) alloy after oxidation at 750 °C for 500 h. From Fig. 4.8 in chapter 4, the recrystallization did not occur in Sn-containing alloy and this may be due to the low N concentration at the interface (line A-B in Fig. 5.16). As shown in

Fig. 5.16, Sn segregated at the interface, which suggested that N diffusion may be suppressed by the Sn-rich layer.

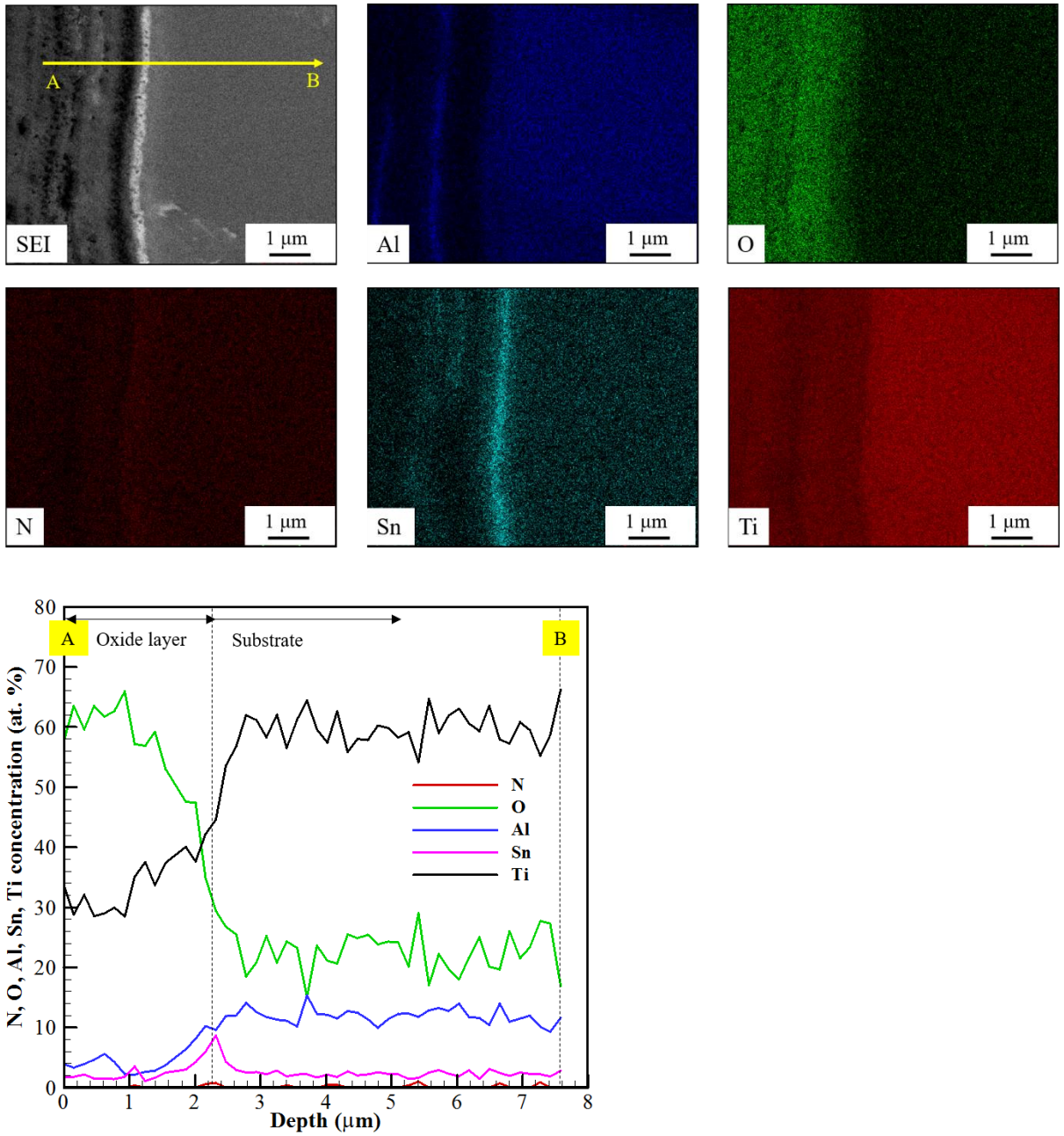

Figure 5.16. Elemental mapping images and concentration profiles of N, O, Al, Sn, and Ti for TKT39 (Sn-containing) at 750 °C for 500 h.

5.5 Conclusions

The oxidation behaviour of Ga-containing near-α Ti alloy with a bimodal structure was investigated at temperatures of 650, 700, and 750 °C and exposure

times as high as 500 h. From the obtained results, the following conclusions can be drawn.

(1) According to the data obtained via weight gain analysis, the alloy oxidation process followed a parabolic relationship at 650 °C and parabolic-cubic relationships at 700 and 750 °C. The densification of the oxide layers near the substrate was observed at 700 and 750 °C.

(2) Alloy recrystallization near the oxide/metal interface occurred at temperatures of 700 and 750 °C, but not at 650 °C.

(3) The estimated activation energy for the alpha-case formation was equal to 156 kJ/mol, which was similar to the magnitudes obtained for conventional alloys. The recrystallization process had little effect on the alloy weight gain due to oxygen penetration.

(4) The abundance of Al_2O_3 species in the oxide layers increased with increasing temperature.

(5) An increase in the concentration of N at the oxide/metal interface may promote the formation of Ti_3AlN and Ti_2N, and the strain caused by lattice misfit at the interface triggered recrystallization near the interface.

5.6 References

[1] G. Lütjering, and J. C. Williams, Titanium, second ed., Springer, Berlin, 2003.

[2] T. Kitashima, K. S. Suresh, and Y. Yamabe-Mitarai, Present stage and future prospects of development of compressor material, Crystal Research and Technology, 50 (2015) 28-37.

[3] J. H. Perepezko, The hotter the engine, the better, Science, 326 (2009) 1068-1069.

[4] T. J. Johnson, M. H. Loretto, and M. W. Kearns, Oxidation of high temperature titanium alloys, in: Proceedings of the Seventh World Titanium Conference, Warrendale, PA, TMS, (1992) 2035-2042.

[5] K. S. Mcreynolds, and S. Tamirisakandala, A study on alpha-case depth in Ti-6Al-2Sn-4Zr-2Mo, Metallurgical and Materials Transactions A, 42 (2011) 1732 -1736.

[6] R. N. Shenoy, J. Unnam, and R. K. Clark, Oxidation and embrittlement of Ti-6Al-2Sn-4Zr-2Mo alloy, Oxidation of Metals, 26 (1986) 105-124.

[7] Z. Liu, and G. Welsch, Effects of oxygen and heat treatment on the mechanical properties of alpha and beta titanium alloys, Metallurgical Transactions A, 19 (1988) 527-542.

[8] T. Kitashima, L. J. Liu, and H. Murakami, Numerical analysis of oxygen transport in alpha titanium during isothermal oxidation, Journal of The Electrochemical Society, 160 (2013) C441-C444.

[9] D. A. P. Reis, C. R. M. Silva, M. C. A. Nono, M. J. R. Barboza, F. Piorino Neto, and E. A. C. Perez, Effect of environment on the creep behavior of the Ti-6Al-4V alloy, Materials Science and Engineering A, 399 (2005) 276-280.

[10] P. Kofstad, K. Hanffe, and H. Kjollesdal, Investigation on the oxidation mechanism of titanium, Acta Chemica Scandinavica, 12 (1958) 239-266.

[11] P. Kofstad, High-temperature oxidation of titanium, Journal of the Less Common Metals, 12 (1967) 449-464.

[12] S. Frangini, and A. Mignone, Various aspects of the air oxidation behaviour of a Ti-6Al-4V alloy at temperatures in the range 600–700 °C, Journal of Materials Science, 29 (1994) 714-720.

[13] H. Guleryuz, and H. Cimenoglu, Oxidation of Ti-6Al-4V alloy, Journal of Alloys and Compounds, 472 (2009) 241-246.

[14] H. L. Du, P. K. Datta, D. B. Lewis, and J. S. Burnell-Gray, Air oxidation behaviour of Ti-6Al-4V alloy between 650 and 850 °C, Corrosion Science, 36 (1994) 631-642.

[15] H. L. Du, P. K. Datta, D. B. Lewis, and J. S. Burnell-Gray, High-temperature corrosion of Ti and Ti-6Al-4V alloy, Oxidation of Metals, 45 (1996) 507-527.

[16] D. Poquillon, C. Armand, and J. Huez, Oxidation and oxygen diffusion in Ti–6Al–4V alloy: improving measurements during sims analysis by rotating the sample, Oxidation of Metals, 79 (2013) 249-259.

[17] R. Gaddam, B. Sefer, R. Pederson, and M. Antti, Oxidation and alpha-case formation in Ti-6Al-2Sn-4Zr-2Mo alloy, Materials Characterization, 99 (2015) 166-174.

[18] C. Leyens, M. Peters, and W. A Kaysser, Oxidation behavior of near-α titanium alloys and their protection by coatings, in the Titanium ’95: Science and

Technology, Proceedings of the 8th World Conference on Titanium, London: Institute of Materials, Birmingham, England, (1996) 1935-1942.

[19] R. W. Evans, R. J. Hull, and B. Wilshire, The effects of alpha-case formation on the creep fracture properties of the high-temperature titanium alloy IMI834, Journal of Materials Processing Technology, 56 (1996) 492-501.

[20] W. J. Jia, W. D. Zeng, X. M. Zhang, Y. G. Zhou, J. R. Liu, and Q. J. Wang, Oxidation behaviour and effect of oxidation on tensile properties of Ti60 alloy, Journal of Materials Science, 46 (2011) 1351-1358.

[21] T. Kitashima, Y. Yamabe-Mitarai, S. Iwasaki, and S. Kuroda, Effects of Ga and Sn additions on the creep strength and oxidation resistance of near-α Ti alloys, Metallurgical and Materials Transactions A, 47 (2016) 6394-6403.

[22] C. E. Shamblen, and T. K. Redden, Creep resistance and high-temperature metallurgical stability of titanium alloys containing gallium, Metallurgical and Materials Transactions B, 3 (1972) 1299-1305.

[23] C. E. Shamblen, and C. J. Rosa, Ti_3Ga and α-Ti interdiffusion between 660 and 860° C, Metallurgical and Materials Transactions B, 2 (1971) 1925-1931.

[24] T. Kitashima, Y. Yamabe-Mitarai, S. Iwasaki, and S. Kuroda, Effects of alloying elements on the tensile and oxidation properties of alpha and near-alpha Ti alloys, in Proceedings of the 13th World Conference on Titanium, Wiley, California, USA, (2015) 479-485.

[25] E. M. Kenina, I. I. Kornilov, and V. V. Vanilova, Effect of oxygen on the scale resistance of titanium-tin alloys, Metal Science and Heat Treatment, 14 (1972) 396-398.

[26] B. Champin, L. Graff, M. Armand, G. Beranger, and C. Coddet, Oxydation des alliages de titane au voisinage des températures d'utilisation dans les turbomoteurs, Journal of the Less Common Metals, 69 (1980) 163-183.

[27] P. Kofstad, High temperature corrosion, Elsevier Applied Science, London, 1988.

[28] D. Liu, W. A. Miller, and K. T. Aust, Diffusion induced grain boundary migration and recrystallization during oxidation of a Ni-48.5 Pet Cu alloy, Metallurgical and Materials Transactions A, 19 (1988) 1667-1675.

[29] T. A. Parthasarathy, and P. G. Shewmon, Vapor transport and DIGM in the Ni-Fe system, Metallurgical Transactions A, 14 (1983) 2560-2563.

[30] W. R. Tyson, Solution hardening of titanium by oxygen, Scripta Metallurgica, 3 (1969) 917-921.

[31] C. J. Rosa, Oxygen diffusion in alpha and beta titanium in the temperature range of 932 to 1142 °C, Metallurgical and Materials Transactions B, 1 (1970) 2517-2522.

[32] F. M. Guclu, H. Cimenoglu, and E. S. Kayali, The recrystallization and thermal oxidation behaviour of CP-titanium, Materials Science and Engineering: C, 26 (2006) 1367-1372.

[33] C. Leyens, M. Peters, and W. A. Kaysser, Influence of microstructure on oxidation behaviour of near-α titanium alloys, Materials Science and Technology, 12 (1996) 213-218.

[34] Q. Chen, and B. Sundman, Thermodynamic assessment of the Ti-Al-N system, Journal of Phase Equilibria, 19 (1998) 146-160.

Chapter 6 Summary and conclusion

The main objective of this study was the investigation of the effects of elements (Ga, Sn) and microstructures on oxidation behaviors of near-α Ti alloys at elevated temperatures (650-750 °C) after long exposure time (up to 500 h) in ambient air.

In Chapter 2, it has been shown that alloying elements, temperature, time and microstructures affect oxidation behaviors. Some additional alloying elements decrease oxygen vacancies in TiO_2 thus decreasing the overall oxidation rate through valence control rule, some elements can form a discrete layer working as a barrier to prevent oxygen diffusion, and some elements affect the adherence of the oxide layer to the metal substrate. For conventional Ti alloys, a logarithmic law has been obtained at low temperature, and changed to parabolic and linear law or mixed rate law with increasing temperature and time. The change of oxidation kinetics were combined with the change in oxide formation and oxygen diffusion, such as the porosity of oxide scale, the composition of oxides, temperature dependency of oxygen diffusivity etc. In addition, microstructures, like bimodal and lamellar microstructures, also affect oxidation process especially on oxygen diffusion process.

To investigate the effects of alloying elements on oxidation behavior, a Ga-containing and a Sn-containing near-α Ti alloys were studied. The microstructures' effects were also considered as discussed in chapter 4. It was shown that the replacement of Sn with Ga decreased the weight gain of the

oxidation sample during oxidation, suppressed oxide growth, and improved adherence between the oxide and substrate. In Ga-containing alloy, there was no Ga segregation at the oxide/substrate interface, and the formation of $(Al, Ga)_2O_3$ and $(Ga, Al)_2TiO_5$ was suggested. Unlike conventional Ti alloys, recrystallization occurred near the oxide/substrate interface, which may contribute to the release of stress, improvement of the adherence between the oxide and substrate, and prevention of the spallation of oxides. In both alloys, lamellar structures showed a smaller weight gain compared to the bimodal structures.

As the Ga-containing alloy showed better oxidation resistance compared to that of Sn-containing alloy and recrystallization was observed near the oxide/substrate interface, the effects of temperature and time on the oxidation behaviour (especially on oxidation reaction rate and α-case formation) of the Ga-containing near-α Ti alloy and the temperature dependence of its recrystallization process were examined as discussed in chapter 5. It was shown that oxidation follows a parabolic relationship at 650 °C and a parabolic-cubic relationship at 700 and 750 °C with the abundance of Al_2O_3 in oxide layers. The amount of Al_2O_3 increased with temperature after the dissolution of Ga_2O_3 species in the Al_2O_3 phase. The activation energy of α-case formation was close to the magnitudes obtained for conventional titanium alloys despite its temperature-dependent recrystallization observed near the oxide/metal interface at 700 and 750 °C. Recrystallization also occurred in the substrate at the oxide/metal interface in Ti-

4Al and Ti-8Al system. N showed higher concentration at the oxide/metal interface in Ti-4Al, Ti-8Al, and Ga-containing alloy except for Sn-containing alloy. Based on the element analysis and the phase diagram of Ti-Al-N system, the formation of grains with Ti_3AlN and Ti_2N were suggested at the interface due to the high concentration of N. Fine recrystallized grains were observed near the interface due to lattice misfit strain.

In summary, this dissertation investigates the oxidation behaviors of a Sn-containing Ti alloy and a Ga-containing Ti alloy. The mechanism on the effects of alloying elements, temperature and time on oxidation behaviors was studied.